



Terms and Conditions of Use of Digitised Theses from Trinity College Library Dublin

Copyright statement

All material supplied by Trinity College Library is protected by copyright (under the Copyright and Related Rights Act, 2000 as amended) and other relevant Intellectual Property Rights. By accessing and using a Digitised Thesis from Trinity College Library you acknowledge that all Intellectual Property Rights in any Works supplied are the sole and exclusive property of the copyright and/or other IPR holder. Specific copyright holders may not be explicitly identified. Use of materials from other sources within a thesis should not be construed as a claim over them.

A non-exclusive, non-transferable licence is hereby granted to those using or reproducing, in whole or in part, the material for valid purposes, providing the copyright owners are acknowledged using the normal conventions. Where specific permission to use material is required, this is identified and such permission must be sought from the copyright holder or agency cited.

Liability statement

By using a Digitised Thesis, I accept that Trinity College Dublin bears no legal responsibility for the accuracy, legality or comprehensiveness of materials contained within the thesis, and that Trinity College Dublin accepts no liability for indirect, consequential, or incidental, damages or losses arising from use of the thesis for whatever reason. Information located in a thesis may be subject to specific use constraints, details of which may not be explicitly described. It is the responsibility of potential and actual users to be aware of such constraints and to abide by them. By making use of material from a digitised thesis, you accept these copyright and disclaimer provisions. Where it is brought to the attention of Trinity College Library that there may be a breach of copyright or other restraint, it is the policy to withdraw or take down access to a thesis while the issue is being resolved.

Access Agreement

By using a Digitised Thesis from Trinity College Library you are bound by the following Terms & Conditions. Please read them carefully.

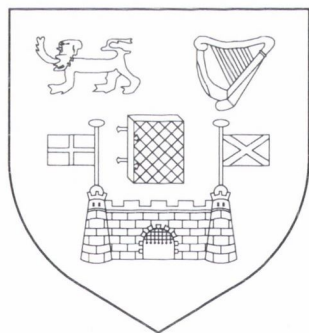
I have read and I understand the following statement: All material supplied via a Digitised Thesis from Trinity College Library is protected by copyright and other intellectual property rights, and duplication or sale of all or part of any of a thesis is not permitted, except that material may be duplicated by you for your research use or for educational purposes in electronic or print form providing the copyright owners are acknowledged using the normal conventions. You must obtain permission for any other use. Electronic or print copies may not be offered, whether for sale or otherwise to anyone. This copy has been supplied on the understanding that it is copyright material and that no quotation from the thesis may be published without proper acknowledgement.

Optimization Techniques in Elastic Proton-Proton Collisions

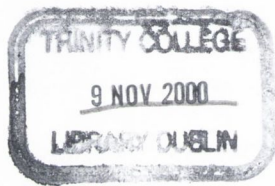
by

Alan T. Bates

A thesis submitted to the School of Mathematics, University of Dublin,
Trinity College, for the degree of Ph.D.



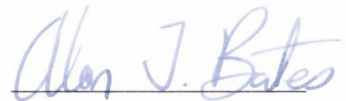
April 2000



Thesis
5901

Declaration

This thesis has not been submitted as an exercise for a degree at any other university. Except where otherwise stated, the work presented herein has been carried out by the author alone. The library of Trinity College, Dublin may lend or copy this thesis upon request. The copyright belongs jointly to the University of Dublin and Alan T. Bates.



Alan T. Bates

Acknowledgements

With pleasure I thank my supervisor Dr. Nigel Buttimore for his advice, encouragement and support at all stages throughout my research. I also wish to thank Dr. Michael Fry and Prof. Siddhartha Sen for their help I received at the beginning of my postgraduate studies. A big thanks to the system administration staff for providing an excellent service. I am kindly grateful for the financial support I received from Enterprise Ireland (SC/96/778) and Dublin Corporation. I would also like to mention my friends—Alex (Pelé), Alfredo, Alison, Beatrice, Carlos, Colm, Conall, David, Emil, Enda, Eoin, Fabian, Ger, James, Justino, Miyuki, Marco, Ollie, Samik and Rui—who all made the atmosphere special. Thanks to my family, in particular my parents, for their constant understanding and support. A special thanks to Giovanna for the laughs, smiles and warmth. Finally I want to mention my city of Dublin which greets me with inspiration every day.

Summary

The proton spin puzzle has intrigued experimentalists and theorists since the surprising result from the EMC experiment at CERN in 1988, which found a smaller than expected contribution to the spin of the proton from the component quarks. The question, “where does the spin of the proton come from?” remains unanswered. Recent data suggests a value of $31 \pm 4\%$ for the fraction of the spin carried by the *up*, *down* and *strange* quarks. The contribution from the gluons and from the orbital angular momentum of the quarks and gluons is not completely known. The Relativistic Heavy Ion Collider at Brookhaven National Laboratory plans to probe the proton structure using the deep inelastic scattering of protons at high center-of-mass energies ($\sqrt{s} = 50 - 500$ GeV) and momentum transfers ($p_T \geq 10$ GeV/ c). To measure the contribution of the gluons to the spin of the proton, with sufficient accuracy, a polarized proton beam with a maximum beam polarization error of 5% is necessary. One method of measuring the polarization of a proton beam uses the analyzing power in elastic proton collisions at small scattering angles. The accuracy of the polarization measurement depends on the size of the helicity single-flip amplitude. In the thesis, bounds on the imaginary part of the helicity single-flip amplitude are derived which provide important information related to the evaluation of polarization. Extended to include equality and inequality constraints, the Lagrange multiplier method

of optimization is successfully employed to bound the imaginary single-flip amplitude, modified by a kinematical factor, in the low momentum transfer region at center-of-mass energies about 50 GeV. An upper bound of 0.84 is found when the elastic cross section, the imaginary spin average non-flip amplitude at small momentum transfers and the total cross section are expressed as equality constraints, with unitarity expressed as an inequality constraint. This bound, at low momentum transfers in the energy range of the Relativistic Heavy Ion Collider, limits the analyzing power to positive values.

Contents

General Introduction	1
1 Polarization Measurement	13
1 Proton-Proton Polarimetry	14
1.1 Analyzing Power in the CNI Region	14
2 Proton-Carbon Polarimetry	18
2 Helicity Single-Flip Amplitude	20
1 Models based on Regge Theory	21
2 Experimental Data	24
3 Bound from Positivity Properties	26
4 Spin 0-Spin 1/2 Bound	26
3 Optimization with Lagrange Multipliers	29
1 Terminology	31
1.1 Maximization with Equality Constraints	32

1.2	Maximization with Inequality Constraints	34
2	MacDowell-Martin Bound; An Example	35
2.1	Observables and Constraints	36
2.2	Optimization	38
2.3	Unitarity Classes	39
2.4	Reconstructing the Constraints	40
4	Observables in Proton-Proton Scattering	43
1	Helicity Amplitudes	44
2	Total Cross Section	48
3	Imaginary Non-Flip Amplitude	49
4	Elastic Cross Section	50
5	Imaginary Single-Flip Amplitude	53
6	Unitarity	54
5	Optimization under σ_{el} and Unitarity	56
1	Lagrange Formalism	57
2	Unitarity Classes	59
2.1	I^W and B^W Unitarity Classes	60
2.2	I^X and B^X Unitarity Classes	61
3	Reconstruction of σ_{el}	64
4	Results	68

6	Bound including the Spin-Average Amplitude	76
1	Lagrange Formalism	77
2	Unitarity Classes	79
2.1	I^W and B^W Unitarity Classes	80
2.2	I^X and B^X Unitarity Classes	82
3	Solution of Interior Unitarity Class	84
3.1	Results	88
4	Solution of Boundary Unitarity Class	92
5	Interior and Boundary Unitarity Classes	93
5.1	Numerical Technique	95
5.2	Results	100
7	Optimization including σ_{tot}	107
1	Lagrange Formalism	108
2	Unitarity Classes	110
2.1	I^W and B^W Unitarity Classes	111
2.2	I^X and B^X Unitarity Classes	113
3	Solution of Interior Unitarity Class	115
3.1	Results	121
4	Solution of Interior and Boundary Classes	126

Appendices

A Partial Wave Phase Shifts	137
B Mathematica Code	138
C Euler-MacLaurin Expansion	141

List of Figures

4.1	Regions associated with the expressions of $d_{\lambda\mu}^J(\theta)$ in terms of Jacobi polynomials.	46
5.1	a_{11}^J, a_{21}^J under σ_{el} and unitarity; $\sqrt{s} = 19.5$ GeV, $t = -0.001$ (GeV/c) ²	72
5.2	a_{11}^J, a_{21}^J under σ_{el} and unitarity; $\sqrt{s} = 23.5$ GeV.	72
5.3	a_{11}^J, a_{21}^J under σ_{el} and unitarity; $\sqrt{s} = 30.7$ GeV.	72
5.4	a_{11}^J, a_{21}^J under σ_{el} and unitarity; $\sqrt{s} = 44.7$ GeV.	73
5.5	a_{11}^J, a_{21}^J under σ_{el} and unitarity; $\sqrt{s} = 52.8$ GeV.	73
5.6	a_{11}^J, a_{21}^J under σ_{el} and unitarity; $\sqrt{s} = 62.5$ GeV.	73
5.7	a_{11}^J, a_{21}^J under σ_{el} and unitarity; $\sqrt{s} = 19.5$ GeV, $t = -0.01$ (GeV/c) ²	74
5.8	a_{11}^J, a_{21}^J under σ_{el} and unitarity; $\sqrt{s} = 23.5$ GeV.	74
5.9	a_{11}^J, a_{21}^J under σ_{el} and unitarity; $\sqrt{s} = 30.7$ GeV.	74
5.10	a_{11}^J, a_{21}^J under σ_{el} and unitarity; $\sqrt{s} = 44.7$ GeV.	75
5.11	a_{11}^J, a_{21}^J under σ_{el} and unitarity; $\sqrt{s} = 52.8$ GeV.	75
5.12	a_{11}^J, a_{21}^J under σ_{el} and unitarity; $\sqrt{s} = 62.5$ GeV.	75

6.1	Behaviour of the polynomial $f_1(J)$	90
6.2	a_k^J ($k = 0, 1, 11, 22$) and a_{21}^J optimized under σ_{el} , $\text{Im } \phi_+$ and unitarity in the interior unitarity class; $\sqrt{s} = 52.8$ GeV, $t = -0.001$ (GeV/c) ²	91
6.3	a_k^J ($k = 0, 1, 11, 22$) and a_{21}^J optimized under σ_{el} , $\text{Im } \phi_+$ and unitarity in the interior unitarity class; $\sqrt{s} = 52.8$ GeV, $t = -0.01$ (GeV/c) ²	91
6.4	a_{11}^J and a_{21}^J optimized under σ_{el} , $\text{Im } \phi_+$ and unitarity constraints in the $I \cup B$ unitarity class; $\sqrt{s} = 52.8$ GeV, $t = -0.001$ (GeV/c) ²	106
6.5	a_{11}^J and a_{21}^J optimized under σ_{el} , $\text{Im } \phi_+$ and unitarity constraints in the $I \cup B$ unitarity class; $\sqrt{s} = 52.8$ GeV, $t = -0.01$ (GeV/c) ²	106
7.1	Behaviour of $h(t)$ over the CNI region.	120
7.2	a_k^J ($k = 0, 1, 11, 22$) and a_{21}^J optimized under σ_{el} , $\text{Im } \phi_+$, σ_{tot} and unitarity in the interior class; $\sqrt{s} = 52.8$ GeV, $t = -0.001$ (GeV/c) ²	123
7.3	a_k^J ($k = 0, 1, 11, 22$) and a_{21}^J optimized under σ_{el} , $\text{Im } \phi_+$, σ_{tot} and unitarity in the interior class; $\sqrt{s} = 52.8$ GeV, $t = -0.01$ (GeV/c) ²	123
7.4	The behaviour of the polynomial $f_2(J)$	126

7.5	a_{11}^J and a_{21}^J optimized under σ_{el} , $\text{Im}\phi_+$, σ_{tot} and unitarity in the boundary unitarity class with $\Sigma_{\text{el}}^B = 0.1\Sigma_{\text{el}}$; $\sqrt{s} =$ 52.8 GeV, $t = -0.001 \text{ (GeV/c)}^2$	129
7.6	a_{11}^J and a_{21}^J optimized under σ_{el} , $\text{Im}\phi_+$, σ_{tot} and unitarity in the boundary unitarity class with $\Sigma_{\text{el}}^B = 0.01\Sigma_{\text{el}}$; $\sqrt{s} =$ 52.8 GeV, $t = -0.001 \text{ (GeV/c)}^2$	129
7.7	a_{11}^J and a_{21}^J optimized under σ_{el} , $\text{Im}\phi_+$, σ_{tot} and unitarity in the boundary unitarity class with $\Sigma_{\text{el}}^B = 0.001\Sigma_{\text{el}}$; $\sqrt{s} =$ 52.8 GeV, $t = -0.001 \text{ (GeV/c)}^2$	130

List of Tables

2.1	The Regge meson exchanges with the corresponding s_e and l_e .	22
2.2	Models for the helicity-flip amplitude	24
2.3	Analyzing power data from Fermilab E704.	25
5.1	Interior and Boundary unitarity class contributions associated with optimization under the elastic cross section and unitarity.	62
5.2	σ_{el} and Σ_{el} as a function of center-of-mass energy	66
5.3	σ_{tot} , g and A_0 as a function of center-of-mass energy.	67
5.4	Results including upper bound on $ \text{Im } r_5 $ optimized under σ_{el} and unitarity constraints at $t = -0.001 \text{ (GeV/c)}^2$ as a function of \sqrt{s}	69
5.5	Results including upper bound on $ \text{Im } r_5 $ optimized under σ_{el} and unitarity constraints at $t = -0.01 \text{ (GeV/c)}^2$ as a function of \sqrt{s}	70

6.1	The equality multipliers r and β under σ_{el} , $\text{Im } \phi_+$ and unitarity constraints.	86
6.2	$ \text{Im } r_5 $ as a function of center-of-mass energy and momentum transfer optimized under σ_{el} , $\text{Im } \phi_+$ and unitarity constraints. .	88
6.3	Contributions from the $I \cup B$ unitarity classes with σ_{el} , $\text{Im } \phi_+$ and unitarity constraints; $\sqrt{s} = 52.8 \text{ GeV}$, $t = -0.001 (\text{GeV}/c)^2$.	100
6.4	Contributions from $I \subset I \cup B$ with σ_{el} , $\text{Im } \phi_+$ and unitarity constraints; $t = -0.001 (\text{GeV}/c)^2$	101
6.5	Contributions from $B \subset I \cup B$ with σ_{el} , $\text{Im } \phi_+$ and unitarity constraints; $t = -0.001 (\text{GeV}/c)^2$	102
6.6	Contributions from $I \subset I \cup B$ with σ_{el} , $\text{Im } \phi_+$ and unitarity constraints; $t = -0.01 (\text{GeV}/c)^2$	104
6.7	Contributions from $B \subset I \cup B$ with σ_{el} , $\text{Im } \phi_+$ and unitarity constraints; $t = -0.01 (\text{GeV}/c)^2$	105
7.1	$ \text{Im } r_5 $ optimized under σ_{el} , $\text{Im } \phi_+$, σ_{tot} and unitarity inside the interior region at $t = -0.001 (\text{GeV}/c)^2$	121
7.2	$ \text{Im } r_5 $ optimized under σ_{el} , $\text{Im } \phi_+$, σ_{tot} and unitarity inside the interior region at $t = -0.01 (\text{GeV}/c)^2$	122
7.3	$ \text{Im } r_5 _{\text{max}}$, with an approximation for g , over the CNI region.	125
7.4	Summary of the bounds on $ \text{Im } r_5 $; at $\sqrt{s} = 52.8 \text{ GeV}$ and $t = -0.001 (\text{GeV}/c)^2$	136

General Introduction

The expression

$$\frac{1}{2} = \frac{1}{2} \Delta\Sigma + \Delta G + L_q + L_G \quad (0.1)$$

indicates the different contributions which sum to give the proton its spin of one half. The various contributions arise from the component quarks ($\Delta\Sigma$), the spin of the gluonic fields (ΔG) and the orbital angular momentum of the quarks (L_q) and of the gluons (L_G). In the deep inelastic scattering regime only the light flavour quarks (*up*, *down* and *strange*) contribute to the spin of the proton. The net helicity of the quark flavour q in the direction of the proton spin, in the quark parton-model [1, 2, 3], is given by

$$\Delta q = \int_0^1 \Delta q(x) dx \equiv \int_0^1 \{q^\uparrow(x) - q^\downarrow(x) + \bar{q}^\uparrow(x) - \bar{q}^\downarrow(x)\} dx \quad (0.2)$$

where x is the Bjorken scaling variable and $q(x)$ is the difference between the number density of quarks with spin parallel to the nucleon spin ($q^\uparrow(x) + \bar{q}^\uparrow(x)$) and those with spin anti-parallel ($q^\downarrow(x) + \bar{q}^\downarrow(x)$).

Probing the proton: Measurements of the cross-section differences, with particular spin configurations of incoming leptons and target nucleons, provide information on the polarized spin structure functions. For a longitudinally polarized target, in $l+p \rightarrow l'+X$, the longitudinal spin-spin asymmetry

$$A_{\parallel} \equiv \left(d\sigma^{\overrightarrow{\leftarrow}} - d\sigma^{\overrightarrow{\rightarrow}} \right) / \left(d\sigma^{\overleftarrow{\leftarrow}} + d\sigma^{\overleftarrow{\rightarrow}} \right) \quad (0.3)$$

is the quantity which is measured in polarized lepton-nucleon deep inelastic scattering experiments. Initial leptons can be longitudinally polarized along (\rightarrow) or opposite (\leftarrow) the direction of motion and nucleons are longitudinally polarized along (\Rightarrow) or opposite (\Leftarrow) the initial lepton direction of motion. In the Bjorken limit, or deep inelastic region,

$$-q^2 = Q^2 \rightarrow \infty, \quad \nu = E - E' \rightarrow \infty, \quad x = \frac{Q^2}{2M\nu} \quad \text{fixed} \quad (0.4)$$

where Q^2 is the four-momentum transfer squared, E and E' are the energies of the incoming and outgoing leptons, in the Lab frame, respectively and M is the nucleon mass. In the Bjorken limit the unpolarized structure functions, $W_1(x, Q^2)$ and $W_2(x, Q^2)$, are known to scale approximately [1, 2]:

$$\lim_{Bj} M W_1(x, Q^2) = F_1(x), \quad \lim_{Bj} \nu W_2(x, Q^2) = F_2(x). \quad (0.5)$$

Similarly the polarized structure functions, $G_1(x, Q^2)$ and $G_2(x, Q^2)$, are expected to scale approximately in the Bjorken limit [1, 2]:

$$\lim_{Bj} M^2 \nu G_1(x, Q^2) = g_1(x), \quad \lim_{Bj} M \nu^2 G_2(x, Q^2) = g_2(x). \quad (0.6)$$

The longitudinal spin-spin asymmetry can be expressed in terms of the unpolarized and polarized structure functions:

$$A_{\parallel} = \frac{Q^2 \{(E + E' \cos \theta) MG_1 - Q^2 G_2\}}{2EE' \{2W_1 \sin^2 \theta/2 + W_2 \cos^2 \theta/2\}} \quad (0.7)$$

where θ is lepton scattering angle. The asymmetry A_{\parallel} expressed in terms of the virtual Compton scattering asymmetries $A_{1,2}$ is

$$A_{\parallel} = D(A_1 + \eta A_2) \quad (0.8)$$

where the coefficients D and η are known. Analysis of A_{\parallel} leads to the expression [1, 2]

$$A_{\parallel} \approx DA_1 \quad (0.9)$$

and

$$g_1(x) \approx \frac{A_{\parallel}}{D} \frac{F_2(x)}{2x \{1 + R(x)\}} \quad (0.10)$$

where R is the ratio of the longitudinal to transverse cross-section,

$$R = \frac{W_2}{W_1} \left(1 + \frac{\nu^2}{Q^2} \right) - 1. \quad (0.11)$$

In the quark-parton model the polarized structure function $g_1(x)$ can be interpreted as the difference between the number density of quarks with spin parallel to the nucleon spin ($q^\uparrow(x) + \bar{q}^\uparrow(x)$) and those with spin anti-parallel ($q^\downarrow(x) + \bar{q}^\downarrow(x)$) averaged over the quark flavour charges e_q [1, 2, 3]:

$$g_1(x) = \frac{1}{2} \sum_q e_q^2 \Delta q(x) = \frac{1}{2} \left\{ \frac{4}{9} \Delta u(x) + \frac{1}{9} \Delta d(x) + \frac{1}{9} \Delta s(x) \right\} \quad (0.12)$$

where $\Delta q(x) = q^\uparrow(x) - q^\downarrow(x) + \bar{q}^\uparrow(x) - \bar{q}^\downarrow(x)$. Measurements of the longitudinal and transverse spin-spin asymmetries, in polarized lepton-nucleon deep inelastic scattering, can lead to information on the polarized structure functions which can be utilized to calculate the contribution from the quarks to the spin of the proton.

Sum rules: The Bjorken sum rule [4] relates the integral over the proton and neutron spin structure functions;

$$\int_0^1 g_1^p(x, Q^2) dx - \int_0^1 g_1^n(x, Q^2) dx = \frac{a_3}{6} \left\{ 1 - \mathcal{O}\left(\frac{\alpha_s}{\pi}\right) \right\} \quad (0.13)$$

where $a_3 = \Delta u - \Delta d$ is a nucleon axial coupling constant sometimes expressed as the ratio of the axial and vector coupling constant (G_A/G_V) of weak decays. The factor $(1 - \mathcal{O}(\alpha_s/\pi))$ arises from QCD radiative corrections. This sum rule reflects the difference in polarization asymmetry in deep inelastic scattering from proton and neutrons. The polarized structure function $g_1(x)$ is extracted for a proton and a neutron separately using different polarized targets. With measurements of $g_1(x)$ one can test the Bjorken sum rule which is independent of nucleon spin structure details and is a fundamental sum rule.

The Ellis-Jaffe [5] sum rules have been derived using the same assumptions as for the Bjorken sum rule—a quark structure for the hadronic, electromag-

netic and weak currents—and by assuming the SU(3) symmetry in decays of the octet baryons with a zero net polarization of the strange quark sea of the nucleon;

$$\Gamma_1^p(Q^2) \equiv \int_0^1 g_1^p(x) dx = \frac{1}{12} a_3 + \frac{5}{36} a_8 \quad (0.14)$$

$$\Gamma_1^n(Q^2) \equiv \int_0^1 g_1^n(x) dx = -\frac{1}{12} a_3 + \frac{5}{36} a_8 \quad (0.15)$$

where the nucleon axial coupling constants a_3 and a_8 are related to the SU(3) couplings F and D by

$$a_3 = F + D, \quad a_8 = 3F - D. \quad (0.16)$$

The SU(3) couplings F and D describe the β - decays of the baryon octet members. The Ellis-Jaffe sum rule predicts $\Gamma_1^p(Q^2) = 0.171 \pm 0.006$ at $Q^2 = 10 \text{ GeV}^2$ and a contribution of approximately 60% from the quarks to the spin of the proton.

EMC data: In 1988 the European Muon Collaboration (EMC) at CERN measured $\Gamma_1^p(Q^2)$ at $Q^2 = 10 \text{ GeV}^2$ [6]. The result $\Gamma_1^p(Q^2) = 0.123 \pm 0.013 \pm 0.019$ was unexpectedly lower than the value predicted by the Ellis-Jaffe sum rule. The contribution from the quarks $\Delta\Sigma = 14 \pm 18\%$ was also found to be surprisingly low with $77 \pm 6\%$ coming from the *up* quarks, $-49 \pm 6\%$ from the *down* quarks and a non-zero contribution of $-15 \pm 6\%$ from the *strange* quarks. This startling result, suggesting a *proton spin crisis* in the parton

model, created much theoretical interest [7] which lead to the discovery of the anomalous gluon contribution. In the modified picture $\Delta\Sigma$ is replaced by the linear combination $\Delta\Sigma - (3\alpha_s/2\pi) \Delta G$ which can be made small by a cancellation between quark and gluon contributions. A new experimental programme to investigate the phenomenon further also commenced. More recent data from the Spin Muon Collaboration (SMC) at CERN [8] suggests $\Delta\Sigma = 31 \pm 4\%$ with the *up* quarks providing about $83.2 \pm 1.5\%$, the *down* quarks about $-42.5 \pm 1.5\%$ and the large negative fraction of $-9.7 \pm 1.8\%$ coming from the *strange* quarks. The questions “Where does the spin of the proton come from? The gluons (ΔG)? Could it be in the orbital angular momentum of the quarks (L_q) and the gluons (L_G)?” remain unanswered [9].

Gluon Contribution: To probe the gluon polarization $\Delta G(Q^2)$, where

$$\Delta G(Q^2) = \int_0^1 \Delta G(x, Q^2) dx, \quad (0.17)$$

and thus measure the gluon contribution to the proton’s spin, a high energy polarized proton beam scattering at high momentum transfers is required. Studies of the gluon polarization suggest $\Delta G(Q^2) \approx 0 - 2$ at $Q^2 \sim 1 \text{ GeV}^2$ and $\Delta G(Q^2)$ is expected to grow with Q^2 . At the Relativistic Heavy Ion Collider (RHIC), Brookhaven, it is planned to use the polarized quarks of one beam of polarized protons to probe the spin structure of the protons in the second beam with high energies ($\sqrt{s} = 50 - 500 \text{ GeV}$) and momentum

transfers ($p_T \geq 10 \text{ GeV}/c$).

The longitudinal spin-spin asymmetry in the direction of the beam, one of the observables planned to be measured at RHIC, is given by

$$A_{LL} = \frac{1}{P_a P_b} \left[\frac{(N_{++} - N_{+-}) + (N_{--} - N_{-+})}{(N_{++} + N_{+-}) + (N_{--} + N_{-+})} \right], \quad (0.18)$$

where N_{++} , N_{+-} , N_{-+} and N_{--} are the number of specific physical events observed with each combination of longitudinal beam polarization directions and P_a , P_b are the polarizations of the beams. The double spin asymmetry A_{LL} will play a vital rôle in finding the gluonic contribution to the proton's spin [10]. To probe the gluon polarization, the process, $\vec{p} + \vec{p} \rightarrow \gamma + X$, or the QCD Compton subprocess, $g + q \rightarrow q + \gamma$, offers good sensitivity to the gluon polarization. In this process the longitudinal spin-spin asymmetry is directly related to the gluon polarization. As well as QCD Compton scattering, jet production probes the gluon polarization with good sensitivity. The asymmetry A_{LL} for the process, $\vec{p} + \vec{p} \rightarrow \text{jets}$, or the elastic gluon-gluon subprocess, $g + g \rightarrow g + g$, is proportional to the square of the gluon polarization and the jet rate production is high.

The RHIC collider, filled with polarized protons ($P \approx 70\%$) and equipped with Siberian Snakes and Spin Rotators [11], is expected to provide a luminosity of $2 \times 10^{32} \text{ cm}^{-2} \text{ s}^{-1}$. By late 2000 the first spin physics run is expected to start. RHIC has an approved program of spin physics for two major exper-

iments, STAR [12] and PHENIX [13], and one elastic scattering experiment (PP2PP) [14]. In the coming years data from the RHIC accelerator will help unravel the *Proton Spin Puzzle* and give us a deeper understanding of the rôle of spin in high energy physics.

To measure the gluon contribution to the proton spin, with sufficient accuracy, a polarized proton beam is required and the beam polarization error should be less than five percent, $\Delta P/P < 5\%$ [15]. There are many possible choices of polarimeters but there are uncertainties on the accuracy of the measured beam polarization [16, 17, 18]. One such polarimeter uses the analyzing power in elastic proton collisions at small scattering angles, where for a known analyzing power, the polarization of the proton beam is calculated by measuring the single spin transverse asymmetry. This small angle scattering region is the Coulomb Nuclear Interference (CNI) region. Due to the size of the scattering angle there is limited data for the analyzing power in this kinematical region. The value of the analyzing power, in the CNI region, is sensitive to the modified imaginary helicity single-flip amplitude $\text{Im } r_5$. To determine the behaviour of the CNI analyzing power the amplitude $\text{Im } r_5$ must be accurately known or alternatively an upper bound on $|\text{Im } r_5|$ can be used to limit the size of the analyzing power. An upper bound of $(\mu_p - 1)/2 \times 5\% \approx 4.48\%$ on $|\text{Im } r_5|$ is sufficient for the proton analyzing

power to be used as a polarimeter with $\Delta P/P < 5\%$ where $\mu_p = 2.793$ is the proton's magnetic moment.

Outline of the Thesis

Polarimetry is introduced in Chapter 1 with a description of why polarized beams are necessary in experiments measuring the gluonic contribution to the proton's spin followed by a section on proton polarimetry in the Coulomb Nuclear Interference (CNI) region, where the helicity amplitudes are first introduced and an expression for the analyzing power is derived. To end the Chapter a brief summary of proton-carbon polarimetry is given which is another possible candidate for polarimetry at RHIC. In the thesis the modified helicity single-flip amplitude $\text{Im } r_5$, for elastic proton collisions in the CNI region, is bounded using the Lagrange multiplier technique of optimization. In general the method of Lagrange multipliers can be used to optimize a function in a system with constraints. The constraints are related to physical quantities or functions in the system, which are known. A simple example is the problem of minimizing the surface area of a cylinder given the volume of the cylinder. The function to be optimized is the surface area, volume is an equality constraint and the minimum surface area is found by optimizing the system. Similarly the Froissart bound [19], an asymptotic bound on the total

cross section, can be derived by including unitarity and the elastic cross section as constraints with the total cross section as the objective function. In the same way a bound on $\text{Im } r_5$, the imaginary helicity single-flip amplitude modified by a kinematical factor, is derived where the system constraints are the elastic cross section, the total cross section and the imaginary spin average non-flip amplitude, all of which are experimentally known. The Lagrange multiplier method also allows inequality constraints to be used when optimizing the system. Unitarity, appearing as an inequality, is input as a constraint when optimizing $\text{Im } r_5$. Many models indicate a value of ≈ 0.1 for $\text{Im } r_5$ [20], where the value of 0.1 is above the threshold value of $(\mu_p - 1)/2 \times 5\%$ for polarimetry with $\Delta P/P < 5\%$.

In the second Chapter a Regge model calculation is used to obtain a value for the amplitude $\text{Im } r_5$ at zero momentum transfer and a synopsis of models for the helicity-flip component is given. Experimental data from Fermilab E704 is presented where a 200 GeV polarized proton beam was used to measure the analyzing power for proton-proton elastic collisions in the CNI region. Other bounds on the amplitude $\text{Im } r_5$ are discussed.

The Lagrange method of optimization is introduced in Chapter 3 with a review of the formalism of Einhorn and Blankenbecler [21]–[25]. Other bounds in particle scattering are mentioned, particularly the work of Martin and collaborators, who have greatly contributed to this field since the pioneering

work of Froissart. Ending Chapter 3 is an example of the Lagrange method of optimization where the MacDowell-Martin bound for spinless particles is derived.

In the fourth Chapter the observables, to be used as constraints when optimizing $\text{Im } r_5$, are expressed in terms of partial wave amplitudes. The observables are the total cross section, the imaginary spin average helicity non-flip amplitude, the elastic cross section and unitarity. The helicity representation of Jacob and Wick [26] is used to express the five helicity amplitudes in elastic proton collisions as partial wave expansions. The observables expressed in terms of helicity amplitudes are written as partial wave series and the imaginary helicity single-flip amplitude is expanded as Taylor series in the CNI region.

The amplitude $|\text{Im } r_5|$ is first optimized in Chapter 5 with unitarity and the elastic cross section expressed as inequality and equality constraints, respectively. The bound, not a ‘strict’ bound, limits the value of $|\text{Im } r_5|$ in the CNI region. The unitarity constraints divide the solutions into different classes which allows the optimal solution to be selected. The system of constraints in this Chapter, and subsequent Chapters, is numerically solved using a combination of analytic calculations and `mathematica 3.0`.

A new constraint is added to the system in Chapter 6, the new constraint being the imaginary spin average helicity non-flip amplitude at some fixed

momentum transfer in the Coulomb Nuclear Interference region. As expected the bound on $|\text{Im } r_5|$ is improved but the bound is far from the desired value of $(\mu_p - 1)/2 \times 5\%$. The unitarity constraints play a more important rôle in this system of constraints, the different solutions generated by the unitarity constraints are compared and the resultant upper bounds on $|\text{Im } r_5|$ are discussed.

In the seventh and final Chapter, the full set of constraints are used to optimize $|\text{Im } r_5|$ in the CNI region. The extra constraint is the total cross section. The derived bound has a value of ≈ 0.89 at $\sqrt{s} = 50$ GeV. This bound on $|\text{Im } r_5|$, with a value less than $(\mu_p - 1)/2$, ensures that the analyzing power in the CNI region is positive; $\mu_p = 2.793$ is the proton's magnetic moment. The optimal solution again is determined by the unitarity constraints. A summary of all the derived bounds on $|\text{Im } r_5|$ in the CNI region is followed by a brief discussion on the applications of optimization techniques in other physical and non-physical problems.

Chapter 1

Polarization Measurement

Details about the gluon polarization can be found by measuring the double spin longitudinal asymmetry, A_{LL} , in a particular process, ultimately leading to a value of the contribution from the gluons to the proton's spin [10]. The double spin longitudinal asymmetry is written as

$$A_{LL} = \frac{1}{P_a P_b} \left[\frac{(N_{++} - N_{+-}) + (N_{--} - N_{-+})}{(N_{++} + N_{+-}) + (N_{-+} + N_{--})} \right], \quad (1.1)$$

where N_{++} , N_{+-} , N_{-+} and N_{--} are the number of specific physical events observed with each combination of beam polarization directions and P_a , P_b are the polarizations of the beams. The asymmetry, to be measured, is dependent on the square of the beam polarization error and consequently it is essential to have an accurate knowledge of the beam polarization. To probe the gluon polarization with sufficient accuracy, the maximum beam

polarization error $\Delta P/P$ cannot be larger than 5% [15]. One method of polarimetry uses the analyzing power in pp elastic collisions at small angles.

1 Proton-Proton Polarimetry

It is believed that polarization in elastic scattering vanishes at high energy where the amplitudes are eventually dominated by diffraction energy. Recent studies of hadronic scattering indicate that this may not be the case [20]. For high energy pp elastic scattering in the Coulomb Nuclear Interference (CNI) region ($t \approx -0.0012 (\text{GeV}/c)^2$), the analyzing power \mathcal{A}_{pp} possesses a small but considerable value [27, 28].

1.1 Analyzing Power in the CNI Region

The analyzing power \mathcal{A}_{pp} for a proton and the transverse single spin asymmetry A_N are related through the expression

$$\mathcal{A}_{pp} P = A_N \tag{1.2}$$

where P is the beam polarization and the target is unpolarized; for 100% beam polarization the asymmetry and analyzing power are equal ¹. The beam polarization can be measured by counting the scatters with the beam

¹In some literature the analyzing power \mathcal{A}_{pp} is referred to as the transverse single spin asymmetry A_N .

polarized up (N^\uparrow) and then down (N^\downarrow) in a polarimeter with a known analyzing power \mathcal{A}_{pp} :

$$P = \frac{1}{\mathcal{A}_{pp}} \left[\frac{N^\uparrow - N^\downarrow}{N^\uparrow + N^\downarrow} \right] = \frac{1}{\mathcal{A}_{pp}} A_N . \quad (1.3)$$

The analyzing power \mathcal{A}_{pp} expressed in terms of the s -channel helicity amplitudes is [29]

$$\mathcal{A}_{pp} \frac{d\sigma}{dt} = -\text{Im} [\phi_5^* (\phi_1 + \phi_2 + \phi_3 - \phi_4)] \quad (1.4)$$

where $d\sigma/dt$ is the differential cross section-

$$\frac{d\sigma}{dt} = \frac{\pi}{2k^2 s} \left\{ |\phi_1(s, t)|^2 + |\phi_2(s, t)|^2 + |\phi_3(s, t)|^2 + |\phi_4(s, t)|^2 + 4|\phi_5(s, t)|^2 \right\} , \quad (1.5)$$

k is the centre-of-mass momentum and ϕ_1, \dots, ϕ_5 are the five independent helicity amplitudes used to describe elastic pp collisions [26, 30]:

$$\phi_1(s, t) = \langle ++ | \phi | ++ \rangle , \quad (1.6)$$

$$\phi_2(s, t) = \langle ++ | \phi | -- \rangle , \quad (1.7)$$

$$\phi_3(s, t) = \langle +- | \phi | +- \rangle , \quad (1.8)$$

$$\phi_4(s, t) = \langle +- | \phi | -+ \rangle , \quad (1.9)$$

$$\phi_5(s, t) = \langle ++ | \phi | +- \rangle . \quad (1.10)$$

The helicity amplitudes can be written as a sum of hadronic and electromagnetic amplitudes;

$$\phi_i = \phi_i^h + e^{i\delta} \phi_i^{em} \quad (i = 1, \dots, 5) . \quad (1.11)$$

The Coulomb phase shift δ is given by [31]

$$\delta = -\alpha \ln \left| \frac{bt}{2} + \frac{4t}{\Lambda^2} \right| - 0.577\alpha \quad (1.12)$$

where α is the fine structure constant, b is the nuclear slope parameter and $\Lambda^2 = 0.71(\text{GeV}/c)^2$ the dipole Sachs form factor parameter. Neglecting the amplitudes ϕ_2 , ϕ_4 and $\phi_1 - \phi_3$, at high energies in the CNI region ², we can write the analyzing power as

$$\mathcal{A}_{pp} \frac{d\sigma}{dt} = -\text{Im} [\phi_5^* (\phi_1 + \phi_3)] = -2 \text{Im} [\phi_5^* \phi_+] \quad (1.13)$$

where ϕ_+ is the spin average non-flip amplitude, $(\phi_1 + \phi_3)/2$. Expressing the helicity amplitudes as $\phi_i = \phi_i^h + e^{i\delta} \phi_i^{em}$ ($i = 1, \dots, 5$), and neglecting the Coulomb phase, the analyzing power in the CNI region can be rewritten as

$$\begin{aligned} \mathcal{A}_{pp} \frac{d\sigma}{dt} &= -2 \text{Im} \left[(\phi_5^h + \phi_5^{em})^* (\phi_+^h + \phi_+^{em}) \right] \\ &\propto \left(\text{Im} \phi_+^h \right) \phi_5^{em} - \phi_+^{em} \left(\text{Im} \phi_5^h \right). \end{aligned} \quad (1.14)$$

The electromagnetic helicity amplitudes are known, the one-photon-exchange amplitudes are given in [32], and the optical theorem [29, 33] gives $\text{Im} \phi_+^h \propto \sigma_{\text{tot}}$ but very little is known about the hadronic single helicity-flip amplitude

²The double helicity-flip amplitude ϕ_4 at small values of $-t$ can be ignored because of a kinematical factor $(-t)$. Measurements of the transverse-spin and longitudinal-spin total cross sections suggest, at high energies, that the contribution from ϕ_2 and $\phi_1 - \phi_3$ to the CNI proton analyzing power is negligible [20].

$\text{Im } \phi_5^h$, experimentally or theoretically, and thus the use of the pp analyzing power as a polarimeter depends on the contribution from the hadronic single helicity-flip amplitude.

Looking in more detail we can write the analyzing power in the CNI region as [33]

$$\mathcal{A}_{pp} = \frac{\sqrt{-t}}{m} \frac{(\kappa_p - 2 \text{Im } r_5) \frac{t_c}{t} + 2 \text{Re } r_5 - 2\rho \text{Im } r_5}{\left(\frac{t_c}{t}\right)^2 - 2(\rho + \delta) \frac{t_c}{t} + 1 + \rho^2} \quad (1.15)$$

with ϕ_2 , ϕ_4 , and $\phi_1 - \phi_3$ not contributing where $\rho = \text{Re } \phi_+ / \text{Im } \phi_+$, $\kappa_p + 1 = \mu_p = 2.793$ is the proton's magnetic moment, m is the proton mass and the ratio r_5 includes a scaling by the imaginary part of the spin-average hadronic amplitude and by a kinematical factor of $m/\sqrt{-t}$:

$$r_5(s, t) = \frac{m}{\sqrt{-t}} \frac{\phi_5(s, t)}{\text{Im } \phi_+(s, t)}. \quad (1.16)$$

In the CNI region when $t \approx t_c$, where

$$t_c = -8\pi\alpha/\sigma_{\text{tot}} \approx -0.0012 \text{ (GeV}/c)^2, \quad (1.17)$$

interference between the non-flip amplitude and the single-flip amplitude is most prominent. This is reflected in the $(\kappa_p - 2 \text{Im } r_5) \frac{t_c}{t}$ term. When $|\rho|$ is small, as is the case at $\sqrt{s} \approx 20 \text{ GeV}$ [33], the main contribution to \mathcal{A}_{pp} , in the CNI region ($t \leq t_c$), comes from $\text{Im } r_5$ and at larger momentum transfers outside the CNI region ($t > t_c$) the real part of r_5 is dominant. The maximum

value of \mathcal{A}_{pp} in the CNI region, 4.7% with $\text{Im } r_5 = 0$, is modified by about 5.5% when $\text{Im } r_5 = \pm 0.05$. The position of the maximum of \mathcal{A}_{pp} is

$$t_{max} = \left[\sqrt{3} + \frac{8}{\kappa} (\rho \text{Im } r_5 - \text{Re } r_5) - (\rho + \delta) \right] t_c \approx \sqrt{3} t_c \quad (1.18)$$

where the Coulomb phase δ is small and can be neglected for pp scattering in the CNI region [20]. A large bound of $|\text{Im } r_5|$ results in an uncertainty on the maximum value of \mathcal{A}_{pp} and to successfully use the pp analyzing power as a polarimeter with $\Delta P/P \leq 5\%$ a maximum upper bound of $(\mu_p - 1)/2 \times 5\% \approx 4.48\%$ on $|\text{Im } r_5|$ is paramount.

2 Proton-Carbon Polarimetry

Similar to proton-proton elastic collisions, the analyzing power \mathcal{A}_{pC} for elastic proton-carbon scattering in the CNI region has a non-zero value which can be used to measure the polarization of a proton beam [28, 34]. The analyzing power expressed in terms of the s -channel helicity amplitudes is [35]

$$\mathcal{A}_{pC} \frac{d\sigma}{dt} = \text{Im} (f_{++}^* f_{+-}) \quad (1.19)$$

where f_{++} and f_{+-} are the helicity non-flip and flip amplitudes, respectively. The modified helicity-flip amplitude, in pC elastic scattering is

$$r = \frac{m}{\sqrt{-t}} \frac{f_{+-}}{\text{Im } f_{++}}. \quad (1.20)$$

Decomposing the helicity amplitudes into hadronic and electromagnetic components enables the analyzing power to be written in terms the flip and non-flip amplitudes [35]. In the case of pC scattering, interference between the flip and non-flip amplitudes is most prominent at $t = t_c$ where

$$t_c = \frac{-8\pi Z\alpha}{\sigma_{\text{tot}}} \approx -0.0013(\text{GeV}/c)^2 \quad (1.21)$$

with $Z = 6$ for a carbon target [28, 35]. Although the spin 0-spin 1/2 system is in many ways simpler than the spin 1/2-spin 1/2 system, the maximum value of the pC analyzing power in the CNI region, like the pp analyzing power, is sensitive to the imaginary modified helicity-flip amplitude $\text{Im } r$ and to use the pC analyzing power as a polarimeter an accurate knowledge of $|\text{Im } r|$ is necessary. Due to the simplicity of the detector system [34] this relative polarimeter, with a theoretically predicted accuracy of 10 – 15%, is one of the candidates for a polarimeter at RHIC.

One challenge is to calculate the size of the imaginary modified helicity-flip amplitude $|\text{Im } r_5|$ in the case of pp collisions or $|\text{Im } r|$ in the case of pC collisions. The Lagrange multiplier method, to be introduced in Chapter 3, is used to optimize $|\text{Im } r_5|$ resulting in an upper bound which limits the value of the analyzing power in the CNI region. All present knowledge of the amplitude $|\text{Im } r_5|$, in the low momentum transfer region, is presented in the next Chapter including experimental data from Fermilab, Regge models, QCD models and derived bounds.

Chapter 2

Helicity Single-Flip Amplitude

In order to use the pp analyzing power as a polarimeter an accurate knowledge of the modified helicity single-flip amplitude $\text{Im } r_5$ must be known. For a 5% beam polarization error a maximum upper bound of $(\mu_p - 1)/2 \times 5\% \approx 4.48\%$ on $|\text{Im } r_5|$ is allowed. What is known about the modified single helicity-flip amplitude $\text{Im } r_5$, theoretically or experimentally? In this chapter all present knowledge of $\text{Im } r_5$, theoretical and experimental, is presented. A Regge model is used to calculate the value 0.09 for $\text{Im } r_5$ at zero momentum transfer followed by a summary of Regge and QCD helicity-flip models. Experimental data from Fermilab E704 is presented which indicates a positive pp analyzing power over the CNR region. Lastly a bound on the spin 0-spin 1/2 modified helicity flip amplitude at low momentum transfers is analyzed. A bound on

In r_5 , based on the positivity properties of the coefficients in the partial wave series for the differential cross section, is also discussed.

1 Models based on Regge Theory

In Regge theory [36] the scattering amplitude has a variable asymptotic behaviour and this behaviour can be connected to a family of bound states and resonances of different masses and spins [37]. For pp scattering there are five independent helicity amplitudes [26, 30],

$$\phi_1(s, t) = \langle ++ | \phi | ++ \rangle = \phi_{++}^{++}(s, t) \quad (2.1)$$

$$\phi_2(s, t) = \langle ++ | \phi | -- \rangle = \phi_{--}^{-+}(s, t) \quad (2.2)$$

$$\phi_3(s, t) = \langle +- | \phi | +- \rangle = \phi_{--}^{++}(s, t) \quad (2.3)$$

$$\phi_4(s, t) = \langle +- | \phi | -+ \rangle = \phi_{-+}^{+-}(s, t) \quad (2.4)$$

$$\phi_5(s, t) = \langle ++ | \phi | +- \rangle = \phi_{+-}^{++}(s, t) \quad (2.5)$$

The contribution of a single t -channel meson Regge pole at $\alpha(t)$, to an s -channel helicity amplitude for the process $ab \rightarrow cd$, is given by [38, 39]

$$\phi_{\lambda_d \lambda_b}^{\lambda_c \lambda_a} = \mp \left(\frac{\sqrt{-t}}{2m_p} \right)^{|\lambda_c - \lambda_a|} \left(\frac{\sqrt{-t}}{2m_p} \right)^{|\lambda_d - \lambda_b|} \beta_e^{\lambda_c \lambda_a} \beta_{\lambda_d \lambda_b}^e \times \frac{1}{2} \left[1 + (-1)^{S_e} e^{-i\pi \alpha_e} \right] \Gamma(l_e - \alpha_e) (\alpha'_e)^{1-l_e} (\alpha'_e s)^{\alpha_e} \quad (2.6)$$

where m_p is the proton mass, s_e is the spin of the corresponding meson exchange and l_e is the minimum value achieved by s_e on the exchange degenerate trajectory; Table 2.1 shows the Regge exchanges and the corresponding s_e [39]. The residues β are simply related to the coupling constants. This model provides a crude description of the helicity structure and s, t dependence of most two body processes. For $\phi_+(s, t)$ and $\phi_5(s, t)$ the leading meson exchanges are ρ, ω, a_2 and f [38] with

$$\alpha_\rho(t) = \alpha_\omega(t) = \alpha_{a_2}(t) = \alpha_f(t) = 0.5 + 0.9t \quad (2.7)$$

and the trajectory slope is $\alpha'_e = 0.9$.

Table 2.1: The Regge meson exchanges with the corresponding s_e and l_e .

e	s_e	l_e
ρ, ω	1	1
a_2, f	2	

For the Pomeron amplitude [38, 39],

$$\phi_{\lambda_d \lambda_b}^{\lambda_c \lambda_a} = -\frac{1}{2} x_P \sqrt{\pi} \beta_f^{\lambda_c \lambda_a} \beta_{\lambda_d \lambda_b}^f \left(\frac{-t}{4m_p^2} \right)^{\frac{1}{2}(|\lambda_c - \lambda_a| + |\lambda_d - \lambda_b|)} e^{At} e^{\frac{1}{2} - i\pi \alpha_P} (\alpha'_P s)^{\alpha_P} \quad (2.8)$$

where the coupling is fixed by the assumption of f dominance and for pp scattering, $x_P = 1.0$, $A = 3.1 \text{ GeV}^{-2}$ [38]. The Pomeron trajectory P is

$$\alpha_P = 1.0 + 0.3t \quad (2.9)$$

and the trajectory slope for the Pomeron exchange is $\alpha'_P = 0.3$. The vertex parity relation is [38, 39]

$$\beta_{\lambda_d \lambda_b}^e = (-1)^{s_e} \eta_e \eta_c \eta_d (-1)^{s_d - \lambda_d - s_b + \lambda_b} \beta_{-\lambda_d - \lambda_b}^e \quad (2.10)$$

while upper and lower vertices are related by

$$\beta_e^{\lambda_d \lambda_b} = (-1)^{s_d - \lambda_d + s_b - \lambda_b} \beta_{\lambda_d \lambda_b}^e \quad (2.11)$$

where η_i is the intrinsic parity of particle i . The signs of the trajectory contributions to the imaginary part of the elastic pp scattering amplitudes are $P + f - \rho - \omega + a_2$ [40] and the contribution to $\text{Im } r_5$ is found to come from the Pomeron exchange, having the value 0.09 at zero momentum transfer.

The spin structure of the helicity-flip amplitude has been investigated by many authors. Table 2.2 lists some models and the corresponding size of the helicity-flip component. A review of each model is given in [20, 33].

The sign and magnitude of $\text{Im } r_5$ differs for each of the approaches mentioned in Table 2.2, however the values suggest $|\text{Im } r_5| < 0.1$ at RHIC energies. This value for $|\text{Im } r_5|$ does not satisfy the requirement, $|\text{Im } r_5| < 4.48\%$,

Table 2.2: Models for the helicity-flip amplitude

Model	Helicity-flip component
dual quark-parton [41]	$r_5 = -0.06$
pion exchange [42]	$\text{Im } r_5 = 0.06$
impact picture [43]	$\text{Im } r_5 \approx -0.06$
two-gluon [44]	$\text{Im } r_5 = 0.13$
compact diquark [45]	$\text{Im } r_5 = 0.05 - 0.10$
chiral symmetry breaking [46]	$ \text{Im } r_5 \approx 0.1$

which, in order to use the pp analyzing power as a polarimeter in the CNI region with a maximum beam polarization error of 5%, is necessary.

2 Experimental Data

The analyzing power in the CNI region has been measured with the 200 GeV/ c polarized proton beam facility at Fermilab. For the first time at high energies polarizations effects have been observed in the CNI region. The use of a polarized beam and a recoil sensitive scintillator target have made the detection possible. In previous experiments with unpolarized beams and polarized targets the CNI region was inaccessible. The experimental data shown in Ta-

ble 2.3 [47] suggests that the analyzing power in the CNI region is small and positive, and the data agrees with the theoretical prediction of a purely CNI analyzing power originating from the interference between the helicity single-flip amplitude and the helicity non-flip amplitude. Analysis of the data [33] indicates a positive value of $8 - 30\%$ for $\text{Im } r_5$.

Table 2.3: Analyzing power data from Fermilab E704.

$-t$ range (GeV/c) ²	$\langle -t \rangle$ (GeV/c) ²	\mathcal{A}_{pp} (%)
$1.50 \times 10^{-3} - 4.00 \times 10^{-3}$	2.88×10^{-3}	4.46 ± 3.16
$4.00 \times 10^{-3} - 1.25 \times 10^{-2}$	8.30×10^{-3}	3.11 ± 1.09
$1.25 \times 10^{-2} - 2.25 \times 10^{-2}$	1.75×10^{-2}	2.62 ± 1.01
$2.25 \times 10^{-2} - 3.25 \times 10^{-2}$	2.73×10^{-2}	3.17 ± 1.07
$3.25 \times 10^{-2} - 4.25 \times 10^{-2}$	3.68×10^{-2}	2.17 ± 1.39
$4.25 \times 10^{-2} - 5.00 \times 10^{-2}$	4.75×10^{-2}	0.27 ± 2.77

The PP2PP experiment, approved by RHIC, plans to complete a detailed study of elastic pp scattering using polarized proton beams with center-of-mass energies in the range $50 - 500$ GeV over the CNI region [14].

3 Bound from Positivity Properties

A fundamental consequence of unitarity is that the absorptive unpolarized differential cross section for the elastic scattering of particles of arbitrary spin must obey the representation [48]–[50]

$$\begin{aligned} \frac{d\sigma^A}{d\Omega} &= \sum_{n=0}^{\infty} (2n+1) c_n(s) P_n(\cos\theta), \quad c_n(s) \geq 0 \\ &\propto \sum_i (\text{Im } \phi_i)^2. \end{aligned} \quad (2.12)$$

$P_n(\cos\theta)$ is a Legendre polynomial whose argument is the cosine of the center-of-mass scattering angle and the absorptive differential cross section satisfies

$$\frac{d\sigma^A}{dt}(s, 0) \geq \frac{d\sigma^A}{dt}(s, t < 0) \quad (2.13)$$

which leads to a bound on $\text{Im } r_5$ given by [51]

$$\text{Im } r_5 \leq 2.5. \quad (2.14)$$

This result limits the size of the analyzing power \mathcal{A}_{pp} to $4.7\% \pm 13.1\%$ at small t and with an upper bound of 2.3 the required value of 5% for the beam polarization accuracy cannot be obtained but the bound limits the value the analyzing power can take in the CNI region.

4 Spin 0-Spin 1/2 Bound

A study of bounds on the single helicity-flip amplitude ϕ_5 may provide important information related to the behaviour of the analyzing power \mathcal{A}_{pp}

in the CNI region. The optimization technique of Lagrange multipliers, extended by Einhorn and Blankenbecler [21] to include equality and inequality constraints, is used to derive bounds on the modified single helicity-flip amplitude $\text{Im } \tilde{\phi}_5$, based on unitarity and experimental quantities, where

$$\text{Im } \tilde{\phi}_5(s, t) = \frac{k}{\sqrt{-t}} \text{Im } \phi_5(s, t) \quad (2.15)$$

and

$$\text{Im } r_5 = \frac{m}{k} \frac{\text{Im } \tilde{\phi}_5(s, t)}{\text{Im } \phi_+(s, t)} \Big|_{-t \sim 0}. \quad (2.16)$$

Hodgkinson [52] used σ_{el} and the slope g to drive a bound on the helicity-flip amplitude for spin 0-spin 1/2 collisions;

$$\frac{|\text{Im } f_{+-}(s, t)|}{\text{Im } f_{++}(s, 0)} \leq 3g^{2/3} \sqrt{-t} \left(\frac{\pi \sigma_{\text{el}}}{60\sigma_{\text{tot}}^2} \right)^{1/6} \times \left\{ 1 + \frac{5g^{2/3}}{84} \left(\frac{60\sigma_{\text{tot}}^2}{\pi \sigma_{\text{el}}} \right)^{1/6} t + \mathcal{O}(t^2) \right\} \quad (2.17)$$

with

$$|t| \leq \left(\frac{7.48}{g^{2/3}} \right) \left(\frac{\pi \sigma_{\text{el}}}{60\sigma_{\text{tot}}^2} \right)^{1/3}$$

where f_{++} and f_{+-} are the helicity non-flip and flip amplitudes respectively.

The optimum

$$|\text{Im } r_5| \leq 2.3 \quad (2.18)$$

is obtained if a similar bound for pp collisions is assumed over the energy range $\sqrt{s} = 50 - 500$ GeV. This upper bound on $|\text{Im } r_5|$ is significantly greater than the critical value of 4.48% for polarimetry with $\Delta P/P \leq 5\%$.

In the following chapters the variational formalism of Einhorn and Blankenbecler [21] is introduced. A number of equality and inequality constraints for pp elastic scattering in the CNI region are found, and with the variational method of Einhorn and Blankenbecler an upper bound on $|\text{Im } r_5|$ in the CNI region is derived.

Chapter 3

Optimization with Lagrange

Multipliers

To optimize a function subject to constraints, equality and inequality constraints, the method of Lagrange multipliers can be employed [21]–[25]. The method is used to derive bounds on the helicity single-flip amplitude in elastic pp scattering with unitarity constraints, appearing as inequalities, and various experimental quantities, appearing as equality constraints. Such experimental quantities are the total and elastic cross sections, and the slope of the spin average helicity non-flip amplitude.

The Froissart bound [19] was the first bound on the asymptotic behaviour of the total cross section at high energy ($s \rightarrow \infty$);

$$\sigma_{\text{tot}} < C \log^2 (s/s_0) \quad (3.1)$$

where \sqrt{s} is the center-of-mass energy and s_0 is a constant. Since the result of Froissart many developments of the method of obtaining bounds on scattering amplitudes have been made [53] – [67], ranging from spinless scattering to nucleon-nucleon scattering and scattering of particles of arbitrary spins. In the following Chapters the Lagrange multiplier method of optimization is used to bound the imaginary helicity single-flip amplitude $\text{Im } \phi_5$ in elastic pp collisions. The pp system is a spin 1/2-spin 1/2 system with five independent helicity amplitudes, two non-flip, two double-flip and one single-flip. Compared to the spin 0-spin 0 system or the spin 0-spin 1/2 system, the number of helicity amplitudes is greater and the algebra following optimization can present some challenges. The derivation of the bound is based on unitarity, analyticity in the Lehman-Martin ellipse and on polynomial behaviour, with no dependence on theoretical models.

In this Chapter, before deriving bounds in the pp system, the basic concepts and terminology of the optimization technique is introduced [21] – [25] along with a description of the conditions required to maximize a function and an example of how the Lagrange multiplier method is used to

obtain the MacDowell-Martin bound [68] in spinless scattering.

1 Terminology

Objective function: The function that we want to optimize is called the objective function. This function depends on a set of real variables x_1, x_2, \dots, x_n , denoted by

$$f(x) = f(x_1, x_2, \dots, x_n). \quad (3.2)$$

The objective function is sometimes named the cost or penalty function.

Constraints: We consider equality constraints and inequality constraints.

Equality constraints are written as

$$f_\alpha(x) = 0 \quad \alpha = 1, 2, \dots, p. \quad (3.3)$$

Inequality constraints are written as

$$g_\beta(x) \geq 0, \quad \beta = 1, 2, \dots, q. \quad (3.4)$$

Any point $x = (x_1, x_2, \dots, x_n)$ that satisfies the constraints is called a feasible point and the set of such points is called the feasible set S .

Tangent cone: The set of all (unit length) half-lines h , originating at a point x_0 in S and tangent to a curve in S is called the tangent cone to S at x_0 .

Differentials: Given a function f , we denote its gradient vector at x_0 by $f'(x_0)$. Given any vector v , the linear functional $f'(x_0, v) = (f'(x_0), v)$ is called the first differential of f and is denoted by

$$\delta f = f'(x_0, v) = (f'(x_0), v) = \sum_{i=1}^n \frac{\partial f}{\partial x_i} v_i. \quad (3.5)$$

Similarly, the second differential of f at x_0 is defined by the quadratic form

$$f''(x_0, v) = \sum_{i=1}^n \sum_{j=1}^n \frac{\partial^2 f}{\partial x_i \partial x_j} v_i v_j. \quad (3.6)$$

Regular points of S: Let x_0 be a feasible point and let k be a unit vector satisfying

$$(f'_\alpha(x_0), k) = 0, \quad \forall \alpha. \quad (3.7)$$

If every k satisfying Eqn. (3.7) lies in the tangent cone C at x_0 , then x_0 is a regular point of S .

Normal points of S: If the gradients $f'(x_0)$ are linearly independent, x_0 is a normal point. Every normal point is a regular point.

1.1 Maximization with Equality Constraints

The standard method of Lagrange multipliers determines all local maxima (or minima) that are regular points. It is summarized by the following two theorems:

Theorem 3.1 *Let x_0 be a regular point of S and let x_0 be a local maximum of $f(x)$ on S .*

(i) *Then there exists multipliers λ_α such that the auxiliary function*

$$L = f + \sum_{\alpha=1}^p \lambda_\alpha f_\alpha$$

has a vanishing gradient

$$L'(x_0) = \frac{\partial L}{\partial x_i} = 0 \quad i = 1, 2, \dots, n. \quad (3.8)$$

(ii) *For a maximum*

$$L''(x_0, h) \leq 0 \quad (3.9)$$

for all h in the tangent cone at x_0 .

(iii) *If x_0 is normal, the multipliers λ_α are unique.*

Theorem 3.2 *If Eqn. (3.8) is satisfied and if $L''(x_0, h)$ is strictly negative for all h in the tangent cone at x_0 , then x_0 is a local maximum of $f(x)$.*

In practice the theorems are used as follows: Solve the n gradient equations, $L'(x_0) = 0$, for x_0 as a function of the unknown multipliers λ_α . The solutions $x_0 = x_0(\lambda_\alpha)$ are inserted into the constraint functions $f_\alpha(x_0)$ and the multipliers are chosen to satisfy the constraint conditions $f_\alpha(x_0) = 0$. The solutions are limited to those for which $L''(x_0, h) < 0$ (for a maximum).

1.2 Maximization with Inequality Constraints

The definitions of normal points and regular points extend to inequality constraints if we divide these into interior constraints β in $I(x_0)$, and boundary constraints β in $B(x_0)$, defined by

$$I(x_0) = \{\beta \mid g_\beta(x_0) > 0\} \quad (3.10)$$

$$B(x_0) = \{\beta \mid g_\beta(x_0) = 0\}. \quad (3.11)$$

Consider the maximization of $f(x)$ subject to the constraints

$$f_\alpha(x) = 0, \quad \alpha = 1, 2, \dots, p, \quad (3.12)$$

$$g_\beta(x) \geq 0, \quad \beta = 1, 2, \dots, q. \quad (3.13)$$

For any feasible x_0 , let $I(x_0)$ be the set of indices β for which $g_\beta(x_0) > 0$ and $B(x_0)$ be those β for which $g_\beta(x_0) = 0$. The following two theorems outline the conditions necessary to optimize with inequality constraints.

Theorem 3.3 *Let x_0 be a regular point and a local maximum of f in the feasible set S . Then*

(i) *There exists multipliers λ_α , and $\mu_\beta \geq 0$ such that the auxiliary function*

$$L = f + \sum_{\alpha=1}^p \lambda_\alpha f_\alpha + \sum_{\beta=1}^q \mu_\beta g_\beta$$

has a vanishing gradient

$$L'(x_0) = 0. \quad (3.14)$$

(ii) If $\beta \in I(x_0)$ we may choose $\mu_\beta = 0$; we may ignore any inequality constraint g_β for which $g_\beta(x_0) > 0$.

(iii) Let S_1 be the subset of S for which $g_\beta(x) = 0$ for all $\beta \in B(x_0)$ for which $\mu_\beta > 0$. Then

$$L''(x_0, h) \leq 0 \quad (3.15)$$

for all h in the tangent cone of S_1 at x_0 .

(iv) If x_0 is a normal point, the multipliers are unique.

Theorem 3.4 *If Eqn. (3.14) is satisfied and if*

$$L''(x_0, h) < 0 \quad (3.16)$$

for all h in the tangent cone at x_0 , then x_0 is a local maximum of $f(x)$.

In Theorems 3.3 and 3.4 the inequality constraint g_β , for which the corresponding multiplier μ_β is positive, effectively is an equality constraint.

2 MacDowell-Martin Bound; An Example

MacDowell and Martin found a lower bound on the logarithmic derivative based on unitarity for elastic spinless scattering [68]:

$$g \geq \frac{1}{9} \frac{\sigma_{\text{tot}}^2}{4\pi\sigma_{\text{el}}} - \frac{1}{9k^2} \quad (3.17)$$

where the logarithmic derivative g is given by [69]

$$g = \frac{d}{dt} \log (\operatorname{Im} F(s, t))|_{t=0} . \quad (3.18)$$

Using the method of Lagrange multipliers the MacDowell-Martin bound can be obtained. For equal mass elastic scattering the center-of-mass energy \sqrt{s} and the momentum transfer t are written as

$$\sqrt{s} = \sqrt{4k^2 + 4m^2} \quad (3.19)$$

and

$$t = -2k^2 (1 - \cos \theta) \quad (3.20)$$

where k is the center-of-mass momentum and θ is the center-of-mass scattering angle.

2.1 Observables and Constraints

For identical or equal mass spinless scattering the total and absorptive elastic cross sections have partial wave expansions [69]

$$\sigma_{\text{tot}} = \frac{4\pi}{k^2} \sum_l (2l + 1) a_l \quad (3.21)$$

and

$$\sigma_{\text{el}}^A = \frac{4\pi}{k^2} \sum_l (2l + 1) a_l^2 \quad (3.22)$$

where a_l is the imaginary partial wave amplitude. The logarithmic derivative g has the partial wave expansion [69]

$$\left(\frac{32\pi}{s\sigma_{\text{tot}}}\right) \times \frac{1}{8k^2} \sum_l (2l+1) l(l+1) a_l. \quad (3.23)$$

Our aim is to constrain the logarithmic derivative, therefore g is the objective function. The constraints are the total and absorptive elastic cross section plus the positivity constraint

$$U_l = a_l - a_l^2 \geq 0 \quad (3.24)$$

which is a direct consequence of unitarity [26, 69, 70].

Before optimizing the logarithmic derivative it is useful to rewrite the scattering amplitudes as dimensionless amplitudes. We define the normalized dimensionless total cross section $A_0 = (k^2/4\pi) \sigma_{\text{tot}}$, the normalized absorptive elastic cross section $\Sigma_{el} = (k^2/4\pi) \sigma_{el}^A$, and the normalized dimensionless logarithmic derivative $g_0 = (k^2 s \sigma_{\text{tot}}/4\pi) g$, where, in the high energy limit¹

$$A_0 = \sum_l (2l+1) a_l \approx 2 \sum_l l a_l, \quad (3.25)$$

$$\Sigma_{el} = \sum_l (2l+1) a_l^2 \approx 2 \sum_l l a_l^2 \quad (3.26)$$

and

$$g_0 = \sum_l (2l+1) l(l+1) a_l \approx 2 \sum_l l^3 a_l. \quad (3.27)$$

¹In proton-proton scattering the total and elastic cross sections are normalized by the factor k^2/π .

The equality constraints, A_0 and Σ_{el} , are expressed as

$$\alpha \left[A_0 - 2 \sum_l l a_l \right] \quad \text{and} \quad \beta \left[\Sigma_{el} - 2 \sum_l l a_l^2 \right]$$

respectively, where α and β are equality multipliers. The inequality or unitarity constraint $U_l = a_l - a_l^2 \geq 0$ is expressed as

$$(2l + 1) \lambda_l U_l \approx 2l \lambda_l U_l$$

and by definition the inequality multiplier λ_l must be zero or positive [21]–[25].

2.2 Optimization

The auxiliary function with the logarithmic derivative as the objective function is introduced:

$$L = 2 \sum_l l^3 a_l + \alpha \left[A_0 - 2 \sum_l l a_l \right] + \beta \left[\Sigma_{el} - 2 \sum_l l a_l^2 \right] + 2 \sum_l l \lambda_l (a_l - a_l^2) \quad (3.28)$$

where $\lambda_l \geq 0$. To optimize the system we differentiate the auxiliary function L with respect to the imaginary partial wave amplitude a_l , to first order-

$$\frac{\partial L}{\partial a_l} = 2l^3 - 2\alpha l + 2l\lambda_l - 4l(\beta + \lambda_l) a_l \quad (3.29)$$

and second order-

$$\frac{\partial^2 L}{\partial a_l^2} = -4l(\beta + \lambda_l) . \quad (3.30)$$

For an minimum we require $\partial L/\partial a_l = 0$ and $\partial^2 L/\partial a_l^2 > 0$, this leads to the condition $\beta < -\lambda_l$ with

$$a_l = \frac{1}{2(\beta + \lambda_l)} l^2 - \frac{\alpha}{2(\beta + \lambda_l)} + \frac{\lambda_l}{2(\beta + \lambda_l)}. \quad (3.31)$$

2.3 Unitarity Classes

When optimizing the system it is natural to divide the partial waves into two classes [21] – [25]. For each unitarity inequality there are two classes, I and B :

$$I^U \equiv \{J | U_l > 0, \lambda_l = 0\}, \quad B^U \equiv \{J | U_l = 0, \lambda_l \geq 0\}, \quad (3.32)$$

I is called the interior unitarity class and B is called the boundary unitarity class. The interior unitarity class becomes

$$I^U \equiv \{l | 0 < a_l < 1, \lambda_l = 0\} \quad (3.33)$$

and the boundary unitarity class splits into two subclasses;

$$\longrightarrow B^{U_0} \equiv \{l | a_l = 0, \lambda_l \geq 0\} \quad (3.34)$$

$$B^U \equiv \{l | U_l > 0, \lambda_l \geq 0\}$$

$$\longrightarrow B^{U_1} \equiv \{l | a_0^l = 1, \lambda_l \geq 0\}. \quad (3.35)$$

Interior Unitarity Class

The inequality multiplier λ_l is equal to zero and the imaginary partial wave amplitude is

$$a_l = r_1 - r_2 l^2 \quad (3.36)$$

where $r_1 = \alpha/(2|\beta|) > 0$ and $r_2 = 1/(2|\beta|) > 0$. The maximum l for positive partial waves is

$$l_{max} = L = \sqrt{\frac{r_1}{r_2}} \quad (3.37)$$

and the minimum l is $l_{min} = 0$.

Boundary Unitarity Class

The boundary unitarity class $B^{U_0} \equiv \{l | a_l = 0, \lambda_l \geq 0\}$ is non-empty when $l > L = l_{max}$ and there is no contribution from the partial wave amplitude a_l in this unitarity class. The other boundary unitarity class $B^{U_1} \equiv \{l | a_l = 1, \lambda_l \geq 0\}$ is non-empty when $l < 0$ and is empty when $l \geq 0$ and consequently there is also no contribution from this unitarity class.

2.4 Reconstructing the Constraints

In this case we are interested in contributions from the interior unitarity class I^U . The normalized dimensionless total cross section A_0 is reconstructed by substituting the expression for the imaginary partial wave amplitude a_l , given

in Equation (3.36), into

$$A_0 = 2 \sum_{l=1}^L la_l \quad (3.38)$$

to give

$$A_0 = 2 \sum_{l=1}^L l (r_1 - r_2 l^2) \approx \frac{r_1^2}{2r_2} \quad (3.39)$$

for large l . Similarly the normalized dimensionless absorptive elastic cross section Σ_{el} and logarithmic derivative g_0 can be reconstructed;

$$\Sigma_{el} \approx \frac{1}{3} \frac{r_1^3}{r_2}, \quad (3.40)$$

$$g_0^{min} \approx \frac{1}{6} \frac{r_1^3}{r_2^2}. \quad (3.41)$$

The logarithmic derivative g written in terms of the normalized dimensionless logarithmic derivative g_0 is

$$g = \frac{4\pi g_0}{k^2 s \sigma_{tot}} \quad (3.42)$$

or

$$g = \frac{g_0}{s A_0} \quad (3.43)$$

and substitution of Equations (3.39) and (3.41) into this expression for g leads to the bound

$$g > \frac{1}{3s} \frac{r_1}{r_2}. \quad (3.44)$$

The ratio r_1/r_2 , where

$$\frac{r_1}{r_2} = \frac{4}{3} \frac{A_0^2}{\Sigma_{el}}, \quad (3.45)$$

is simply found by solving Equations (3.39) and (3.40). The minimized logarithmic derivative with the $r_1/r_2 = 4 A_0^2/(3 \Sigma_{el})$ is written as

$$g > \frac{1}{9\pi} \frac{k^2}{s} \frac{\sigma_{\text{tot}}^2}{\sigma_{\text{el}}} \quad (3.46)$$

and in the high energy limit, $k \approx \sqrt{s}/2$, the MacDowell-Martin bound

$$g > \frac{1}{36\pi} \frac{\sigma_{\text{tot}}^2}{\sigma_{\text{el}}} \quad (3.47)$$

is obtained.

In deriving the lower bound on g we have only considered leading order l terms. If lower order l terms are included the complete MacDowell-Martin bound

$$g > \frac{1}{36\pi} \frac{\sigma_{\text{tot}}^2}{\sigma_{\text{el}}} - \frac{1}{9k^2} \quad (3.48)$$

can be found.

Chapter 4

Observables in Proton-Proton Scattering

In the elastic scattering of protons there are many observables that can be measured experimentally [29, 71, 72], for example, the total and elastic cross sections, the nuclear slope, single spin asymmetries and double spin asymmetries. The observables, expressed in terms of the five independent helicity amplitudes, ϕ_1, \dots, ϕ_5 , in the representation of Jacob and Wick [26], can be expanded as a partial wave series. In this chapter we will introduce the helicity representation of Jacob and Wick and express some of the proton - proton scattering observables as partial wave expansions.

1 Helicity Amplitudes

For the elastic scattering of two protons at CM energy \sqrt{s} and CM momentum $k = \sqrt{s - 4m^2}/2$, there are sixteen helicity amplitudes which under the following relations [26, 30];

Parity conservation

$$\langle \lambda'_1 \lambda'_2 | \phi | \lambda_1 \lambda_2 \rangle = (-1)^{\mu - \lambda} \langle -\lambda'_1 - \lambda'_2 | \phi | -\lambda_1 - \lambda_2 \rangle \quad (4.1)$$

Time reversal invariance

$$\langle \lambda'_1 \lambda'_2 | \phi | \lambda_1 \lambda_2 \rangle = (-1)^{\mu - \lambda} \langle \lambda_1 \lambda_2 | \phi | \lambda'_1 \lambda'_2 \rangle \quad (4.2)$$

Identical particle scattering

$$\langle \lambda'_1 \lambda'_2 | \phi | \lambda_1 \lambda_2 \rangle = (-1)^{\lambda - \mu} \langle \lambda'_2 \lambda'_1 | \phi | \lambda_2 \lambda_1 \rangle \quad (4.3)$$

Symmetry properties

$$d_{\lambda\mu}^J(\theta) = (-1)^{\lambda - \mu} d_{-\lambda - \mu}^J(\theta), \quad d_{\lambda\mu}^J(\theta) = (-1)^{\lambda - \mu} d_{\mu\lambda}^J(\theta), \quad d_{\lambda\mu}^J(\theta) = d_{-\mu - \lambda}^J(\theta) \quad (4.4)$$

reduce to two non helicity-flip amplitudes, two double helicity-flip amplitudes, and one single helicity-flip amplitude where $\lambda = \lambda_1 - \lambda_2$, $\mu = \lambda'_1 - \lambda'_2$. The non helicity-flip amplitudes ϕ_1 and ϕ_3 , the double helicity-flip amplitudes ϕ_2 and ϕ_4 , and the single helicity-flip amplitude ϕ_5 , have partial wave

expansions [26, 30, 73]:

$$\phi_1(s, t) = \langle ++ | \phi | ++ \rangle = \frac{\sqrt{s}}{2k} \sum_J (2J+1) (f_0^J(s) + f_{11}^J(s)) d_{00}^J(\theta) \quad (4.5)$$

$$\phi_3(s, t) = \langle +- | \phi | +- \rangle = \frac{\sqrt{s}}{2k} \sum_J (2J+1) (f_1^J(s) + f_{22}^J(s)) d_{11}^J(\theta) \quad (4.6)$$

$$\phi_2(s, t) = \langle ++ | \phi | -- \rangle = \frac{\sqrt{s}}{2k} \sum_J (2J+1) (f_{11}^J(s) - f_0^J(s)) d_{00}^J(\theta) \quad (4.7)$$

$$\phi_4(s, t) = \langle +- | \phi | -+ \rangle = \frac{\sqrt{s}}{2k} \sum_J (2J+1) (f_{22}^J(s) - f_1^J(s)) d_{1-1}^J(\theta) \quad (4.8)$$

$$\phi_5(s, t) = \langle ++ | \phi | +- \rangle = \frac{\sqrt{s}}{2k} \sum_J (2J+1) f_{21}^J(s) d_{10}^J(\theta) \quad (4.9)$$

where f_i^J ($i = 0, 1, 11, 22, 21$) denote the s -channel partial wave amplitudes, $\text{Im } f_i^J = a_i^J$, $\text{Re } f_i^J = b_i^J$ and $z = \cos \theta = 1 + t/2k^2$.

In the Coulomb Nuclear Interference (CNI) region, $t \approx -0.0012(\text{Gev}/c)^2$, it is convenient to express the five helicity amplitudes in terms of Jacobi polynomials. For $J - \lambda$ an integer, we can relate $d_{\lambda\mu}^J(\theta)$ to the Jacobi polynomials $P_n^{(\alpha, \beta)}(z)$, where $z = \cos \theta$. To define the $d_{\lambda\mu}^J(\theta)$ function in terms of Jacobi polynomials it is suitable to separate the space of λ and μ into four regions A, B, C, D as shown in Figure 4.1. In region A, the relation is [74]

$$d_{\lambda\mu}^J(\theta) = \left(\sqrt{\frac{(J+\lambda)!(J-\lambda)!}{(J+\mu)!(J-\mu)!}} \left(\frac{1+z}{2}\right)^{\frac{(\lambda+\mu)}{2}} \left(\frac{1-z}{2}\right)^{\frac{(\lambda-\mu)}{2}} \right) \times P_{J-\lambda}^{(\lambda-\mu, \lambda+\mu)}(z), \quad (4.10)$$

where $z = \cos \theta = 1 + t/2k^2$, and $J - \lambda = 0, 1, 2, \dots$.

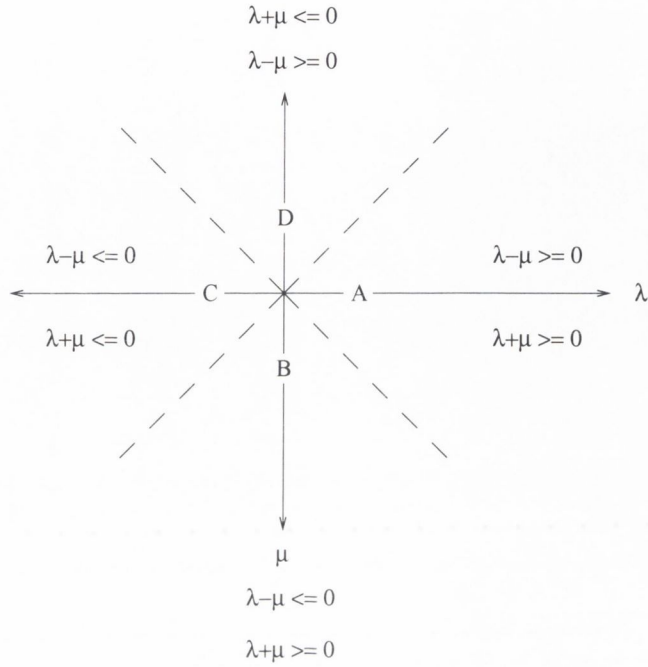


Figure 4.1: Regions associated with the expressions of $d_{\lambda\mu}^J(\theta)$ in terms of Jacobi polynomials.

Equivalent forms in the other regions are obtained by use of symmetry relations [30, 74].

In region B, use

$$d_{\lambda\mu}^J(\theta) = (-1)^{\lambda-\mu} d_{\mu\lambda}^J(\theta). \quad (4.11)$$

In region C, use

$$d_{\lambda\mu}^J(\theta) = (-1)^{\lambda-\mu} d_{-\lambda-\mu}^J(\theta). \quad (4.12)$$

In region D, use

$$d_{\lambda\mu}^J(\theta) = d_{-\mu-\lambda}^J(\theta). \quad (4.13)$$

The $d_{\lambda\mu}^J(\theta)$ functions can now be expressed in terms of Jacobi polynomials:

$$d_{00}^J(\theta) = P_J^{(0,0)}(z), \quad (4.14)$$

$$d_{11}^J(\theta) = \frac{(1+z)}{2} P_{J-1}^{(0,2)}(z), \quad (4.15)$$

$$d_{1-1}^J(\theta) = \frac{(1-z)}{2} P_{J-1}^{(2,0)}(z) \quad (4.16)$$

and

$$d_{10}^J(\theta) = \sqrt{\frac{J+1}{J}} \frac{\sqrt{1-z^2}}{2} P_{J-1}^{(1,1)}(z). \quad (4.17)$$

The five helicity amplitudes in Equations (4.5) - (4.9) can thus be written in terms of Jacobi polynomials;

$$\phi_1(s, t) = \frac{\sqrt{s}}{2k} \sum_J (2J+1) (f_0^J(s) + f_{11}^J(s)) P_J^{(0,0)}(z) \quad (4.18)$$

$$\phi_2(s, t) = \frac{\sqrt{s}}{2k} \sum_J (2J+1) (f_{11}^J(s) - f_0^J(s)) P_J^{(0,0)}(z), \quad (4.19)$$

$$\phi_3(s, t) = \frac{\sqrt{s}(1+z)}{4k} \sum_J (2J+1) (f_1^J(s) + f_{22}^J(s)) P_{J-1}^{(0,2)}(z) \quad (4.20)$$

$$\phi_4(s, t) = \frac{\sqrt{s}(1-z)}{4k} \sum_J (2J+1) (f_{22}^J(s) - f_1^J(s)) P_{J-1}^{(2,0)}(z) \quad (4.21)$$

$$\phi_5(s, t) = \frac{\sqrt{s}\sqrt{1-z^2}}{4k} \sum_J (2J+1) \sqrt{\frac{J+1}{J}} f_{21}^J(s) P_{J-1}^{(1,1)}(z) \quad (4.22)$$

where $z = \cos\theta = 1 + t/(2k^2)$.

2 Total Cross Section

The optical theorem [29, 33] at zero momentum transfer or $z = 1$,

$$\text{Im } \phi_+(s, t)|_{t=0} = \frac{k \sqrt{s}}{2\pi} \sigma_{\text{tot}}(s), \quad (4.23)$$

is used to express the total cross section as a partial wave expansion, given by

$$\begin{aligned} \sigma_{\text{tot}}(s) = \frac{\pi}{k^2} \sum_J (2J+1) \{ & (a_0^J(s) + a_{11}^J(s)) P_J^{(0,0)}(1) \\ & + (a_1^J(s) + a_{22}^J(s)) P_{J-1}^{(0,2)}(1) \}, \end{aligned} \quad (4.24)$$

where $\text{Im } \phi_+(s, t) = (\text{Im } \phi_1(s, t) + \text{Im } \phi_3(s, t))/2$ is the imaginary spin average helicity non-flip amplitude. For $z = 1$ or $t = 0$, the Jacobi polynomials can be written as [75]

$$P_n^{(\alpha, \beta)}(1) = \frac{\Gamma(\alpha + n + 1)}{\Gamma(\alpha + 1)n!}, \quad (4.25)$$

leading to $P_J^{(0,0)}(1) = 1$ and $P_{J-1}^{(0,2)}(1) = 1$. The partial wave expansion for the total cross section is thus

$$\sigma_{\text{tot}}(s) = \frac{\pi}{k^2} \sum_J (2J+1) \{ a_0^J(s) + a_1^J(s) + a_{11}^J(s) + a_{22}^J(s) \}. \quad (4.26)$$

The normalized dimensionless total cross section, defined as $A_0 = k^2 \sigma_{\text{tot}}/\pi$ ¹, is given by

$$A_0 = \sum_J (2J+1) \{ a_0^J(s) + a_1^J(s) + a_{11}^J(s) + a_{22}^J(s) \}. \quad (4.27)$$

¹In spinless scattering the total and elastic cross sections are normalized by the factor $k^4/(4\pi)$.

3 Imaginary Non-Flip Amplitude

The imaginary spin average non-flip amplitude inside the Coulomb Nuclear Interference (CNI) region, written as a Taylor expansion, is

$$\text{Im } \phi_+(s, t) \approx \text{Im } \phi_+(s, 0) + t \left(\frac{d}{dt} \text{Im } \phi_+(s, t) \right) \Big|_{t=0}. \quad (4.28)$$

To calculate $\frac{d}{dt} \text{Im } \phi_+(s, t) \Big|_{t=0}$, Equation (4.25) with the additional property [75]

$$\frac{d^m}{dz^m} P_n^{(\alpha, \beta)}(z) = 2^{-m} \frac{\Gamma(m + n + \alpha + \beta + 1)}{\Gamma(n + \alpha + \beta + 1)} P_{n-m}^{(\alpha+m, \beta+m)}(z) \quad (4.29)$$

is employed and for $m = 1$

$$\frac{d}{dz} P_n^{(\alpha, \beta)}(z) = \frac{(n + \alpha + \beta + 1)}{2} P_{n-1}^{(\alpha+1, \beta+1)}(z). \quad (4.30)$$

To calculate the slope of the imaginary non-flip amplitude, the properties given in Equations (4.25) and (4.30) are used to find

$$\frac{d}{dz} P_J^{(0,0)}(z) \Big|_{z=1} = \frac{1}{2} J(J + 1) \quad (4.31)$$

and

$$\frac{d}{dz} P_{J-1}^{(0,2)}(z) \Big|_{z=1} = \frac{1}{2} (J + 2)(J - 1). \quad (4.32)$$

The imaginary non-flip amplitude thus has the partial wave expansion

$$\text{Im } \phi_+(s, t) =$$

$$\frac{\sqrt{s}}{4k} \sum_J (2J + 1) \left\{ a_0^J(s) + a_1^J(s) + a_{11}^J(s) + a_{22}^J(s) \right\} \left(1 - \frac{\zeta}{4} J(J + 1) \right) \quad (4.33)$$

with momentum transfers in the CNI region, where $\zeta = -t/k^2$. The logarithmic derivative of the imaginary spin average non-flip amplitude is defined as [69]

$$g = \frac{d}{dt} \ln \text{Im } \phi_+(s, t)|_{t=0} = \frac{1}{\text{Im } \phi_+(s, 0)} \left(\frac{d}{dt} \text{Im } \phi_+(s, t) \right) \Big|_{t=0}, \quad (4.34)$$

therefore

$$\left(\frac{d}{dt} \text{Im } \phi_+(s, t) \right) \Big|_{t=0} = g \text{Im } \phi_+(s, 0). \quad (4.35)$$

The Taylor expansion of $\text{Im } \phi_+(s, t)$ in the CNI region, given by Equation (4.28), can thus be written as

$$\text{Im } \phi_+(s, t) = \text{Im } \phi_+(s, 0) \{1 - (-t g)\}. \quad (4.36)$$

In the CNI region the term $1 - (-t g)$ can be approximated with the exponential e^{gt} and using the optical theorem the imaginary spin average non-flip amplitude can be expressed as

$$\text{Im } \phi_+(s, t) = \frac{k\sqrt{s} \sigma_{\text{tot}}(s)}{4\pi} e^{gt}. \quad (4.37)$$

4 Elastic Cross Section

The elastic cross section can be expressed as a partial wave expansion by integrating the differential cross section over momentum transfer t :

$$\sigma_{\text{el}}(s) = \int_{-4k^2}^0 dt \frac{d\sigma(s, t)}{dt}. \quad (4.38)$$

The differential cross section written in terms of the helicity amplitudes is

$$\frac{d\sigma(s, t)}{dt} = \frac{\pi}{2k^2 s} \left\{ |\phi_1(s, t)|^2 + |\phi_2(s, t)|^2 + |\phi_3(s, t)|^2 + |\phi_4(s, t)|^2 + 4|\phi_5(s, t)|^2 \right\} \quad (4.39)$$

and the elastic cross section also written in terms of the helicity amplitudes is

$$\sigma_{\text{el}}(s) = \frac{\pi}{2k^2 s} \int_{-4k^2}^0 dt \left\{ |\phi_1(s, t)|^2 + |\phi_2(s, t)|^2 + |\phi_3(s, t)|^2 + |\phi_4(s, t)|^2 + 4|\phi_5(s, t)|^2 \right\} . \quad (4.40)$$

Using the expression

$$t = -2k^2(1 - z), \quad (4.41)$$

the t variable can be replaced with the z variable, where t is the momentum transfer, k is the center-of-mass three-momentum, and $z = \cos\theta$. The elastic cross section expressed as an integral over z becomes

$$\sigma_{\text{el}}(s) = \frac{\pi}{s} \int_{-1}^{+1} dz \left\{ |\phi_1(s, t)|^2 + |\phi_2(s, t)|^2 + |\phi_3(s, t)|^2 + |\phi_4(s, t)|^2 + 4|\phi_5(s, t)|^2 \right\} . \quad (4.42)$$

To express the elastic cross section as a partial wave expansion, the integrals $\int_{-1}^{+1} dz |\phi_i(s, t)|^2$ are calculated, where $i = 1, \dots, 5$. The integration formula [76]

$$\int_{-1}^{+1} (1 - z)^\alpha (1 + z)^\beta P_n^{(\alpha, \beta)}(z) P_m^{(\alpha, \beta)}(z) dz = \begin{cases} 0 & m \neq n \\ \frac{2^{\alpha+\beta+1} \Gamma(\alpha+n+1) \Gamma(\beta+n+1)}{n! (\alpha+\beta+2n+1) \Gamma(\alpha+\beta+n+1)} \delta_{m, n} \end{cases} \quad (4.43)$$

is used to find

$$\int_{-1}^{+1} d_{\lambda\mu}^J(\theta) d_{\lambda\mu}^M(\theta) dz = \frac{2}{2J+1} \delta_{M,J} \quad (4.44)$$

which leads to

$$\int_{-1}^{+1} |\phi_1(s, t)|^2 dz = \frac{s}{2k^2} \sum_J (2J+1) |f_0^J(s) + f_{11}^J(s)|^2 \quad (4.45)$$

$$\int_{-1}^{+1} |\phi_2(s, t)|^2 dz = \frac{s}{2k^2} \sum_J (2J+1) |f_0^J(s) - f_{11}^J(s)|^2 \quad (4.46)$$

$$\int_{-1}^{+1} |\phi_3(s, t)|^2 dz = \frac{s}{2k^2} \sum_J (2J+1) |f_1^J(s) + f_{22}^J(s)|^2 \quad (4.47)$$

$$\int_{-1}^{+1} |\phi_4(s, t)|^2 dz = \frac{s}{2k^2} \sum_J (2J+1) |f_1^J(s) - f_{22}^J(s)|^2 \quad (4.48)$$

$$\int_{-1}^{+1} |\phi_5(s, t)|^2 dz = \frac{s}{2k^2} \sum_J (2J+1) |f_{21}^J(s)|^2. \quad (4.49)$$

Equations (4.45)-(4.49) substituted into Equation (4.42) gives the partial wave expansion for the elastic cross section;

$$\begin{aligned} \sigma_{\text{el}}(s) = \frac{\pi}{k^2} \sum_J (2J+1) \left\{ |f_0^J(s)|^2 + |f_1^J(s)|^2 + |f_{11}^J(s)|^2 \right. \\ \left. + |f_{22}^J(s)|^2 + 2 |f_{21}^J(s)|^2 \right\}. \quad (4.50) \end{aligned}$$

The normalized dimensionless elastic cross section, defined as $\Sigma_{\text{el}} = k^2 \sigma_{\text{el}} / \pi$, is

$$\Sigma_{\text{el}} = \sum_J (2J+1) \left\{ |f_0^J(s)|^2 + |f_1^J(s)|^2 + |f_{11}^J(s)|^2 + |f_{22}^J(s)|^2 + 2 |f_{21}^J(s)|^2 \right\}. \quad (4.51)$$

5 Imaginary Single-Flip Amplitude

The imaginary single helicity-flip amplitude,

$$\text{Im } \phi_5(s, t) = \frac{\sqrt{s}}{2k} \sum_J (2J+1) a_{21}^J(s) d_{10}^J(\theta), \quad (4.52)$$

written in terms of Jacobi polynomials is

$$\text{Im } \phi_5(s, t) = \frac{\sqrt{s}(1-z^2)^{1/2}}{4k} \sum_J (2J+1) \sqrt{\frac{J+1}{J}} a_{21}^J(s) P_{J-1}^{(1,1)}(z) \quad (4.53)$$

or

$$\frac{\text{Im } \phi_5(s, t)}{(1-z^2)^{1/2}} = \frac{\sqrt{s}}{4k} \sum_J (2J+1) \sqrt{\frac{J+1}{J}} a_{21}^J(s) P_{J-1}^{(1,1)}(z). \quad (4.54)$$

In the Coulomb Nuclear Interference (CNI) region, $t \approx -0.0012 \text{ (Gev}/c)^2$, $P_{J-1}^{(1,1)}(z)$ is expanded as a Taylor series;

$$P_{J-1}^{(1,1)}(z) \approx P_{J-1}^{(1,1)}(z)|_{z=1} - \frac{\zeta}{2} \left(\frac{d}{dz} P_{J-1}^{(1,1)}(z) \right) \Big|_{z=1} \quad (4.55)$$

where $z = 1 + t/(2k^2)$ and $\zeta = -t/k^2$. Using the two properties of Jacobi polynomials in Equations (4.25) and (4.30), the Taylor series for $P_{J-1}^{(1,1)}(z)$ about $z = 1$ is

$$P_{J-1}^{(1,1)}(z) \approx J \left(1 - \frac{\zeta}{8} [J(J+1) - 2] \right), \quad (4.56)$$

and thus

$$\frac{\text{Im } \phi_5(s, t)}{(1-z^2)^{1/2}} \Big|_{z \sim 1} \approx \frac{\sqrt{s}}{4k} \sum_J (2J+1) \sqrt{\frac{J+1}{J}} J \left(1 - \frac{\zeta}{8} [J(J+1) - 2] \right) a_{21}^J(s). \quad (4.57)$$

The approximation $\sin \theta \approx 2 \sin \theta/2$ for $\theta \sim 0$ is used to write $\sqrt{-t} = 2k \sin \theta/2$ as $\sqrt{-t} \approx k \sin \theta = k(1-z^2)^{1/2}$. The ratio $\text{Im } r_5 = m \text{Im } \phi_5 / (\sqrt{-t} \text{Im } \phi_+)$ is

$$\text{Im } r_5 = \frac{m}{k} \frac{\text{Im } \tilde{\phi}_5}{\text{Im } \phi_+(s, t)} \quad (4.58)$$

where

$$\text{Im } \tilde{\phi}_5 = \frac{\text{Im } \phi_5(s, t)}{(1-z^2)^{1/2}}. \quad (4.59)$$

6 Unitarity

The partial wave amplitudes obey the following unitarity inequalities [73]

$$U_1^J = a_0^J - |f_0^J|^2 \geq 0 \quad (4.60)$$

$$U_2^J = a_1^J - |f_1^J|^2 \geq 0 \quad (4.61)$$

$$V_1^J = a_{11}^J - |f_{11}^J|^2 - |f_{21}^J|^2 \geq 0 \quad (4.62)$$

$$V_2^J = a_{22}^J - |f_{22}^J|^2 - |f_{21}^J|^2 \geq 0 \quad (4.63)$$

where f_i^J ($i = 0, 1, 11, 22, 21$) denote the s -channel partial wave amplitudes, $\text{Im } f_i^J = a_i^J$ and $\text{Re } f_i^J = b_i^J$. Combining Equation (4.60) with Equation (4.61) leads to the inequality $W^J = U_1^J + U_2^J$ where

$$W^J = a_0^J + a_1^J - |f_0^J|^2 - |f_1^J|^2 \geq 0 \quad (4.64)$$

and the inequality $X^J = V_1^J + V_2^J$ follows from the combination of Equation (4.62) and Equation (4.63) where

$$X^J = a_{11}^J + a_{22}^J - |f_{11}^J|^2 - |f_{22}^J|^2 - 2|f_{21}^J|^2 \geq 0. \quad (4.65)$$

For the elastic scattering of spin 0 and spin 1/2 particles there are two independent helicity amplitudes, a flip and a non-flip amplitude, with partial wave expansions whose partial wave amplitudes obey unitarity relations similar to relations (4.60) and (4.61). The unitarity relations (4.62) and (4.63) are characteristic of spin 1/2 - spin 1/2 scattering, the f_{21}^J term coming from the single helicity-flip amplitude ϕ_5 . The partial wave amplitudes, expressed in terms of partial wave phase shifts, are given in the Appendix.

Chapter 5

Optimization under σ_{el} and Unitarity

The Lagrange method of optimization [21]– [25] is used to derive an upper bound on amplitude $|\text{Im } r_5|$. The amplitude $|\text{Im } r_5|$ is bounded by optimizing the modified single helicity-flip amplitude $\text{Im } \tilde{\phi}_5$ with unitarity, expressed as inequality constraints, and the elastic cross section, appearing as an equality constraint. The imaginary modified helicity single-flip amplitude, $\text{Im } \tilde{\phi}_5 = \text{Im } \phi_5 / \sqrt{1 - z^2}$, has the partial wave expansion

$$\text{Im } \tilde{\phi}_5(s, t) = \frac{\sqrt{s}}{4k} \sum_J (2J + 1) \sqrt{\frac{J+1}{J}} J \left(1 - \frac{\zeta}{8} [J(J+1) - 2] \right) a_{21}^J(s) \quad (5.1)$$

and

$$\text{Im } r_5 = \frac{m}{k} \frac{\text{Im } \tilde{\phi}_5(s, t)}{\text{Im } \phi_+(s, t)} \quad (5.2)$$

with momentum transfers t inside the CNI region where $\zeta = -t/k^2$. The normalized dimensionless elastic cross section expressed as a partial wave expansion is

$$\Sigma_{\text{el}} = \sum_J (2J + 1) \left\{ |f_0^J(s)|^2 + |f_1^J(s)|^2 + |f_{11}^J(s)|^2 + |f_{22}^J(s)|^2 + 2|f_{21}^J(s)|^2 \right\}. \quad (5.3)$$

The partial wave unitarity relations, a direct consequence of S -matrix unitarity, are

$$W^J = a_0^J + a_1^J - |f_0^J|^2 - |f_1^J|^2 \geq 0 \quad (5.4)$$

and

$$X^J = a_{11}^J + a_{22}^J - |f_{11}^J|^2 - |f_{22}^J|^2 - 2|f_{21}^J|^2 \geq 0. \quad (5.5)$$

1 Lagrange Formalism

The modified single helicity-flip amplitude $\text{Im } \tilde{\phi}_5$ is optimized by introducing the normalized dimensionless elastic cross section Σ_{el} , expressed as an equality constraint, and the partial wave unitarity relations, expressed as inequality constraints. The modified single helicity-flip amplitude $\text{Im } \tilde{\phi}_5$ is the

objective or penalty function in the Lagrangian [77]:

$$\begin{aligned}
\mathcal{L} = & \operatorname{Im} \tilde{\phi}_5 + \beta \left[\Sigma_{el} - \sum_J (2J+1) \left(|f_0^J|^2 + |f_1^J|^2 + |f_{11}^J|^2 + |f_{22}^J|^2 + 2|f_{21}^J|^2 \right) \right] \\
& + \sum_J (2J+1) \mu_J \left(a_{11}^J + a_{22}^J - |f_{11}^J|^2 - |f_{22}^J|^2 - 2|f_{21}^J|^2 \right) \\
& + \sum_J (2J+1) \lambda_J \left(a_0^J + a_1^J - |f_0^J|^2 - |f_1^J|^2 \right) \tag{5.6}
\end{aligned}$$

where β is an equality multiplier and the inequality multipliers, λ_J and μ_J , are non-negative by definition. In the high energy or large J limit only the leading order J terms are included; $2J+1$ terms are replaced by $2J$, $J(J+1)$ terms are replaced by J^2 , and $\sqrt{s} \approx 2k$. The Lagrange function of Equation (5.6), in the large J limit becomes

$$\begin{aligned}
\mathcal{L} = & \operatorname{Im} \tilde{\phi}_5 + \beta \left[\Sigma_{el} - 2 \sum_J J \left(|f_0^J|^2 + |f_1^J|^2 + |f_{11}^J|^2 + |f_{22}^J|^2 + 2|f_{21}^J|^2 \right) \right] \\
& + 2 \sum_J J \mu_J \left(a_{11}^J + a_{22}^J - |f_{11}^J|^2 - |f_{22}^J|^2 - 2|f_{21}^J|^2 \right) \\
& + 2 \sum_J J \lambda_J \left(a_0^J + a_1^J - |f_0^J|^2 - |f_1^J|^2 \right) \tag{5.7}
\end{aligned}$$

with

$$\operatorname{Im} \tilde{\phi}_5 \approx \sum_J J^2 \left(1 - \frac{\zeta}{8} J^2 \right) a_{21}^J(s) \tag{5.8}$$

and $\zeta = -t/k^2$. The system is optimized by taking first and second derivatives with respect to the real and imaginary partial wave amplitudes, b_i^J and a_i^J . This gives the optimized set of partial waves, at some fixed t in the CNI region;

$$b_i^J = 0 \quad \forall i, \tag{5.9}$$

$$a_0^J = a_1^J = \frac{\tilde{\lambda}_J}{1 + 2\tilde{\lambda}_J} \quad (5.10)$$

$$a_{11}^J = a_{22}^J = \frac{\tilde{\mu}_J}{1 + 2\tilde{\mu}_J} \quad (5.11)$$

$$a_{21}^J = \frac{\frac{J}{8\beta} \left[1 - \frac{\zeta}{8} J^2 \right]}{1 + 2\tilde{\mu}_J}, \quad (5.12)$$

where $\tilde{\lambda}_J = \lambda_J/2\beta$, $\tilde{\mu}_J = \mu_J/2\beta$, and $\beta > 0$ for a maximum (or $\beta < 0$ for a minimum).

2 Unitarity Classes

Optimization imposes the conditions:

$$b_i^J = 0 \quad \forall i \implies f_i^J = a_i^J + b_i^J = a_i^J, \quad (5.13)$$

$$a_0^J = a_1^J \quad \text{and} \quad a_{11}^J = a_{22}^J. \quad (5.14)$$

The partial wave amplitudes therefore obey the following unitarity inequalities

$$W^J = a_0^J - a_0^{J2} \geq 0 \quad (5.15)$$

and

$$X^J = a_{11}^J - a_{11}^{J2} - a_{21}^{J2} \geq 0. \quad (5.16)$$

When optimizing the system it is natural to divide the partial waves into two classes [21]. For each unitarity inequality there are two classes, I and B :

$$I^W = \{J \mid W_J > 0, \tilde{\lambda}_J = 0\}, \quad B^W = \{J \mid W_J = 0, \tilde{\lambda}_J \geq 0\} \quad (5.17)$$

$$I^X = \{J | X_J > 0, \tilde{\mu}_J = 0\}, \quad B^X = \{J | X_J = 0, \tilde{\mu}_J \geq 0\} \quad (5.18)$$

I is called the interior unitarity class and B is called the boundary unitarity class.

2.1 I^W and B^W Unitarity Classes

The interior unitarity class I^W is rewritten as

$$I^W \equiv \{J | 0 < a_0^J < 1, \tilde{\lambda}_J = 0\}, \quad (5.19)$$

and the boundary unitarity class B^W splits into two subclasses, B_0^W and B_1^W ;

$$\longrightarrow B^{W_0} \equiv \{J | a_0^J = 0, \tilde{\lambda}_J \geq 0\} \quad (5.20)$$

$$B^W \equiv \{J | W_J > 0, \tilde{\lambda}_J \geq 0\}$$

$$\longrightarrow B^{W_1} \equiv \{J | a_0^J = 1, \tilde{\lambda}_J \geq 0\} \quad (5.21)$$

Consider the unitarity class I^W . The inequality multiplier $\tilde{\lambda}_J$ is equal to zero and from Equation (5.10), $a_0^J = 0$ with $\tilde{\lambda}_J = 0$. Therefore there is no contribution from the interior unitarity class I^W . The boundary unitarity class B^{W_0} with $a_0^J = 0$ restricts the value $\tilde{\lambda}_J$ to zero. Since $\tilde{\lambda}_J \geq 0$ is required the unitarity class B^{W_0} is non-empty, however with $a_0^J = 0$ there is no contribution from this unitarity class. The other boundary unitarity class B^{W_1} with $a_0^J = 1$ restricts the value $\tilde{\lambda}_J$ to a negative value of -1 . Since $\tilde{\lambda}_J \geq 0$ is required the unitarity class B^{W_1} is empty and consequently there

is also no contribution from this unitarity class. Table 5.1 summarizes the contributions from the various unitarity classes.

2.2 I^X and B^X Unitarity Classes

The interior unitarity class I^X under the optimization becomes

$$I^X \equiv \left\{ J \mid a_{11}^J - a_{11}^{J^2} - a_{21}^{J^2} > 0, \tilde{\mu}_J = 0 \right\}, \quad (5.22)$$

and the boundary unitarity class B^X is written as

$$B^X \equiv \left\{ J \mid a_{11}^J - a_{11}^{J^2} - a_{21}^{J^2} = 0, \tilde{\mu}_J \geq 0 \right\}. \quad (5.23)$$

There is no contribution from the interior unitarity class I^X . The inequality multiplier $\tilde{\mu}_J$ is equal to zero and from Equation (5.11), $a_{11}^J = 0$ with $\tilde{\mu}_J = 0$. The boundary unitarity class B^X with $a_{11}^J - a_{11}^{J^2} - a_{21}^{J^2} = 0$ and $\tilde{\mu}_J \geq 0$ is non-empty and there is a contribution from the unitarity class B^X . Table 5.1 gives a synopsis of the contributions from the various unitarity classes.

There are four possible unions of unitarity classes in this optimized system;

$\mathbf{I}^W \cup \mathbf{I}^X$: Both of these unitarity classes are non-empty but all the partial wave amplitudes are zero and there is no contribution from this union of classes.

Table 5.1: Interior and Boundary unitarity class contributions associated with optimization under the elastic cross section and unitarity.

Unitarity Class	Contribution
I^W	non-empty class with zero contribution
B^{W_0}	non-empty class with zero contribution
B^{W_1}	empty class
I^X	non-empty class with zero contribution
B^W	non-empty class with non-zero contribution

$\mathbf{I}^W \cup \mathbf{B}^X$: This union of unitarity classes is also non-empty. There is a contribution from the boundary class B^X but there is no contribution from the interior class I^W .

$\mathbf{B}^W \cup \mathbf{I}^X$: This union of unitarity classes splits into two subclasses, one empty subclass $B^{W_1} \cup I^X$, and one non-empty subclass $B^{W_0} \cup I^X$. There is no contribution from the non-empty subclass $B^{W_0} \cup I^X$ and therefore there is no contribution from the entire unitarity class $B^W \cup I^X$.

$\mathbf{B}^W \cup \mathbf{B}^X$: This union of unitarity classes also splits into two subclasses, one empty subclass $B^{W_1} \cup B^X$, and one non-empty subclass $B^{W_0} \cup B^X$ with a non-zero contribution.

The unitarity classes $I^W \cup B^X$ and $B^{W_0} \cup B^X$ are equivalent, since in both of these unions of classes the partial amplitude a_0^J is equal to zero or both I^W and B^{W_0} are non-contributing unitarity classes. The only non-empty contributing set of unitarity classes is the set; $B^{W_0} \cup B^X \subset B^W \cup B^X$ or $I^W \cup B^X$ where

$$a_0^J = a_1^J = 0, \quad (5.24)$$

$$a_{11}^J = a_{22}^J = \frac{\tilde{\mu}_J}{1 + 2\tilde{\mu}_J} \quad (5.25)$$

and

$$a_{21}^J = \frac{\frac{J}{8\beta} \left[1 - \frac{\zeta}{8} J^2 \right]}{1 + 2\tilde{\mu}_J}. \quad (5.26)$$

The boundary unitarity class condition

$$B^X \equiv \left\{ J \mid a_{11}^J - a_{11}^{J^2} - a_{21}^{J^2} = 0, \tilde{\mu}_J \geq 0 \right\}, \quad (5.27)$$

on substitution of Equations (5.25) and (5.26), can be expressed as

$$B^X \equiv \left\{ J \mid \tilde{\mu}_J^2 + \tilde{\mu}_J - \left[\frac{J}{8\beta} \left(1 - \frac{\zeta}{8} J^2 \right) \right]^2 = 0, \tilde{\mu}_J \geq 0 \right\}. \quad (5.28)$$

The quadratic equation

$$\tilde{\mu}_J^2 + \tilde{\mu}_J - \left[\frac{J}{8\beta} \left(1 - \frac{\zeta}{8} J^2 \right) \right]^2 = 0, \quad (5.29)$$

has solutions

$$\tilde{\mu}_J = \frac{1}{2} \left\{ \pm \sqrt{1 + 4 \left[\frac{J}{8\beta} \left(1 - \frac{\zeta}{8} J^2 \right) \right]^2} - 1 \right\}. \quad (5.30)$$

By definition $\tilde{\mu}_J \geq 0$ and the positive solution is selected;

$$\tilde{\mu}_J = \frac{1}{2} \left\{ \sqrt{1 + 4 \left[\frac{J}{8\beta} \left(1 - \frac{\zeta}{8} J^2 \right) \right]^2} - 1 \right\}. \quad (5.31)$$

3 Reconstruction of σ_{el}

The optimized partial waves can be written as

$$a_{11}^J = a_{22}^J = \frac{1}{2} \left(1 - \frac{4\beta}{Q(J)} \right) \quad (5.32)$$

and

$$a_{21}^J = \frac{J}{2} \frac{\left(1 - \frac{\zeta}{8} J^2 \right)}{Q(J)}, \quad (5.33)$$

with

$$Q(J) = 1 + 2\tilde{\mu}_J = \sqrt{16\beta^2 + J^2 - \frac{\zeta}{4} J^4 + \frac{\zeta^2}{64} J^6} \quad (5.34)$$

and $J \leq M$, where M is the maximum J corresponding to positive partial wave amplitudes and is given by

$$M = \text{Floor} \left[\sqrt{8/\zeta} \right]. \quad (5.35)$$

The Floor function gives the greatest integer less than or equal to $\sqrt{8/\zeta}$. We now reconstruct Σ_{el} and $\text{Im } \tilde{\phi}_5$ by substituting Equations (5.32) and (5.33)

into

$$\Sigma_{\text{el}} = 4 \sum_{J=0}^M J \left(a_{11}^{J^2} + a_{21}^{J^2} \right) \quad (5.36)$$

and

$$\text{Im } \tilde{\phi}_5 = \sum_{J=0}^M J^2 \left(1 - \frac{\zeta}{8} J^2 \right) a_{21}^J \quad (5.37)$$

to give

$$\Sigma_{\text{el}} = \sum_{J=0}^M \left(J - \frac{8\beta J}{Q(J)} + \frac{16\beta^2 J}{Q(J)^2} + \frac{J^3}{Q(J)^2} - \frac{\zeta J^5}{4Q(J)^2} + \frac{\zeta^2 J^7}{64Q(J)^2} \right) \quad (5.38)$$

and

$$\text{Im } \tilde{\phi}_5 = \sum_{J=0}^M \left(\frac{J^3}{2Q(J)} - \frac{\zeta J^5}{8Q(J)} + \frac{\zeta^2 J^7}{128Q(J)} \right). \quad (5.39)$$

For large J , using the Euler-MacLaurin expansion [78, 79], the summation over J is replaced by an integration over J , leading to

$$\Sigma_{\text{el}} \approx \frac{M^2}{2} - 8\beta I_1(M) + 16\beta^2 I_2(M) + I_4(M) - \frac{\zeta}{4} I_6(M) + \frac{\zeta^2}{64} I_8(M) \quad (5.40)$$

and

$$\text{Im } \tilde{\phi}_5 \approx \frac{1}{2} I_3(M) - \frac{\zeta}{8} I_5(M) + \frac{\zeta^2}{128} I_7(M). \quad (5.41)$$

The Jacobi-Elliptical integrals, I_j ($j = 1, \dots, 8$), are given by

$$\begin{aligned} I_1(M) &= \int_0^M dJ \frac{J}{Q(J)} & I_2(M) &= \int_0^M dJ \frac{J}{Q(J)^2} \\ I_3(M) &= \int_0^M dJ \frac{J^3}{Q(J)} & I_4(M) &= \int_0^M dJ \frac{J^3}{Q(J)^2} \\ I_5(M) &= \int_0^M dJ \frac{J^5}{Q(J)} & I_6(M) &= \int_0^M dJ \frac{J^5}{Q(J)^2} \\ I_7(M) &= \int_0^M dJ \frac{J^7}{Q(J)} & I_8(M) &= \int_0^M dJ \frac{J^7}{Q(J)^2}. \end{aligned} \quad (5.42)$$

To solve Equation (5.40), for the equality multiplier β , the value of the normalized dimensionless elastic cross section $\Sigma_{\text{el}} = k^2\sigma_{\text{el}}/\pi$ must be known. The experimental data for σ_{el} and the Σ_{el} value as a function of center-of-mass energy ¹ is shown in Table 5.2 [80]. The system was solved at two

Table 5.2: σ_{el} and Σ_{el} as a function of center-of-mass energy

\sqrt{s} (GeV)	k (GeV)	σ_{el} (mb)	Σ_{el}
19.4	9.65	6.88	524
23.5	11.71	6.87	770
30.7	15.32	6.94	1332
44.7	22.33	7.23	2947
52.8	26.38	7.40	4214
62.5	31.23	7.63	6088

values of momentum transfer, $t = -0.001$ (GeV/c)² and -0.01 (GeV/c)², over the energy range $\sqrt{s} = 19.4 - 62.5$ GeV. The system could not be solved analytically because of the nature of the Jacobi-Elliptical integrals. To compute the solutions of the system `mathematica 3.0` [81] was used to solve Equation (5.40) for β ; the complete `mathematica` code is given in the Appendix. After solving the system for β at a given t and \sqrt{s} , the

¹To convert mb to GeV⁻² divide by 0.3894

optimized value of the modified helicity single-flip amplitude $\text{Im } \tilde{\phi}_5$ is found by substituting the value of β into Equation (5.39) or Equation (5.41). The ratio $\text{Im } r_5$ is given by

$$\text{Im } r_5 = \frac{m}{k} \frac{\text{Im } \tilde{\phi}_5(s, t)}{\text{Im } \phi_+(s, t)}. \quad (5.43)$$

The experimental data for σ_{tot} [80], g [82] and the value of the normalized dimensionless total cross section $A_0 = k^2 \sigma_{\text{tot}} / \pi$, necessary to calculate $\text{Im } \phi_+(s, t)$, is given in Table 5.3. A fit was used to calculate values of σ_{el}

Table 5.3: σ_{tot} , g and A_0 as a function of center-of-mass energy.

\sqrt{s} (GeV)	$2g$ (GeV ²)	σ_{tot} (mb)	A_0
19.4	11.74	38.76	2953
23.5	11.80	39.23	4399
30.7	12.20	40.14	7702
44.7	12.80	41.29	16832
52.8	12.87	42.90	24412
62.5	13.02	44.01	35106

and σ_{tot} [80] where the values given in Tables 5.2 and 5.3 are nominal values. Error analysis gives an error of $\sim 30\%$ on σ_{el} , $\sim 1\%$ on σ_{tot} and $\sim 2\%$ on g which result in an error of $\sim 5\%$ on the $|\text{Im } r_5|$ upper bound.

4 Results

An upper bound on $\text{Im } r_5$ is computed and a lower bound is obtained by changing the sign of the equality multiplier; $\text{Im } \tilde{\phi}_5$ is minimized. Under this translation the lower bound on $\text{Im } \tilde{\phi}_5$ is simply minus the upper bound and therefore if $\text{Im } r_5 \leq a$ then $\text{Im } r_5 \geq -a$ and the upper bound on the modulus of $\text{Im } r_5$ is given by $|\text{Im } r_5| \leq a$.

Upper Bound at $t = -0.001 \text{ (GeV/c)}^2$

Table 5.4 gives the upper bound on $|\text{Im } r_5|$ at $t = -0.001 \text{ (GeV/c)}^2$ over the energy range $\sqrt{s} = 19.4 - 62.5 \text{ GeV}$. The bound on $|\text{Im } r_5|$ is not a very ‘strong’ bound; to use the pp analyzing power as a polarimeter $|\text{Im } r_5|$ must be less than $(\mu_p - 1)/2 \times 5\% \approx 4.48\%$. The calculated bound may not be a useful bound but the technique can be repeated with additional constraints in the system. The addition of constraints into the Lagrange function will at least give the same upper bound- the bound cannot get ‘wider’, an improvement on the bound is more likely. It is well accepted that the greater the number of constraints in the system, the better the bound becomes.

Table 5.4: Results including upper bound on $|\text{Im } r_5|$ optimized under σ_{el} and unitarity constraints at $t = -0.001 \text{ (GeV/c)}^2$ as a function of \sqrt{s} .

\sqrt{s} (GeV)	$\text{Im } \phi_+$	J_{max}	β	$ \text{Im } r_5 $
19.4	1474	863	1659	114.8
23.5	2193	1047	2015	113.5
30.7	3835	1370	2622	111.7
44.7	8369	1997	3746	110.9
52.8	12136	2359	4372	108.1
62.5	17447	2793	5099	107.0

Upper Bound at $t = -0.01 \text{ (GeV/c)}^2$

Table 5.5 shows the upper bound on $|\text{Im } r_5|$ at $t = -0.01 \text{ (GeV/c)}^2$ over the energy range $\sqrt{s} = 19.4 - 62.5 \text{ GeV}$. The bound on $|\text{Im } r_5|$ is an improvement on the bound at $t = -0.001 \text{ (GeV/c)}^2$, a factor of ten smaller. The bound on $|\text{Im } r_5|$ is dependent on $\sqrt{-t}$, as t decreases the bound grows in size, and likewise as t increases the bound reduces in size. This dependency is linear and to derive an upper bound of less than 4.48% on $|\text{Im } r_5|$ the bound must not have such a strong dependence on $\sqrt{-t}$.

Table 5.5: Results including upper bound on $|\text{Im } r_5|$ optimized under σ_{el} and unitarity constraints at $t = -0.01 \text{ (GeV/c)}^2$ as a function of \sqrt{s} .

\sqrt{s} (GeV)	$\text{Im } \phi_+$	J_{max}	β	$ \text{Im } r_5 $
19.4	1399	273	164	12.1
23.5	2080	331	199	11.9
30.7	3630	433	259	11.8
44.7	7901	631	371	11.7
52.8	11453	746	433	11.5
62.5	16454	883	504	11.3

An obvious difference between the two sets of results is the size of the bound on $|\text{Im } r_5|$; as t approaches zero, the bound tends to infinity. The bounds on $|\text{Im } r_5|$ at the two values of momentum transfer are approximately related to each other by a factor of 10. As t falls by a factor of 10 the bound on $|\text{Im } r_5|$ rises by a factor of 10, and similarly, as t rises by a factor of 10 the bound on $|\text{Im } r_5|$ falls by a factor of 10. Therefore, in the CNI region, there is a linear relationship between the bound on $|\text{Im } r_5|$ and the momentum transfer t . This linear behaviour originates in the singular behaviour of $\sqrt{-t}$ in J_{max} where $J_{\text{max}} = \sqrt{8k^2/(-t)}$. The singular nature of $\sqrt{-t}$ in J_{max} causes

the number of partial waves to approach infinity as t tends to zero, and also the bound on $|\text{Im } r_5|$ tends to infinity. In order to improve the bound on $|\text{Im } r_5|$ the contribution from the higher partial waves must be reduced [52]. The addition of constraints in the Lagrange function will reduce the bound on $|\text{Im } r_5|$, such constraints are the total cross section and the slope of the imaginary non-flip amplitude. These extra constraints are introduced into the Lagrange function in the following Chapters, and as expected the bound on $|\text{Im } r_5|$ reduces as more constraints are added to the system, significantly.

Partial Wave Plots, $t = -0.001 \text{ (GeV/c)}^2$

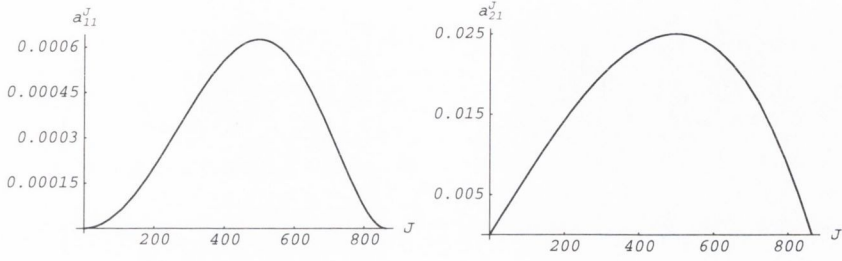


Figure 5.1: a_{11}^J, a_{21}^J under σ_{el} and unitarity; $\sqrt{s} = 19.5 \text{ GeV}$, $t = -0.001 \text{ (GeV/c)}^2$.

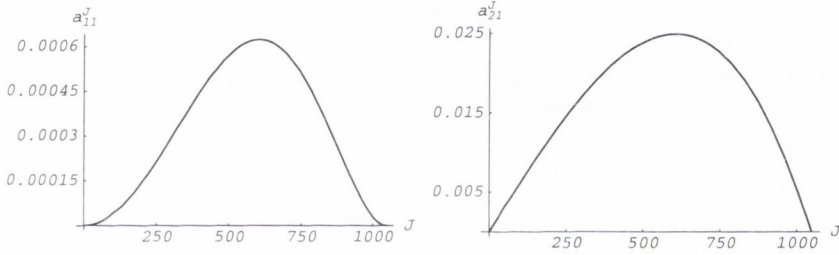


Figure 5.2: a_{11}^J, a_{21}^J under σ_{el} and unitarity; $\sqrt{s} = 23.5 \text{ GeV}$.

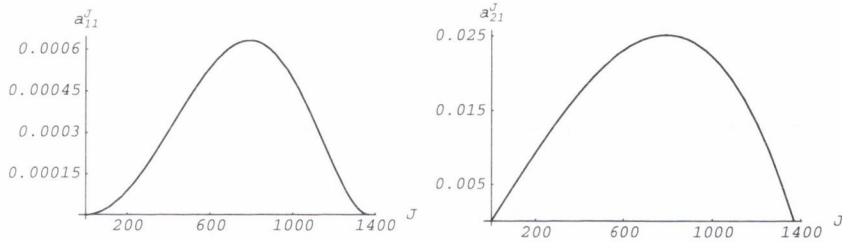


Figure 5.3: a_{11}^J, a_{21}^J under σ_{el} and unitarity; $\sqrt{s} = 30.7 \text{ GeV}$.

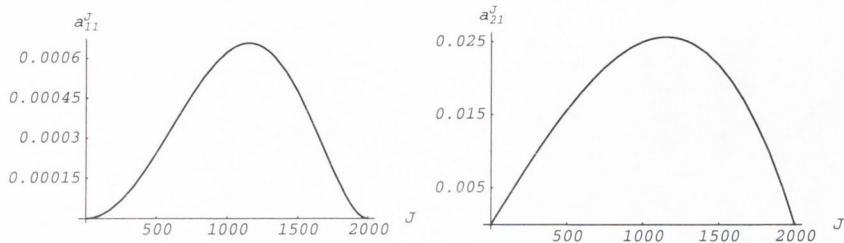


Figure 5.4: a_{11}^J, a_{21}^J under σ_{el} and unitarity; $\sqrt{s} = 44.7$ GeV.

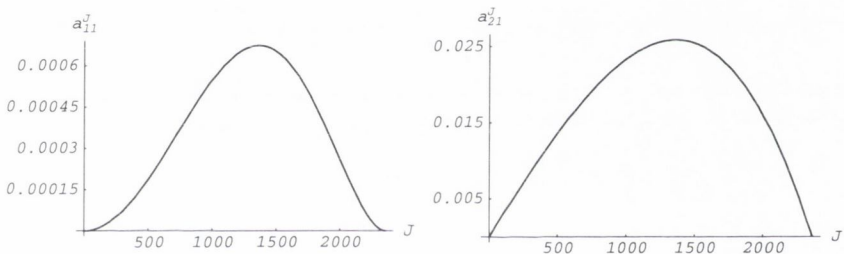


Figure 5.5: a_{11}^J, a_{21}^J under σ_{el} and unitarity; $\sqrt{s} = 52.8$ GeV.

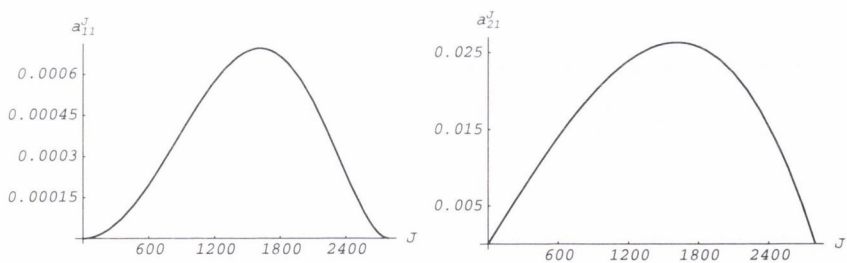


Figure 5.6: a_{11}^J, a_{21}^J under σ_{el} and unitarity; $\sqrt{s} = 62.5$ GeV.

Partial Wave Plots, $t = -0.01 \text{ (GeV/c)}^2$

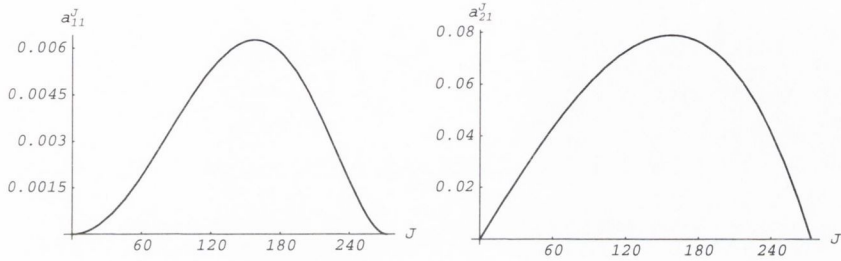


Figure 5.7: a_{11}^J, a_{21}^J under σ_{el} and unitarity; $\sqrt{s} = 19.5 \text{ GeV}$, $t = -0.01 \text{ (GeV/c)}^2$.

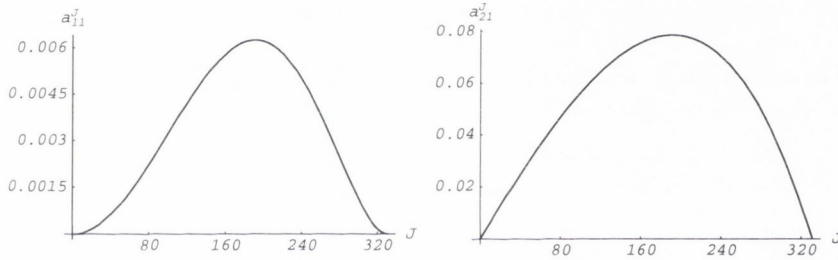


Figure 5.8: a_{11}^J, a_{21}^J under σ_{el} and unitarity; $\sqrt{s} = 23.5 \text{ GeV}$.

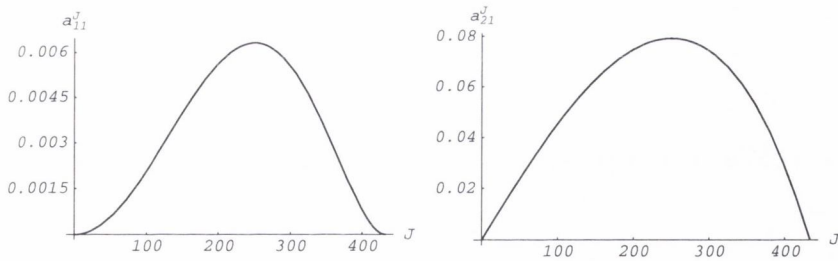


Figure 5.9: a_{11}^J, a_{21}^J under σ_{el} and unitarity; $\sqrt{s} = 30.7 \text{ GeV}$.

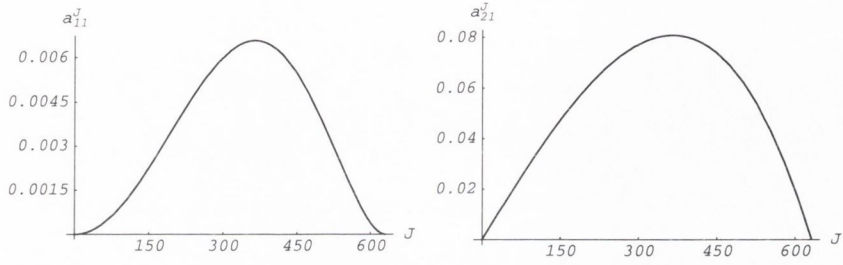


Figure 5.10: a_{11}^J, a_{21}^J under σ_{el} and unitarity; $\sqrt{s} = 44.7$ GeV.

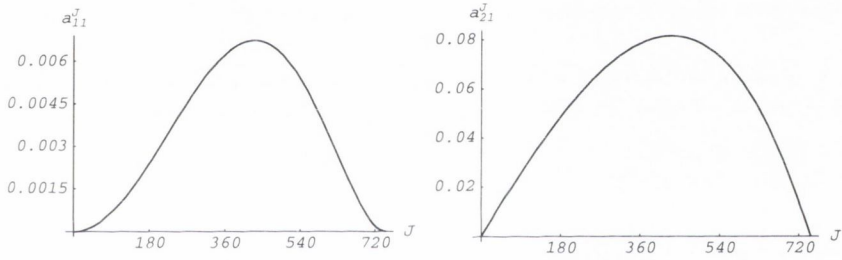


Figure 5.11: a_{11}^J, a_{21}^J under σ_{el} and unitarity; $\sqrt{s} = 52.8$ GeV.

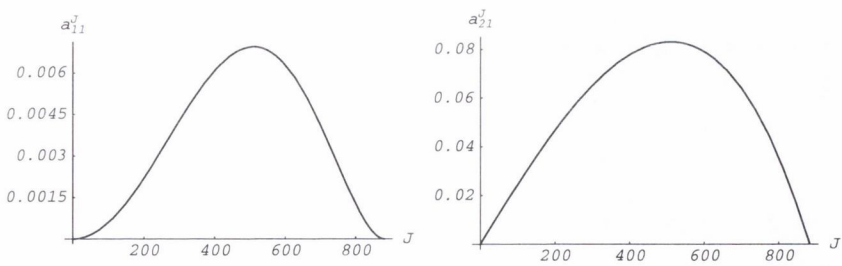


Figure 5.12: a_{11}^J, a_{21}^J under σ_{el} and unitarity; $\sqrt{s} = 62.5$ GeV.

Chapter 6

Bound including the Spin-Average Amplitude

To improve the previous bound on $|\text{Im } r_5|$ extra constraints are added to the Lagrange function. It is known, in general, as the number of constraints in a system are increased, the bound on the objective function improves. The aim is to obtain an improved bound on $|\text{Im } r_5|$ by optimizing the modified single helicity-flip amplitude $\text{Im } \tilde{\phi}_5$ with unitarity, expressed as inequality constraints, the elastic cross section, appearing as an equality constraint, and with the imaginary spin average helicity non-flip amplitude, expressed as an equality constraint. The new constraint, being the imaginary spin average

helicity non-flip amplitude $\text{Im } \phi_+(s, t)$, has the partial wave expansion:

$$\text{Im } \phi_+(s, t) = \frac{\sqrt{s}}{4k} \sum_J (2J + 1) \{a_0^J(s) + a_1^J(s) + a_{11}^J(s) + a_{22}^J(s)\} \left(1 - \frac{\zeta}{4} J(J + 1)\right) \quad (6.1)$$

where $\zeta = -t/k^2$. The unitarity constraints of Equations (4.64) and (4.65), and the partial wave expansion for the dimensionless normalized elastic cross section Σ_{el} , given by Equation (4.51), are again input constraints in the Lagrange function with the objective function $\text{Im } \tilde{\phi}_5$.

1 Lagrange Formalism

The Lagrange function is constructed with the imaginary spin average non-flip amplitude $\text{Im } \phi_+(s, t)$ expressed as an equality constraint, the normalized dimensionless elastic cross section Σ_{el} appearing as an equality constraint, and the partial wave unitarity relations appearing as inequality constraints. The modified single helicity-flip amplitude $\text{Im } \tilde{\phi}_5$ is introduced as the objective or penalty function in the Lagrange function:

$$\begin{aligned}
\mathcal{L} = & \operatorname{Im} \tilde{\phi}_5 + \beta \left[\Sigma_{el} - \sum_J (2J+1) \left(|f_0^J|^2 + |f_1^J|^2 + |f_{11}^J|^2 + |f_{22}^J|^2 + 2|f_{21}^J|^2 \right) \right] \\
& + \gamma \left[\operatorname{Im} \phi_+ - \frac{\sqrt{s}}{4k} \sum_J (2J+1) \left\{ a_0^J(s) + a_1^J(s) + a_{11}^J(s) + a_{22}^J(s) \right\} \left(1 - \frac{\zeta}{4} J(J+1) \right) \right] \\
& + \sum_J (2J+1) \mu_J \left(a_{11}^J + a_{22}^J - |f_{11}^J|^2 - |f_{22}^J|^2 - 2|f_{21}^J|^2 \right) \\
& + \sum_J (2J+1) \lambda_J \left(a_0^J + a_1^J - |f_0^J|^2 - |f_1^J|^2 \right) \tag{6.2}
\end{aligned}$$

where β and γ are equality multipliers. The inequality multipliers, λ_J and μ_J , are non-negative by definition and $\zeta = -t/(k^2)$. The Lagrange function of Equation (6.2), in the large J or high energy limit, becomes

$$\begin{aligned}
\mathcal{L} = & \operatorname{Im} \tilde{\phi}_5 + \beta \left[\Sigma_{el} - 2 \sum_J J \left(|f_0^J|^2 + |f_1^J|^2 + |f_{11}^J|^2 + |f_{22}^J|^2 + 2|f_{21}^J|^2 \right) \right] \\
& + \gamma \left[\operatorname{Im} \phi_+ - \sum_J J \left\{ a_0^J(s) + a_1^J(s) + a_{11}^J(s) + a_{22}^J(s) \right\} \left(1 - \frac{\zeta}{4} J^2 \right) \right] \\
& + 2 \sum_J J \mu_J \left(a_{11}^J + a_{22}^J - |f_{11}^J|^2 - |f_{22}^J|^2 - 2|f_{21}^J|^2 \right) \\
& + 2 \sum_J J \lambda_J \left(a_0^J + a_1^J - |f_0^J|^2 - |f_1^J|^2 \right) \tag{6.3}
\end{aligned}$$

and

$$\operatorname{Im} \tilde{\phi}_5 \approx \sum_J J^2 \left(1 - \frac{\zeta}{8} J^2 \right) a_{21}^J(s). \tag{6.4}$$

The system is optimized by taking first and second derivatives with respect to the real and imaginary partial wave amplitudes, b_i^J and a_i^J . This gives the optimized set of partial waves, for a fixed t in the CNI region;

$$b_i^J = 0 \quad \forall i, \tag{6.5}$$

$$a_0^J = a_1^J = \frac{r \left(1 - \frac{\zeta}{4} J^2\right) + \tilde{\lambda}_J}{1 + 2\tilde{\lambda}_J}, \quad (6.6)$$

$$a_{11}^J = a_{22}^J = \frac{r \left(1 - \frac{\zeta}{4} J^2\right) + \tilde{\mu}_J}{1 + 2\tilde{\mu}_J}, \quad (6.7)$$

and

$$a_{21}^J = \frac{\frac{J}{8\beta} \left(1 - \frac{\zeta}{8} J^2\right)}{1 + 2\tilde{\mu}_J}, \quad (6.8)$$

where $\tilde{\lambda}_J = \lambda_J/2\beta$, $\tilde{\mu}_J = \mu_J/2\beta$, $r = -\gamma/(4\beta)$ and $\beta > 0$ for a maximum (or $\beta < 0$ for a minimum).

2 Unitarity Classes

Optimization under the three constraints imposes the conditions:

$$b_i^J = 0 \quad \forall i \implies f_i^J = a_i^J + b_i^J = a_i^J, \quad (6.9)$$

$$a_0^J = a_1^J \quad \text{and} \quad a_{11}^J = a_{22}^J. \quad (6.10)$$

The partial wave amplitudes therefore obey the following unitarity inequalities

$$W^J = a_0^J - a_0^{J2} \geq 0 \quad (6.11)$$

and

$$X^J = a_{11}^J - a_{11}^{J2} - a_{21}^{J2} \geq 0. \quad (6.12)$$

When optimizing the system it is natural to divide the partial waves into two classes [21]. For each unitarity inequality there are two classes, I and B :

$$I^W = \{J | W_J > 0, \tilde{\lambda}_J = 0\}, \quad B^W = \{J | W_J = 0, \tilde{\lambda}_J \geq 0\} \quad (6.13)$$

$$I^X = \{J | X_J > 0, \tilde{\mu}_J = 0\}, \quad B^X = \{J | X_J = 0, \tilde{\mu}_J \geq 0\} \quad (6.14)$$

I is called the interior unitarity class and B is called the boundary unitarity class.

2.1 I^W and B^W Unitarity Classes

The interior unitarity class I^W , under the three constraints, is expressed as

$$I^W \equiv \{J | 0 < a_0^J < 1, \tilde{\lambda}_J = 0\}. \quad (6.15)$$

In Equation (6.6) $\tilde{\lambda}_J$ is set to zero and the imaginary partial wave amplitude a_0^J in the interior unitarity class becomes

$$a_0^J = r \left(1 - \frac{\zeta}{4} J^2 \right). \quad (6.16)$$

The constraint $0 < a_0^J < 1$ places the restriction

$$\frac{4}{\zeta} \left(1 - \frac{1}{r} \right) < J^2 < \frac{4}{\zeta} \quad (6.17)$$

on J . When $r > 1$ or $r < 0$ the solutions for the optimized system are complex and for real solutions $0 < r < 1$, this limits the value of J to

$$0 \leq J^2 < \frac{4}{\zeta}. \quad (6.18)$$

The boundary unitarity class B^W splits into two sub-classes, B^{W_0} and B^{W_1} :

$$\longrightarrow B^{W_0} \equiv \{J | a_0^J = 0, \tilde{\lambda}_J \geq 0\} \quad (6.19)$$

$$B^W \equiv \{J | W_J > 0, \tilde{\lambda}_J \geq 0\}$$

$$\longrightarrow B^{W_1} \equiv \{J | a_0^J = 1, \tilde{\lambda}_J \geq 0\} . \quad (6.20)$$

In the boundary unitarity class B^{W_0} the imaginary partial wave amplitude a_0^J is equal to zero and from Equation (6.6) the inequality multiplier $\tilde{\lambda}_J$ is given by

$$\tilde{\lambda}_J = -r \left(1 - \frac{\zeta}{4} J^2 \right) . \quad (6.21)$$

The B^{W_0} class begins at $J^2 = 4/\zeta$, and for $J^2 > 4/\zeta$, $0 < r < 1$, the inequality multiplier $\tilde{\lambda}_J$ is positive. Therefore the boundary unitarity class B^{W_0} is non-empty but with $a_0^J = 0$ for all J there are no contributions from this unitarity class. The imaginary partial wave amplitude a_0^J is equal to unity in the boundary unitarity class B^{W_1} and from Equation (6.6) the inequality multiplier $\tilde{\lambda}_J$ is given by

$$\tilde{\lambda}_J = r \left(1 - \frac{\zeta}{4} J^2 \right) - 1 . \quad (6.22)$$

By definition $\tilde{\lambda}_J \geq 0$ or $r(1 - \zeta/4 J^2) \geq 1$. This limits the value of J to

$$J^2 \leq \frac{4}{\zeta} \left(1 - \frac{1}{r} \right) \quad (6.23)$$

and with $0 < r < 1$, J can only take complex values. The B^{W_1} class is therefore an empty unitarity class.

In summary, the unitarity classes, I^W and B^{W_0} , are non-empty and the unitarity class B^{W_1} is empty;

$$I^W \equiv \{J | 0 < a_0^J < 1, 0 \leq J \leq M_1\}, \quad (6.24)$$

$$B^{W_0} \equiv \{J | a_0^J = 0, M_1 + 1 \leq J \leq M_2\} \quad (6.25)$$

where $M_1 = \text{Floor} \left[\sqrt{4/\zeta} \right]$, $M_2 = \text{Floor} \left[\sqrt{8/\zeta} \right]$ and $\zeta = -t/k^2$.

2.2 I^X and B^X Unitarity Classes

The interior unitarity class I^X under the optimization becomes

$$I^X \equiv \{J | a_{11}^J - a_{11}^{J^2} - a_{21}^{J^2} > 0, \tilde{\mu}_J = 0\}, \quad (6.26)$$

Substituting Equations (6.7) and (6.8), with $\tilde{\mu}_J = 0$, into the interior constraint $a_{11}^J - a_{11}^{J^2} - a_{21}^{J^2} > 0$ leads to the equation;

$$f_1(J) = a_1 + a_2 J^2 + a_3 J^4 + a_4 J^6 > 0 \quad (6.27)$$

where $a_1 = r(1 - r)$, $a_2 = r\zeta(2r - 1)/4 - 1/(64\beta^2)$, $a_3 = \zeta/(256\beta^2) - r^2\zeta^2/16$, $a_4 = -\zeta^2/(64\beta)^2$, and only solutions with positive J are allowed.

The solution is of the form

$$0 \leq J^2 < \eta_1^2 \frac{4}{\zeta} \quad (6.28)$$

where η_1 is a function of r , β and ζ . The function η_1 will be shown to be equal to unity. The boundary unitarity class B^X is written as

$$B^X \equiv \{J | a_{11}^J - a_{11}^{J^2} - a_{21}^{J^2} = 0, \tilde{\mu}_J \geq 0\}. \quad (6.29)$$

The constraint $a_{11}^J - a_{11}^{J^2} - a_{21}^{J^2} = 0$ can be written as a quadratic equation:

$$\tilde{\mu}_J^2 + \tilde{\mu}_J + f_1(J) = 0, \quad (6.30)$$

where

$$f_1(J) = a_1 + a_2 J^2 + a_3 J^4 + a_4 J^6. \quad (6.31)$$

The solutions are

$$\tilde{\mu}_J = \frac{1}{2} \left\{ \pm \sqrt{1 - 4f_1(J)} - 1 \right\}. \quad (6.32)$$

The function $f_1(J)$ is negative for $J^2 > 4/\zeta$ and therefore $\tilde{\mu}_J$ is positive for such J values. By definition $\tilde{\mu}_J \geq 0$. Consequently, only the positive solution is chosen;

$$\tilde{\mu}_J = \frac{1}{2} \left\{ \sqrt{1 - 4f_1(J)} - 1 \right\}. \quad (6.33)$$

To summarize $I^X \equiv \{J | a_{11}^J - a_{11}^{J^2} - a_{21}^{J^2} > 0, 0 \leq J \leq M_1\}$ non-empty:

$$I^X \equiv \{J | a_{11}^J - a_{11}^{J^2} - a_{21}^{J^2} > 0, 0 \leq J \leq M_1\}, \quad (6.34)$$

$$B^X \equiv \{J | a_{11}^J - a_{11}^{J^2} - a_{21}^{J^2} = 0, M_1 + 1 \leq J \leq M_2\}, \quad (6.35)$$

with $\eta_1 = 1$, where $M_1 = \text{Floor} \left[\sqrt{4/\zeta} \right]$, $M_2 = \text{Floor} \left[\sqrt{8/\zeta} \right]$ and $\zeta = -t/k^2$. It is important to notice that with $\eta_1 = 1$ both interior unitarity classes, I^W and I^X , are non-empty over the same region, $J \in [0, M_1]$. Similarly the boundary unitarity classes, B^W and B^X , are non-empty over the same region, $J \in [M_1 + 1, M_2]$. In other words there is no mixing of unitarity classes, all classes either interior unitarity classes or boundary unitarity are classes for a given J .

The unitarity classes $I^W \cup I^X$, $B^W \cup B^X$ and the union $I^W \cup I^X \cup B^W \cup B^X$ are considered.

3 Solution of Interior Unitarity Class

Consider the set of interior classes $I \equiv I^W \cup I^X$. The inequality multipliers, $\tilde{\lambda}_J$ and $\tilde{\mu}_J$, in the interior region are equal to zero. The imaginary partial wave amplitudes are

$$a_k^J = r \left(1 - \frac{\zeta}{4} J^2 \right) \quad (6.36)$$

and

$$a_{21}^J = \frac{J}{8\beta} \left(1 - \frac{\zeta}{8} J^2 \right), \quad (6.37)$$

$k = 0, 1, 11, 22$, with $0 \leq J \leq M_1$, where M_1 is the maximum J corresponding to positive partial wave amplitudes ($a_k^J > 0$) and is equal to $\text{Floor} \left[\sqrt{4/\zeta} \right]$. The $\text{Floor} \left[\sqrt{4/\zeta} \right]$ function gives the greatest integer less than or equal to $\sqrt{4/\zeta}$. The imaginary spin average non-flip amplitude $\text{Im } \phi_+^I$ is reconstructed by substituting Equation (6.36) into the partial wave expansion

$$\text{Im } \phi_+^I = \sum_{J=0}^{M_1} J \left\{ a_0^J(s) + a_1^J(s) + a_{11}^J(s) + a_{22}^J(s) \right\} \left(1 - \frac{\zeta}{4} J^2 \right) \quad (6.38)$$

to give

$$\text{Im } \phi_+^I = 4r \sum_{J=0}^{M_1} J \left(1 - \frac{\zeta}{4} J^2 \right)^2 \quad (6.39)$$

where superscript I denotes the contribution from the interior unitarity class $I \equiv I^W \cup I^X$. The Euler-MacLaurin expansion [78, 79] for large J is used to write the imaginary spin average non-flip amplitude as an integration over J :

$$\text{Im } \phi_+^I \approx 4r \int_0^{M_1} dJ \left(J - \frac{\zeta}{2} J^3 + \frac{\zeta^2}{16} J^5 \right) \quad (6.40)$$

$$\approx 2rM_1^2 - \frac{r\zeta}{2}M_1^4 + \frac{r\zeta^2}{24}M_1^6. \quad (6.41)$$

Substituting $M_1 \approx \sqrt{4/\zeta}$ into this Euler-MacLaurin expansion leads to

$$\text{Im } \phi_+^I \approx \frac{8}{3\zeta} r. \quad (6.42)$$

Similarly Σ_{el}^I is reconstructed by substituting Equations (6.36) and (6.37) into the partial wave expansion

$$\Sigma_{\text{el}}^I = 2 \sum_{J=0}^{M_1} J \left(a_0^{J^2} + a_1^{J^2} + a_{11}^{J^2} + a_{22}^{J^2} + 2a_{21}^{J^2} \right) \quad (6.43)$$

to give

$$\Sigma_{\text{el}}^I \approx \frac{32}{6\zeta} r^2 + \frac{1}{\beta^2} \frac{11}{96\zeta^2} \quad (6.44)$$

for large J . The equality multiplier

$$r = \frac{3}{8} \zeta \text{Im } \phi_+^I \quad (6.45)$$

is found by manipulating Equation (6.42). The solution of Equation (6.44)

is simply

$$\frac{1}{\beta} = \sqrt{\frac{96}{11}} \zeta \left(\Sigma_{\text{el}}^I - \frac{32}{6\zeta} r^2 \right)^{1/2} \quad (6.46)$$

or

$$\frac{1}{\beta} = \sqrt{\frac{96}{11}} \zeta \left(\Sigma_{\text{el}}^I - \frac{3}{4} \zeta \text{Im} \phi_+^{I 2} \right)^{1/2}. \quad (6.47)$$

The experimental data for σ_{el} and $\text{Im} \phi_+$, given in Tables 5.2, 5.4 and 5.5, is used to find the values of the equality multipliers, r and β , at $t = -0.001 \text{ (GeV/c)}^2$ and $t = -0.01 \text{ (GeV/c)}^2$ over the energy range $\sqrt{s} = 19.4 - 62.5 \text{ GeV}$. The values of r and β are shown in Table 6.1.

Table 6.1: The equality multipliers r and β under σ_{el} , $\text{Im} \phi_+$ and unitarity constraints.

\sqrt{s} (GeV)	$t = -0.001 \text{ (GeV/c)}^2$		$t = -0.01 \text{ (GeV/c)}^2$	
	r	β	r	β
19.4	0.00593	1401	0.0562	164
23.5	0.00599	1702	0.0568	200
30.7	0.00612	2216	0.0579	263
44.7	0.00629	3166	0.0594	376
52.8	0.00653	3699	0.0617	445
62.5	0.00670	4316	0.0632	521

The modified imaginary single-flip amplitude $\text{Im} \tilde{\phi}_5^I$ is reconstructed by

substituting Equation (6.37) into

$$\text{Im } \tilde{\phi}_5^I = \sum_{J=0}^{M_1} J^2 \left(1 - \frac{\zeta}{8} J^2\right) a_{21}^J(s) \quad (6.48)$$

to give

$$\text{Im } \tilde{\phi}_5^I = \frac{1}{8\beta} \sum_{J=0}^{M_1} J^3 \left(1 - \frac{\zeta}{8} J^2\right)^2. \quad (6.49)$$

For large J the modified imaginary single-flip amplitude is written as

$$\text{Im } \tilde{\phi}_5^I \approx \frac{1}{\beta} \frac{11}{48\zeta^2}. \quad (6.50)$$

An analytic expression for modified single-flip amplitude is found by substituting the expression for β into Equation (6.50), this gives

$$\text{Im } \tilde{\phi}_5^I = \sqrt{\frac{11}{24}} \frac{1}{\zeta} \left(\Sigma_{\text{el}}^I - \frac{3}{4} \zeta \text{Im } \phi_+^{I^2}\right)^{1/2}. \quad (6.51)$$

In this unitarity class $\text{Im } \phi_+^I = \text{Im } \phi_+$, $\Sigma_{\text{el}}^I = \Sigma_{\text{el}}$ and $\text{Im } \tilde{\phi}_5^I = \text{Im } \tilde{\phi}_5$, that is, the contribution to the optimized modified single-flip amplitude completely originates in the interior unitarity class, $I \equiv I^W \cup I^X$, and

$$\text{Im } \tilde{\phi}_5 \leq \sqrt{\frac{11}{24}} \frac{1}{\zeta} \left(\Sigma_{\text{el}} - \frac{3}{4} \zeta \text{Im } \phi_+^2\right)^{1/2}. \quad (6.52)$$

The lower bound on $\text{Im } \tilde{\phi}_5$ is simply minus the upper bound;

$$\text{Im } \tilde{\phi}_5 \geq -\sqrt{\frac{11}{24}} \frac{1}{\zeta} \left(\Sigma_{\text{el}} - \frac{3}{4} \zeta \text{Im } \phi_+^2\right)^{1/2}. \quad (6.53)$$

The bound on $|\text{Im } r_5|$, given by $m|\text{Im } \tilde{\phi}_5|/(k \text{Im } \phi_+)$, is

$$|\text{Im } r_5| \leq \sqrt{\frac{11}{24}} \frac{m}{k\zeta} \frac{\left(\Sigma_{\text{el}} - \frac{3}{4} \zeta \text{Im } \phi_+^2\right)^{1/2}}{\text{Im } \phi_+} \quad (6.54)$$

where $\zeta = -t/k^2$.

3.1 Results

Table 6.2 shows the bound on $|\text{Im } r_5|$ evaluated in the CNI region at $t = -0.001, -0.01 \text{ (GeV}/c)^2$ over the kinematical range, $\sqrt{s} = 19.5 - 62.5 \text{ GeV}$.

A number of comments can be made about the bound on $|\text{Im } r_5|$. The bound,

Table 6.2: $|\text{Im } r_5|$ as a function of center-of-mass energy and momentum transfer optimized under σ_{el} , $\text{Im } \phi_+$ and unitarity constraints.

$\sqrt{s} \text{ (GeV)}$	$t = -0.001 \text{ (GeV}/c)^2$	$t = -0.01 \text{ (GeV}/c)^2$
19.4	93.6	8.4
23.5	92.5	8.3
30.7	91.0	8.1
44.7	90.3	8.0
52.8	87.9	7.7
62.5	87.0	7.6

with the imaginary spin average non-flip amplitude, the elastic cross section and unitarity as constraints is an improvement on the previous bound with the elastic cross section and unitarity as constraints. This is expected; the bound improves as more constraints are added to the system. The bound on $|\text{Im } r_5|$ decreases as t increases and the bound has a linear dependence on

the momentum transfer t .

In the interior unitarity class $J_{max} = M_1 = \text{Floor}[\sqrt{4/\zeta}]$ and the partial wave amplitudes are zero for higher J . The partial wave series for the imaginary partial wave amplitude a_{21}^J terminate at $J = M_1$, the largest value of J allowed in the interior unitarity class. For positive values of a_{21}^J , $J_{max} = M_2 = \text{Floor}[\sqrt{8/\zeta}]$. The partial wave series for a_{21}^J is truncated at $J = M_1$ which may result in the loss of information and the bound on $|\text{Im } r_5|$ may be unnecessarily high. The boundary unitarity class $B^W \cup B^X$ is non-empty for $M_1 + 1 \leq J \leq M_2$. In the boundary class none of the partial wave series are truncated and all the amplitudes become zero as J approaches M_2 . The next case to consider is the boundary unitarity class $B \equiv B^W \cup B^X$. The behaviour of the partial wave amplitudes at $\sqrt{s} = 52.8$ GeV, in the interior unitarity class, is shown in Figures 6.2 and 6.3 where the partial wave series terminate at $J = M_1$. Consider the polynomial $f_1(J)$ given by

$$f_1(J) = a_1 + a_2 J^2 + a_3 J^4 + a_4 J^6 > 0 \quad (6.55)$$

where $a_1 = r(1-r)$, $a_2 = r\zeta(2r-1)/4 - 1/(64\beta^2)$, $a_3 = \zeta/(256\beta^2) - r^2\zeta^2/16$ and $a_4 = -\zeta^2/(64\beta)^2$. The interior unitarity class I^X defined in Equation (6.35) can be redefined as

$$I^X \equiv \{J \mid f_1(J) > 0, \tilde{\mu}_J = 0\} . \quad (6.56)$$

The value of J satisfying $f_1(J) > 0$ was found to be

$$0 \leq J^2 < \eta_1^2 \frac{4}{\zeta} \quad (6.57)$$

with η_1^2 set to unity. The polynomial $f_1(J)$, shown in Figure 6.1, can be plot by substituting the numerical values for r and β , at $\sqrt{s} = 52.8$ GeV and $t = -0.001$ (GeV/c)². The maximum J , with $\eta_1^2 = 1$, at $\sqrt{s} = 52.8$ GeV is 1668. The maximum J for $f_1(J) > 0$, from Figure 6.1, is 1668 implying $\eta_1 \sim 1$. The is true for all kinematical values considered in the Thesis.

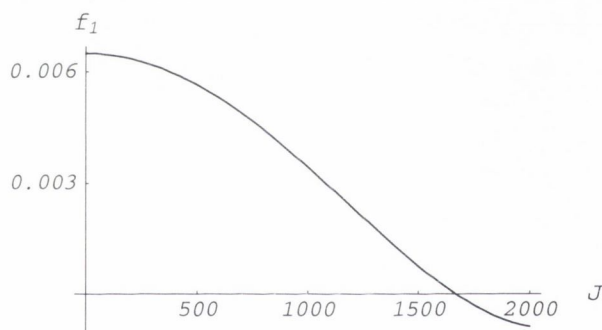


Figure 6.1: Behaviour of the polynomial $f_1(J)$.

Partial Wave Plots

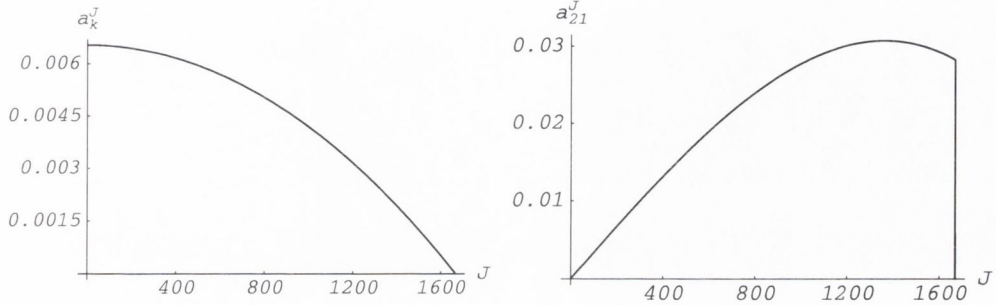


Figure 6.2: a_k^J ($k = 0, 1, 11, 22$) and a_{21}^J optimized under σ_{el} , $\text{Im } \phi_+$ and unitarity in the interior unitarity class; $\sqrt{s} = 52.8$ GeV, $t = -0.001$ (GeV/c)².

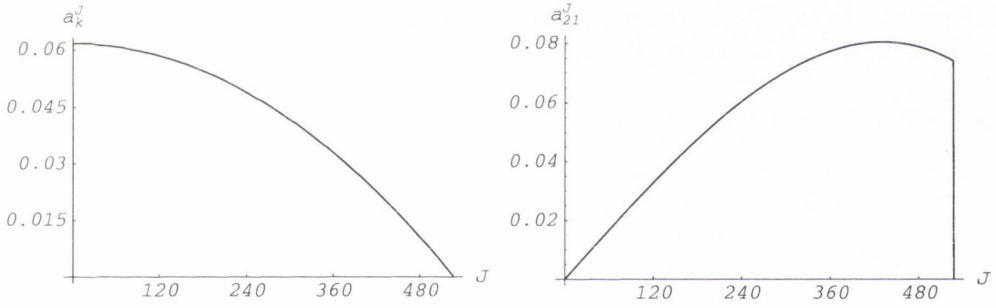


Figure 6.3: a_k^J ($k = 0, 1, 11, 22$) and a_{21}^J optimized under σ_{el} , $\text{Im } \phi_+$ and unitarity in the interior unitarity class; $\sqrt{s} = 52.8$ GeV, $t = -0.01$ (GeV/c)².

4 Solution of Boundary Unitarity Class

In this unitarity class the value of J is limited to

$$M_1 + 1 \leq J \leq M_2 \quad (6.58)$$

where $M_1 = \text{Floor}[\sqrt{4/\zeta}]$, $M_2 = \text{Floor}[\sqrt{8/\zeta}]$ and $\zeta = -t/k^2$. The unitarity constraint in the boundary unitarity class, $a_{11}^J - a_{11}^{J^2} - a_{21}^{J^2} = 0$, leads to the expression for the partial wave amplitude a_{11}^J :

$$a_{11}^J = \frac{1}{2} \left\{ 1 \pm \sqrt{1 - 4 a_{21}^{J^2}} \right\}. \quad (6.59)$$

Therefore the partial wave amplitude a_{11}^J must be positive in the boundary unitarity class. The expression for the imaginary spin average helicity non-flip amplitude is

$$\text{Im } \phi_+^B = 2 \sum_{J=M_1+1}^{M_2} J a_{11}^J \left(1 - \frac{\zeta}{4} J^2 \right). \quad (6.60)$$

For $M_1 + 1 \leq J \leq M_2$, the term $(1 - \zeta/4 J^2)$ is negative and a_{11}^J is positive, consequently $\text{Im } \phi_+^B$ is negative inside the boundary unitarity class. The experimental value of $\text{Im } \phi_+$ is positive and by including only the boundary unitarity class, where $\text{Im } \phi_+^B = \text{Im } \phi_+$, the system is not solvable. To solve the system in the boundary unitarity class, the interior unitarity class must also be considered, where $\text{Im } \phi_+^I + \text{Im } \phi_+^B = \text{Im } \phi_+$.

5 Interior and Boundary Unitarity Classes

The set of unitarity classes $I \cup B$ or $I^W \cup I^X \cup B^W \cup B^X$ is considered. In summary, inside the interior unitarity class I , the value J can take is limited to $0 \leq J \leq M_1$. The system constraints are given by

$$\text{Im } \phi_+^I = \frac{8}{3\zeta} r \quad (6.61)$$

$$\Sigma_{\text{el}}^I = \frac{32}{6\zeta} r^2 + \frac{1}{\beta^2} \frac{11}{96\zeta^2} \quad (6.62)$$

with imaginary partial wave amplitudes

$$a_k^J = r \left(1 - \frac{\zeta}{4} J^2 \right) \quad (6.63)$$

and

$$a_{21}^J = \frac{J}{8\beta} \left(1 - \frac{\zeta}{8} J^2 \right) \quad (6.64)$$

where $k = 0, 1, 11, 22$ and $\zeta = -t/k^2$. The modified helicity single-flip amplitude is

$$\text{Im } \tilde{\phi}_5^I \approx \frac{1}{\beta} \frac{11}{48\zeta^2}. \quad (6.65)$$

The equality multiplier β expressed in terms of the system constraints is

$$\frac{1}{\beta} = \sqrt{\frac{96}{11}} \zeta \left(\Sigma_{\text{el}}^I - \frac{3}{4} \zeta \text{Im } \phi_+^{I^2} \right)^{1/2}. \quad (6.66)$$

Consider the case when

$$\Sigma_{\text{el}}^I = \frac{3}{4} \zeta \text{Im } \phi_+^{I^2}. \quad (6.67)$$

The reciprocal of the equality multiplier β is zero and as a result the imaginary partial wave amplitude a_{21}^J is zero inside the interior unitarity class, I . If the imaginary partial wave amplitude a_{21}^J is zero then

$$\text{Im } \tilde{\phi}_5^I = 0. \quad (6.68)$$

Therefore there is no contribution to the modified imaginary helicity single-flip amplitude inside the interior unitarity region I . The system constraints are rewritten as

$$\text{Im } \phi_+^I = \frac{8}{3\zeta} r \quad (6.69)$$

$$\Sigma_{\text{el}}^I = \frac{32}{6\zeta} r^2 \quad (6.70)$$

with imaginary partial wave amplitudes

$$a_k^J = r \left(1 - \frac{\zeta}{4} J^2 \right) \quad (6.71)$$

and

$$a_{21}^J = 0 \quad (6.72)$$

and the equality multipliers, r and β , in the interior unitarity class I are given by

$$r = \frac{\Sigma_{\text{el}}^I}{2 \text{Im } \phi_+^I} \quad (6.73)$$

and

$$\frac{1}{\beta} = 0. \quad (6.74)$$

5.1 Numerical Technique

To solve the system, with both interior and boundary unitarity classes, a numerical technique is required. The system cannot be solved analytically because of the complex nature of Jacobi-Elliptical integrals and solutions cannot be obtained with the use of `mathematica`. The numerical technique, combining `mathematica` with analytic calculations, is successfully applied and a bound on $|\text{Im } r_5|$ is derived. A detailed description of the numerical technique follows.

What fraction of Σ_{el} falls into the interior class I? The contribution in the interior region Σ_{el}^I is a fraction of the total normalized dimensionless elastic cross section Σ_{el} given by

$$\Sigma_{\text{el}}^I = n \Sigma_{\text{el}} \quad (6.75)$$

where $0 \leq n \leq 1$. In the interior region $\Sigma_{\text{el}}^I = 3/4 \zeta \text{Im } \phi_+^I{}^2$ and the fraction n is the ratio $\Sigma_{\text{el}}^I / \Sigma_{\text{el}}$;

$$n = \frac{3}{4} \zeta \frac{\text{Im } \phi_+^I{}^2}{\Sigma_{\text{el}}}. \quad (6.76)$$

The contribution to Σ_{el} from the boundary unitarity class B is therefore

$$\Sigma_{\text{el}}^B = (1 - n) \Sigma_{\text{el}}. \quad (6.77)$$

What fraction of the imaginary spin average amplitude falls into the interior class I? Assume the contribution to $\text{Im } \phi_+$ in the interior

class is 100% and the contribution from the boundary class B is zero, that is,

$$\text{Im } \phi_+ = \text{Im } \phi_+^I + \text{Im } \phi_+^B = \text{Im } \phi_+^I + 0 = \text{Im } \phi_+^I. \quad (6.78)$$

It will be shown, using an iterative technique, that $\text{Im } \phi_+^B < 0$ and $\text{Im } \phi_+^I > \text{Im } \phi_+$ such that $\text{Im } \phi_+^I + \text{Im } \phi_+^B = \text{Im } \phi_+$. In the boundary unitarity class $B \equiv B^W \cup B^X$, by setting $\text{Im } \phi_+^B = 0$, the system is constrained by partial wave unitarity and by the elastic cross section; $\text{Im } \phi_+$ is not a constraint in the boundary unitarity class.

In Chapter 5, the system, with partial wave unitarity and the elastic cross section as constraints, was solved in the boundary unitarity class. The same method is followed. In the boundary unitarity class, $B \equiv B^W \cup B^X$, the optimized partial waves, at a fixed t in the CNI region, can be written as

$$a_{11}^J = a_{22}^J = \frac{1}{2} \left(1 - \frac{4\beta}{Q(J)} \right) \quad (6.79)$$

and

$$a_{21}^J = \frac{J}{2} \frac{\left(1 - \frac{\zeta}{8} J^2 \right)}{Q(J)}, \quad (6.80)$$

where

$$Q(J) = \sqrt{16\beta^2 + J^2 - \frac{\zeta}{4} J^4 + \frac{\zeta^2}{64} J^6}, \quad (6.81)$$

with $M_1 + 1 \leq J \leq M_2$. When $J = M_1$ the interior unitarity class terminates and M_2 is the maximum J corresponding to positive partial wave amplitudes

where

$$M_1 = \text{Floor} \left[\sqrt{4/\zeta} \right] \quad (6.82)$$

and

$$M_2 = \text{Floor} \left[\sqrt{8/\zeta} \right]. \quad (6.83)$$

The $\text{Floor}[x]$ function gives the greatest integer less than or equal to x .

The observable Σ_{el} and the objective function $\text{Im} \tilde{\phi}_5^B$ are reconstructed by substituting Equations (6.79) and (6.80) into

$$\Sigma_{\text{el}}^B = 4 \sum_{J=M_1+1}^{M_2} J \left(a_{11}^J{}^2 + a_{21}^J{}^2 \right) \quad (6.84)$$

and

$$\text{Im} \tilde{\phi}_5^B = \sum_{J=M_1+1}^{M_2} J^2 \left(1 - \frac{\zeta}{8} J^2 \right) a_{21}^J \quad (6.85)$$

to give

$$\Sigma_{\text{el}}^B = \sum_{J=M_1+1}^{M_2} \left(J - \frac{8\beta J}{Q(J)} + \frac{16\beta^2 J}{Q(J)^2} + \frac{J^3}{Q(J)^2} - \frac{\zeta J^5}{4Q(J)^2} + \frac{\zeta^2 J^7}{64Q(J)^2} \right) \quad (6.86)$$

and

$$\text{Im} \tilde{\phi}_5^B = \sum_{J=M_1+1}^{M_2} \left(\frac{J^3}{2Q(J)} - \frac{\zeta J^5}{8Q(J)} + \frac{\zeta^2 J^7}{128Q(J)} \right). \quad (6.87)$$

For large J we can replace the summation over J by an integration over J [78, 79] which leads to

$$\Sigma_{\text{el}}^B \approx \frac{1}{2} \left(M_2^2 - (M_1 + 1)^2 \right) - 8\beta I_1 + 16\beta^2 I_2 + I_4 - \frac{\zeta}{4} I_6 + \frac{\zeta^2}{64} I_8 \quad (6.88)$$

and

$$\text{Im} \tilde{\phi}_5^B \approx \frac{1}{2} I_3 - \frac{\zeta}{8} I_5 + \frac{\zeta^2}{128} I_7. \quad (6.89)$$

The Jacobi-Elliptical integrals, I_j ($j = 1, \dots, 8$), are given by

$$\begin{aligned}
I_1 &= \int_{M_1+1}^{M_2} dJ \frac{J}{Q(J)} & I_2 &= \int_{M_1+1}^{M_2} dJ \frac{J}{Q(J)^2} \\
I_3 &= \int_{M_1+1}^{M_2} dJ \frac{J^3}{Q(J)} & I_4 &= \int_{M_1+1}^{M_2} dJ \frac{J^3}{Q(J)^2} \\
I_5 &= \int_{M_1+1}^{M_2} dJ \frac{J^5}{Q(J)} & I_6 &= \int_{M_1+1}^{M_2} dJ \frac{J^5}{Q(J)^2} \\
I_7 &= \int_{M_1+1}^{M_2} dJ \frac{J^7}{Q(J)} & I_8 &= \int_{M_1+1}^{M_2} dJ \frac{J^7}{Q(J)^2}.
\end{aligned} \tag{6.90}$$

To numerically solve the system and calculate a bound on $|\text{Im } r_5|$, the kinematical values $\sqrt{s} = 52.8$ GeV and $t = -0.001$ (GeV/c)² are chosen as *sample* points. The experimental data in Tables 5.2 and 5.4 give the values $\Sigma_{\text{el}} = 4214$ and $\text{Im } \phi_+ = 12128$. The fraction n of Σ_{el} in the interior unitarity class I , given by Equation (6.76), is 0.003765 and the contribution to Σ_{el} in the boundary unitarity class B , given by Equation (6.77), is 4056. Rewriting Equation (6.88) as

$$4056 = \frac{1}{2} \left(M_2^2 - (M_1 + 1)^2 \right) - 8\beta I_1 + 16\beta^2 I_2 + I_4 - \frac{\zeta}{4} I_6 + \frac{\zeta^2}{64} I_8, \tag{6.91}$$

enables a solution for β to be found, where $\beta = 2487$. When reconstructing Σ_{el}^B , where

$$\Sigma_{\text{el}}^B = 4 \sum_{J=M_1+1}^{M_2} J \left(a_{11}^J{}^2 + a_{21}^J{}^2 \right) \tag{6.92}$$

with

$$a_{11}^J = a_{22}^J = \frac{1}{2} \left(1 - \frac{4\beta}{Q(J)} \right) \tag{6.93}$$

and

$$a_{21}^J = \frac{J}{2} \frac{\left(1 - \frac{\zeta}{8} J^2\right)}{Q(J)}, \quad (6.94)$$

the imaginary partial wave amplitude a_{11}^J is found to be non-zero. The constraint

$$\text{Im } \phi_+^B = 2 \sum_{J=M_1+1}^{M_2} J a_{11}^J \left(1 - \frac{\zeta}{4} J^2\right) \quad (6.95)$$

initially set to zero, is a function of a_{11}^J . Substituting the expression for a_{11}^J , with the solved multiplier value, into $\text{Im } \phi_+^B$ results in the non-zero value of -570 . In the interior unitarity class the contribution to $\text{Im } \tilde{\phi}_5$ is zero when the fraction of Σ_{el} in the class is given by

$$n = \frac{3}{4} \zeta \frac{\text{Im } \phi_+^I{}^2}{\Sigma_{\text{el}}}. \quad (6.96)$$

To satisfy the condition $\text{Im } \phi_+ = 12128 = \text{Im } \phi_+^I + \text{Im } \phi_+^B$ the value of $\text{Im } \phi_+^I$ is adjusted to $\text{Im } \phi_+ - \text{Im } \phi_+^B = 12128 + 569 = 12697$. The value of $\text{Im } \phi_+^I$ increases and consequently the fraction n of Σ_{el} in the interior unitarity class also increases, to a value of 0.04127 . The contribution to Σ_{el} in the boundary unitarity class B becomes $4041 = (1 - n)\Sigma_{\text{el}}$ and the equation

$$4041 = \frac{1}{2} \left(M_2^2 - (M_1 + 1)^2 \right) - 8\beta I_1 + 16\beta^2 I_2 + I_4 - \frac{\zeta}{4} I_6 + \frac{\zeta^2}{64} I_8 \quad (6.97)$$

is solved for β with solution $\beta = 2492$. A value of -567 for $\text{Im } \phi_+^B$ is calculated after reconstruction and the condition $\text{Im } \phi_+^I + \text{Im } \phi_+^B = \text{Im } \phi_+$ is satisfied. Reconstructing $\text{Im } \tilde{\phi}_5$ in Equation (6.87) with $\sqrt{s} = 52.8$ GeV,

$t = -0.001 \text{ (GeV}/c)^2$ and $\beta = 2492$, the bound

$$|\text{Im } r_5| \leq 59.2 \quad (6.98)$$

is calculated. The contributions from the two unitarity classes are shown in Table 6.3.

Table 6.3: Contributions from the $I \cup B$ unitarity classes with σ_{el} , $\text{Im } \phi_+$ and unitarity constraints; $\sqrt{s} = 52.8 \text{ GeV}$, $t = -0.001 \text{ (GeV}/c)^2$.

	$I \equiv I^U \cup I^V \cup I^W \cup I^X$ $0 \leq J \leq 1668$	$B \equiv B^{U_0} \cup B^{V_0} \cup B^W \cup B^X$ $1669 \leq J \leq 2359$
r	0.00685	0
$1/\beta$	0	4.012×10^{-4}
$\text{Im } \phi_+$	12697	-567
Σ_{el}	174	4041
$\text{Im } r_5$	0	59.2

5.2 Results

The bound on $|\text{Im } r_5|$ is calculated by adding the contributions from the interior and boundary unitarity classes. The contribution from the interior

unitarity class is always zero and the contribution to the bound comes entirely from the boundary unitarity class.

Momentum transfer $t = -0.001 \text{ (GeV/c)}^2$

In the kinematical region $\sqrt{s} = 19.4 - 62.5 \text{ GeV}$ at $t = -0.001 \text{ (GeV/c)}^2$ the bound on $|\text{Im } r_5|$ varies from 63.8 down to 58.6, Tables 6.4 and 6.5 list the contributions from the interior and boundary unitarity classes, respectively. To calculate the upper on $|\text{Im } r_5|$ the contributions from the two unitarity classes are simply added and to find the values of the observables the contributions from the two unitarity classes are also added. As expected the

Table 6.4: Contributions from $I \subset I \cup B$ with σ_{el} , $\text{Im } \phi_+$ and unitarity constraints; $t = -0.001 \text{ (GeV/c)}^2$.

$\sqrt{s} \text{ (GeV)}$	$J \text{ range}$	$n \text{ (\%)}$	r	$1/\beta$	Σ_{el}	$\text{Im } \phi_+$	$\text{Im } r_5$
19.4	[0, 610]	3.66	0.00621	0	19	1545	0
23.5	[0, 740]	3.74	0.00628	0	29	2298	0
30.7	[0, 969]	3.86	0.00641	0	52	4016	0
44.7	[0, 1412]	3.92	0.00659	0	116	8769	0
52.8	[0, 1668]	4.12	0.00684	0	174	12705	0
62.5	[0, 1975]	4.21	0.00702	0	257	18268	0

Table 6.5: Contributions from $B \subset I \cup B$ with σ_{el} , $\text{Im } \phi_+$ and unitarity constraints; $t = -0.001 \text{ (GeV}/c)^2$.

\sqrt{s} (GeV)	J range	$(1 - n)$ (%)	r	β	Σ_{el}	$\text{Im } \phi_+$	$\text{Im } r_5$
19.4	[611, 863]	96.34	0	947	505	-70	63.8
23.5	[741, 1047]	96.26	0	1147	742	-104	62.4
30.7	[970, 1370]	96.14	0	1491	1281	-180	61.2
44.7	[1413, 1997]	96.08	0	2132	2831	-398	60.8
52.8	[1669, 2359]	95.88	0	2493	4041	-567	59.2
62.5	[1976, 2793]	95.79	0	2909	5832	-818	58.6

contribution to $|\text{Im } r_5|$ from the interior unitarity class is zero and the majority of the contribution to Σ_{el} comes from the boundary unitarity class. To restrict the bound on $|\text{Im } r_5|$ the contribution to Σ_{el} in the boundary unitarity class, given by $(1 - n)$, must be reduced. The reduction of this contribution has the effect of reducing the contribution from the imaginary partial wave amplitude a_{21}^J . The only partial wave amplitude the bound depends on is a_{21}^J and therefore a reduction in the contribution from the imaginary partial wave amplitude a_{21}^J in the boundary unitarity class should reduce the bound on $|\text{Im } r_5|$. In previous calculations the bound on $|\text{Im } r_5|$ was considerably higher. When solving the system without contributions from the boundary

unitarity class and with contributions only from the interior unitarity class the bound on $|\text{Im } r_5|$, in the same kinematical range, varies from 93.6 down to 87.0. When the system is constrained by partial wave unitarity and the elastic cross section σ_{el} , also in the same kinematical region, the bound on $|\text{Im } r_5|$ varies from 114.8 down to 107.0.

Momentum transfer $t = -0.01 \text{ (GeV/c)}^2$

In the kinematical region $\sqrt{s} = 19.4 - 62.5 \text{ GeV}$ at $t = -0.01 \text{ (GeV/c)}^2$ the bound on $|\text{Im } r_5|$ varies from 5.6 down to 5.0, the complete set of results are given Tables 6.6 and 6.7 The contribution to $|\text{Im } r_5|$ from the interior unitarity class is again zero. The majority of the contribution to Σ_{el} remains in the boundary unitarity class. When solving the system without contributions from the boundary unitarity class and with contributions only from the interior unitarity class the bound on $|\text{Im } r_5|$, in the same kinematical range, varies from 8.4 down to 7.6. When the system is constrained by partial wave unitarity and the elastic cross section σ_{el} , in the same kinematical region, the bound on $|\text{Im } r_5|$ varies from 12.1 down to 11.3.

The bound on $|\text{Im } r_5|$ derived with, partial wave unitarity, the elastic cross section σ_{el} and the imaginary spin average non-flip amplitude $\text{Im } \phi_+$, expressed as constraints, is a definite improvement on the previous $|\text{Im } r_5|$ bound. There is an overall improvement on the $|\text{Im } r_5|$ bound, although the

value is far from the 4.48% threshold necessary to successfully use the pp CNI analyzing power as a polarimeter with a maximum beam polarization error of 5%.

Table 6.6: Contributions from $I \subset I \cup B$ with σ_{el} , $\text{Im} \phi_+$ and unitarity constraints; $t = -0.01 \text{ (GeV}/c)^2$.

\sqrt{s} (GeV)	J range	n (%)	r	$1/\beta$	Σ_{el}	$\text{Im} \phi_+$	$\text{Im} r_5$
19.4	[0, 193]	32.27	0.0583	0	169	1451	0
23.5	[0, 234]	32.99	0.0589	0	254	2157	0
30.7	[0, 306]	33.89	0.0600	0	452	3760	0
44.7	[0, 446]	34.19	0.0615	0	1008	8186	0
52.8	[0, 527]	35.89	0.0638	0	1513	11849	0
62.5	[0, 624]	36.57	0.0654	0	2227	17020	0

Table 6.7: Contributions from $B \subset I \cup B$ with σ_{el} , $\text{Im} \phi_+$ and unitarity constraints; $t = -0.01 \text{ (GeV}/c)^2$.

\sqrt{s} (GeV)	J range	$(1 - n)$ (%)	r	β	Σ_{el}	$\text{Im} \phi_+$	$\text{Im} r_5$
19.4	[194, 273]	67.73	0	112	355	-50	5.6
23.5	[235, 331]	67.01	0	135	516	-74	5.5
30.7	[307, 433]	66.11	0	178	881	-125	5.5
44.7	[447, 631]	65.81	0	255	1939	-274	5.7
52.8	[528, 746]	64.11	0	302	2702	-382	5.1
62.5	[625, 883]	63.43	0	354	3862	-54	5.0

In the next and final Chapter a new bound on $|\text{Im} r_5|$ is derived. The penalty function $\text{Im} \tilde{\phi}_5$ is constrained by an extra observable- the total cross section σ_{tot} . The extra constraint in the system has the desired effect of reducing the bound on $|\text{Im} r_5|$ to a value less than one at $\sqrt{s} = 50 \text{ GeV}$ and with momentum transfers in the CNI region.

Partial Wave Plots

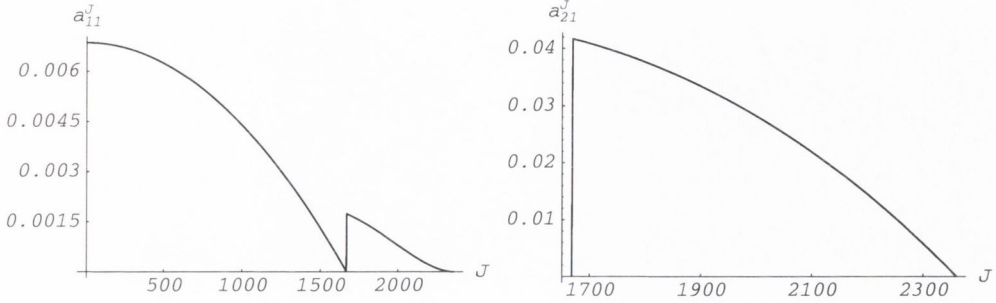


Figure 6.4: a_{11}^J and a_{21}^J optimized under σ_{el} , $\text{Im } \phi_+$ and unitarity constraints in the $I \cup B$ unitarity class; $\sqrt{s} = 52.8 \text{ GeV}$, $t = -0.001 \text{ (GeV/c)}^2$.

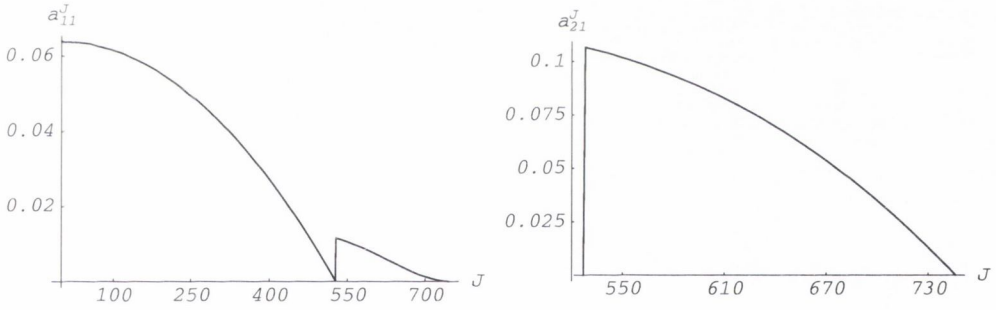


Figure 6.5: a_{11}^J and a_{21}^J optimized under σ_{el} , $\text{Im } \phi_+$ and unitarity constraints in the $I \cup B$ unitarity class; $\sqrt{s} = 52.8 \text{ GeV}$, $t = -0.01 \text{ (GeV/c)}^2$.

Chapter 7

Optimization including σ_{tot}

To improve the previous bound on $|\text{Im } r_5|$ another equality constraint is added to the Lagrange function. This new equality constraint is the total cross section, σ_{tot} , expressed as a normalized dimensionless total cross section with the partial wave expansion

$$A_0 - \sum_J (2J + 1) \{a_0^J + a_1^J + a_{11}^J + a_{22}^J\}. \quad (7.1)$$

Included in the Lagrange function are the equality constraints;

$$\Sigma_{el} - \sum_J (2J + 1) (|f_0^J|^2 + |f_1^J|^2 + |f_{11}^J|^2 + |f_{22}^J|^2 + 2|f_{21}^J|^2) \quad (7.2)$$

and

$$\text{Im } \phi_+ - \frac{\sqrt{s}}{4k} \sum_J (2J + 1) \{a_0^J(s) + a_1^J(s) + a_{11}^J(s) + a_{22}^J(s)\} \left(1 - \frac{\zeta}{4} J(J + 1)\right). \quad (7.3)$$

The unitarity inequalities of Equations (4.64) and (4.65) are again utilized as input inequality constraints. An improved bound on $|\text{Im } r_5|$ in the CNI region is expected. The bound

$$|\text{Im } r_5| \leq m_p \sqrt{g} \left(\frac{36\pi g \sigma_{\text{el}}}{\sigma_{\text{tot}}^2} - 1 \right)^{1/2} \quad (7.4)$$

at zero momentum transfer is derived. At $\sqrt{s} = 52.8$ GeV its value is 0.89, a large improvement on the bounds previously derived in Chapters 5 and 6.

1 Lagrange Formalism

The normalized dimensionless total cross section A_0 , expressed as an equality constraint, is added to the Lagrange function along with the normalized dimensionless elastic cross section Σ_{el} , written as an equality constraint, the imaginary spin average non helicity-flip amplitude $\text{Im } \phi_+$, also expressed as an equality constraint, and the partial wave unitarity relations written as inequality constraints. The modified single helicity-flip amplitude $\text{Im } \tilde{\phi}_5$ is introduced as the objective or penalty function in the Lagrange function:

$$\begin{aligned}
\mathcal{L} = & \operatorname{Im} \tilde{\phi}_5 + \alpha \left[A_0 - \sum_J (2J+1) \{ a_0^J(s) + a_1^J(s) + a_{11}^J(s) + a_{22}^J(s) \} \right] \\
& + \beta \left[\Sigma_{el} - \sum_J (2J+1) (|f_0^J|^2 + |f_1^J|^2 + |f_{11}^J|^2 + |f_{22}^J|^2 + 2|f_{21}^J|^2) \right] \\
& + \gamma \left[\operatorname{Im} \phi_+ - \frac{\sqrt{s}}{4k} \sum_J (2J+1) \{ a_0^J(s) + a_1^J(s) + a_{11}^J(s) + a_{22}^J(s) \} \left(1 - \frac{\zeta}{4} J(J+1) \right) \right] \\
& + \sum_J (2J+1) \mu_J (a_{11}^J + a_{22}^J - |f_{11}^J|^2 - |f_{22}^J|^2 - 2|f_{21}^J|^2) \\
& + \sum_J (2J+1) \lambda_J (a_0^J + a_1^J - |f_0^J|^2 - |f_1^J|^2)
\end{aligned} \tag{7.5}$$

where α , β and γ are equality multipliers. The inequality multipliers, λ_J and μ_J are by definition non-negative and $\zeta = -t/(k^2)$. In the high energy or large J limit only the leading order J terms are included and the Lagrange function of Equation (7.5) becomes

$$\begin{aligned}
\mathcal{L} = & \operatorname{Im} \tilde{\phi}_5 + \alpha \left[A_0 - 2 \sum_J J \{ a_0^J(s) + a_1^J(s) + a_{11}^J(s) + a_{22}^J(s) \} \right] \\
& + \beta \left[\Sigma_{el} - 2 \sum_J J (|f_0^J|^2 + |f_1^J|^2 + |f_{11}^J|^2 + |f_{22}^J|^2 + 2|f_{21}^J|^2) \right] \\
& + \gamma \left[\operatorname{Im} \phi_+ - \sum_J J \{ a_0^J(s) + a_1^J(s) + a_{11}^J(s) + a_{22}^J(s) \} \left(1 - \frac{\zeta}{4} J^2 \right) \right] \\
& + 2 \sum_J J \mu_J (a_{11}^J + a_{22}^J - |f_{11}^J|^2 - |f_{22}^J|^2 - 2|f_{21}^J|^2) \\
& + 2 \sum_J J \lambda_J (a_0^J + a_1^J - |f_0^J|^2 - |f_1^J|^2)
\end{aligned} \tag{7.6}$$

and

$$\operatorname{Im} \tilde{\phi}_5 \approx \sum_J J^2 \left(1 - \frac{\zeta}{8} J^2 \right) a_{21}^J(s). \tag{7.7}$$

The system is optimized by taking first and second derivatives with respect to the real and imaginary partial wave amplitudes, b_i^J and a_i^J . This gives the optimized set of partial waves, at some fixed t in the CNI region;

$$b_i^J = 0 \quad \forall i, \quad (7.8)$$

$$a_0^J = a_1^J = \frac{r_1 + r_2 \left(1 - \frac{\zeta}{4} J^2\right) + \tilde{\lambda}_J}{1 + 2\tilde{\lambda}_J}, \quad (7.9)$$

$$a_{11}^J = a_{22}^J = \frac{r_1 + r_2 \left(1 - \frac{\zeta}{4} J^2\right) + \tilde{\mu}_J}{1 + 2\tilde{\mu}_J} \quad (7.10)$$

and

$$a_{21}^J = \frac{\frac{J}{8\beta} \left(1 - \frac{\zeta}{8} J^2\right)}{1 + 2\tilde{\mu}_J} \quad (7.11)$$

where $\tilde{\lambda}_J = \lambda_J/2\beta$, $\tilde{\mu}_J = \mu_J/2\beta$, $r_1 = -\alpha/(2\beta)$, $r_2 = -\gamma/(4\beta)$ and $\beta > 0$ for a maximum (or $\beta < 0$ for a minimum).

2 Unitarity Classes

Optimization under the four constraints imposes the following conditions:

$$b_i^J = 0 \quad \forall i \implies f_i^J = a_i^J + b_i^J = a_i^J \quad (7.12)$$

$$a_0^J = a_1^J \quad \text{and} \quad a_{11}^J = a_{22}^J. \quad (7.13)$$

The partial wave amplitudes therefore obey the following unitarity inequalities

$$W^J = a_0^J - a_0^{J2} \geq 0 \quad (7.14)$$

and

$$X^J = a_{11}^J - a_{11}^{J^2} - a_{21}^{J^2} \geq 0. \quad (7.15)$$

2.1 I^W and B^W Unitarity Classes

The interior unitarity class I^W , under the four constraints, is expressed as

$$I^W \equiv \{J | 0 < a_0^J < 1, \tilde{\lambda}_J = 0\}. \quad (7.16)$$

In Equation (7.9) $\tilde{\lambda}_J$ is set to zero and the imaginary partial wave amplitude a_0^J in the interior unitarity class becomes

$$a_0^J = r_1 + r_2 \left(1 - \frac{\zeta}{4} J^2\right). \quad (7.17)$$

The constraint $0 < a_0^J < 1$ places the restriction

$$\frac{4}{\zeta} \left(\frac{(r_1 + r_2) - 1}{r_2}\right) < J^2 < \frac{4}{\zeta} \left(1 + \frac{r_1}{r_2}\right) \quad (7.18)$$

on J . When $r_1 + r_2 > 1$ or $r_1 + r_2 < 0$, the solutions for the optimized system are complex and for real solutions the conditions $0 < r_1 + r_2 < 1$ and $r_2 > 0$, must be satisfied. The value of J is limited to

$$0 \leq J^2 < \frac{4}{\zeta} \left(1 + \frac{r_1}{r_2}\right). \quad (7.19)$$

The boundary unitarity class B^W splits into two sub-classes, B^{W_0} and B^{W_1} :

$$\longrightarrow B^{W_0} \equiv \{J | a_0^J = 0, \tilde{\lambda}_J \geq 0\} \quad (7.20)$$

$$B^W \equiv \{J | W_J > 0, \tilde{\lambda}_J \geq 0\} \\ \longrightarrow B^{W_1} \equiv \{J | a_0^J = 1, \tilde{\lambda}_J \geq 0\}. \quad (7.21)$$

In the boundary unitarity class B^{W_0} the imaginary partial wave amplitude a_0^J is equal to zero and from Equation (7.9) the inequality multiplier $\tilde{\lambda}_J$ is given by

$$\tilde{\lambda}_J = -(r_1 + r_2) + r_2 \frac{\zeta}{4} J^2. \quad (7.22)$$

The B^{W_0} class begins at $J^2 = M_1^2 = 4/\zeta (1 + r_1/r_2)$, and for $J \geq M_1 + 1$, with $0 < r_1 + r_2 < 1$ and $r_2 > 0$, the inequality multiplier $\tilde{\lambda}_J$ is positive. Therefore the boundary unitarity class B^{W_0} is non-empty for $J \geq M_1 + 1$ but with $a_0^J = 0$, for all J , there are no contributions from this unitarity class. The imaginary partial wave amplitude a_0^J is equal to unity in the boundary unitarity class B^{W_1} and from Equation (7.9) the inequality multiplier $\tilde{\lambda}_J$ is given by

$$\tilde{\lambda}_J = (r_1 + r_2) - 1 - r_2 \frac{\zeta}{4} J^2. \quad (7.23)$$

By definition $\tilde{\lambda}_J \geq 0$ and the value of J is limited to

$$J^2 \leq \frac{4}{\zeta} \left(\frac{(r_1 + r_2) - 1}{r_2} \right) \quad (7.24)$$

and with $0 < r_1 + r_2 < 1$ and $r_2 > 0$, J^2 is negative, or J is complex. The B^{W_1} class is therefore an empty unitarity class.

In summary, the unitarity classes, I^W and B^{W_0} , are non-empty and the unitarity class B^{W_1} is empty;

$$I^W \equiv \{J | 0 < a_0^J < 1, 0 < J \leq M_1\}, \quad (7.25)$$

$$B^{W_0} \equiv \{J | a_0^J = 0, M_1 + 1 \leq J \leq M_2\} \quad (7.26)$$

where $M_1 = \text{Floor} \left[\sqrt{4/\zeta (1 + r_1/r_2)} \right]$, $M_2 = \text{Floor} \left[\sqrt{8/\zeta} \right]$ and $\zeta = -t/k^2$.

2.2 I^X and B^X Unitarity Classes

The interior unitarity class I^X under the optimization becomes

$$I^X \equiv \{J | a_{11}^J - a_{11}^{J^2} - a_{21}^{J^2} > 0, \tilde{\mu}_J = 0\}, \quad (7.27)$$

Substituting Equations (7.10) and (7.11), with $\tilde{\mu}_J = 0$, into the interior constraint $a_{11}^J - a_{11}^{J^2} - a_{21}^{J^2} > 0$ leads to the equation;

$$f_2(J) = \tilde{a}_1 + \tilde{a}_2 J^2 + \tilde{a}_3 J^4 + \tilde{a}_4 J^6 > 0 \quad (7.28)$$

where $\tilde{a}_1 = (r_1 + r_2)(1 - (r_1 + r_2))$, $\tilde{a}_2 = r_2 \zeta (2(r_1 + r_2) - 1)/4 - 1/(64\beta^2)$, $\tilde{a}_3 = \zeta/(256\beta^2) - r_2^2 \zeta^2/16$, $\tilde{a}_4 = -\zeta^2/(64\beta)^2$, and only positive J solutions are allowed. The solution is of the form

$$0 < J^2 < \eta_2^2 \frac{4}{\zeta} \left(1 + \frac{r_1}{r_2}\right) \quad (7.29)$$

where η_2 is function of r_1 , r_2 , β and ζ . The function η_2 is set to unity, it will be shown later that $\eta_2 \sim 1$ and the bound is slightly adjusted by setting

$\eta_2 = 1$. The boundary unitarity class B^X is written as

$$B^X \equiv \left\{ J \mid a_{11}^J - a_{11}^{J^2} - a_{21}^{J^2} = 0, \tilde{\mu}_J \geq 0 \right\}. \quad (7.30)$$

The constraint $a_{11}^J - a_{11}^{J^2} - a_{21}^{J^2} = 0$ can be written as a quadratic equation:

$$\tilde{\mu}_J^2 + \tilde{\mu}_J + f_2(J) = 0, \quad (7.31)$$

where

$$f_2(J) = \tilde{a}_1 + \tilde{a}_2 J^2 + \tilde{a}_3 J^4 + \tilde{a}_4 J^6 \quad (7.32)$$

The solutions are

$$\tilde{\mu}_J = \frac{1}{2} \left\{ \pm \sqrt{1 - 4f_2(J)} - 1 \right\}. \quad (7.33)$$

The function $f_2(J)$ is negative for $J > M_1 = \text{Floor}[4/\zeta (1 + r_1/r_2)]$ and therefore $\tilde{\mu}_J$ is positive for such J values. By definition $\tilde{\mu}_J \geq 0$, therefore the positive solution is chosen;

$$\tilde{\mu}_J = \frac{1}{2} \left\{ \sqrt{1 - 4f_2(J)} - 1 \right\}. \quad (7.34)$$

To summarize, both the classes, I^X and B^X , are non-empty:

$$I^X \equiv \left\{ J \mid a_{11}^J - a_{11}^{J^2} - a_{21}^{J^2} > 0, 0 \leq J \leq M_1 \right\}, \quad (7.35)$$

$$B^X \equiv \left\{ J \mid a_{11}^J - a_{11}^{J^2} - a_{21}^{J^2} = 0, M_1 + 1 \leq J \leq M_2 \right\}, \quad (7.36)$$

for $\eta_2 = 1$, where

$$M_1 = \text{Floor} \left[\sqrt{4/\zeta (1 + r_1/r_2)} \right], \quad (7.37)$$

$$M_2 = \text{Floor} \left[\sqrt{8/\zeta} \right] \quad (7.38)$$

and $\zeta = -t/k^2$. It is important to notice that with $\eta_2 = 1$ both interior unitarity classes, I^W and I^X , are non-empty over the same region, $J \in [0, M_1]$. Similarly the boundary unitarity classes, B^W and B^X , are non-empty over the same region, $M_1 + 1 \leq J \leq M_2$. In other words there is no mixing of unitarity classes, all classes either interior unitarity classes or boundary unitarity classes for a given J .

The unitarity classes are $I^W \cup I^X$ and the union $I^W \cup I^X \cup B^W \cup B^X$ are considered

3 Solution of Interior Unitarity Class

Consider the set of interior classes, $I \equiv I^W \cup I^X$. The inequality multipliers, $\tilde{\lambda}_J$ and $\tilde{\mu}_J$, in the interior region are equal to zero. The imaginary partial wave amplitudes are therefore written as as

$$a_k^J = r_1 + r_2 \left(1 - \frac{\zeta}{4} J^2 \right) \quad (7.39)$$

and

$$a_{21}^J = \frac{J}{8\beta} \left(1 - \frac{\zeta}{8} J^2 \right), \quad (7.40)$$

$k = 0, 1, 11, 22$, with $0 \leq J \leq M_1$, where $M_1 = \text{Floor} \left[\sqrt{4/\zeta (1 + r_1/r_2)} \right]$ is the maximum J in the interior unitarity class. In this case the contributions

to the observables and to the bound on $\text{Im } \tilde{\phi}_5$ solely comes from this interior unitarity class; $A_0^I = A_0$, $\text{Im } \phi_+^I = \text{Im } \phi_+$, $\Sigma_{\text{el}}^I = \Sigma_{\text{el}}$ and $\text{Im } \tilde{\phi}_5^I = \text{Im } \tilde{\phi}_5$. The normalized dimensionless total cross section is reconstructed by substituting Equation (7.39) into

$$A_0 = \sum_{J=0}^{M_1} J \left(a_0^J + a_1^J + a_{11}^J + a_{22}^J \right) \quad (7.41)$$

to give

$$A_0 = 8 \sum_{J=0}^{M_1} J \left[r_1 + r_2 \left(1 - \frac{\zeta}{4} J^2 \right) \right]. \quad (7.42)$$

The Euler-MacLaurin expansion [78, 79] for large J is used to write the normalized dimensionless total cross section A_0 as an integration over J :

$$A_0 \approx 8 \int_0^{M_1} dJ \left((r_1 + r_2) J - r_2 \frac{\zeta}{4} J^3 \right) \quad (7.43)$$

$$\approx \frac{M_1^2}{2} \left\{ 8(r_1 + r_2) - r_2 \zeta M_1^2 \right\}. \quad (7.44)$$

Similarly the imaginary spin average helicity non-flip amplitude $\text{Im } \phi_+^I$ is reconstructed by substituting Equation (7.39) into

$$\text{Im } \phi_+ = \sum_{J=0}^{M_1} J \left\{ a_0^J + a_1^J + a_{11}^J + a_{22}^J \right\} \left(1 - \frac{\zeta}{4} J^2 \right) \quad (7.45)$$

to give

$$\text{Im } \phi_+ \approx 4 \int_0^{M_1} dJ \left\{ (r_1 + r_2) J - (2r_2 + r_1) \frac{\zeta}{4} J^3 + r_2 \frac{\zeta^2}{16} J^5 \right\} \quad (7.46)$$

$$\approx M_1^2 \left\{ 2(r_1 + r_2) - (2r_2 + r_1) \frac{\zeta}{4} M_1^2 + \frac{r_2 \zeta^2}{24} M_1^4 \right\}. \quad (7.47)$$

The dimensionless normalized elastic cross section Σ_{el}^J , by substituting Equations (7.39) and (7.40) into

$$\Sigma_{\text{el}} = 2 \sum_{J=0}^{M_1} J \left(a_0^{J^2} + a_1^{J^2} + a_{11}^{J^2} + a_{22}^{J^2} + 2a_{21}^{J^2} \right), \quad (7.48)$$

is reconstructed:

$$\begin{aligned} \Sigma_{\text{el}} \approx & \left\{ 4(r_1 + r_2)^2 M_1^2 - (r_1 + r_2)r_2\zeta M_1^4 + \frac{r_2^2\zeta^2}{12} M_1^6 \right\} \\ & + \frac{M_1^4}{64\beta^2} \left\{ 1 - \frac{\zeta}{6} M_1^2 + \frac{\zeta^2}{128} M_1^4 \right\} \end{aligned} \quad (7.49)$$

The modified imaginary single-flip amplitude $\text{Im } \tilde{\phi}_5$ is reconstructed by substituting Equation (7.40) into

$$\text{Im } \tilde{\phi}_5 = \sum_{J=0}^{M_1} J^2 \left(1 - \frac{\zeta}{8} J^2 \right) a_{21}^J \quad (7.50)$$

leading to

$$\text{Im } \tilde{\phi}_5 = \frac{1}{8\beta} \sum_{J=0}^{M_1} J^3 \left(1 - \frac{\zeta}{8} J^2 \right)^2. \quad (7.51)$$

For large J the modified imaginary single-flip amplitude is written as

$$\text{Im } \tilde{\phi}_5 \approx \frac{1}{8\beta} \frac{M_1^4}{4} \left(1 - \frac{\zeta}{6} M_1^2 + \frac{\zeta^2}{128} M_1^4 \right). \quad (7.52)$$

An expression for the equality multiplier β is found by solving Equation (7.49):

$$\beta = \frac{M_1^2 \left\{ 1 - \frac{\zeta}{6} M_1^2 + \frac{\zeta^2}{128} M_1^4 \right\}^{1/2}}{8 \left\{ \Sigma_{\text{el}} - \left(4(r_1 + r_2)^2 M_1^2 - (r_1 + r_2)r_2\zeta M_1^4 + \frac{r_2^2\zeta^2}{12} M_1^6 \right) \right\}^{1/2}}. \quad (7.53)$$

Rewriting the modified imaginary single-flip amplitude one obtains,

$$\begin{aligned} \text{Im } \tilde{\phi}_5 \approx & \left\{ \Sigma_{\text{el}} - \left(4(r_1 + r_2)^2 M_1^2 - (r_1 + r_2)r_2 \zeta M_1^4 + \frac{r_2^2 \zeta^2}{12} M_1^6 \right) \right\}^{1/2} \\ & \times \frac{M_1^2}{4} \left\{ 1 - \frac{\zeta}{6} M_1^2 + \frac{\zeta^2}{128} M_1^4 \right\}^{1/2}. \end{aligned} \quad (7.54)$$

The equality multipliers, r_1 and r_2 , are found by solving Equations (7.44) and (7.47). The solutions are given by

$$r_1 = \frac{A_0^3 \zeta (1 - 3 \text{Im } \phi_+ / A_0)}{36 (1 - 2 \text{Im } \phi_+ / A_0)^2} \quad (7.55)$$

and

$$r_2 = \frac{A_0^2 \zeta}{72 (1 - 2 \text{Im } \phi_+ / A_0)^2} \quad (7.56)$$

where $\zeta = -t/k^2$. The equality multiplier β , with solutions for r_1 and r_2 , is expressed as

$$\beta = \frac{9(A_0 - 2 \text{Im } \phi_+) \sqrt{1 - 2 \text{Im } \phi_+ / A_0 + 36 \text{Im } \phi_+^2 / A_0^2}}{2A_0 \zeta \sqrt{72 \Sigma_{\text{el}} - 2A_0^2 \zeta / (1 - 2 \text{Im } \phi_+ / A_0)}}. \quad (7.57)$$

The optimized modified imaginary single-flip amplitude, expressed as a function of r_1 , r_2 and β , becomes

$$\text{Im } \tilde{\phi}_5 = \frac{(A_0 - 2 \text{Im } \phi_+)}{4A_0 \zeta} \frac{\sqrt{1/2 - 2(1 - \text{Im } \phi_+ / A_0) \text{Im } \phi_+}}{\sqrt{36 \Sigma_{\text{el}} - A_0^2 \zeta / (1 - 2 \text{Im } \phi_+ / A_0)}} \quad (7.58)$$

with

$$J_{\text{max}} = \frac{12}{\zeta} \left(1 - 2 \frac{\text{Im } \phi_+}{A_0} \right). \quad (7.59)$$

For low momentum transfers the imaginary spin average non-flip amplitude $\text{Im } \phi_+$, expanded to order t , is written as

$$\text{Im } \phi_+ \approx \frac{A_0}{2} (1 + gt) . \quad (7.60)$$

Under this approximation the maximum J inside the interior unitarity class is independent of t and in the limit $t \rightarrow 0$ the number of partial waves is finite where

$$J_{\text{max}} = \sqrt{12g} k . \quad (7.61)$$

The equality multipliers in the low t limit become

$$r_1 = \frac{A_0}{72g^2k^2} \left(\frac{1 + 3gt}{t} \right) , \quad (7.62)$$

$$r_2 = -\frac{A_0}{72g^2k^2 t} \quad (7.63)$$

and

$$\beta = \frac{9gk^2}{2\sqrt{72\Sigma_{\text{el}} - 2A_0^2/(gk^2)}} (8 + gt(16 + 9gt))^{1/2} . \quad (7.64)$$

The upper bound on $|\text{Im } r_5|$, where $|\text{Im } r_5| = m_p |\text{Im } \tilde{\phi}_5|/(k \text{Im } \phi_+)$, can be expressed analytically:

$$|\text{Im } r_5| \leq \frac{m_p kg}{2A_0} \sqrt{18\Sigma_{\text{el}} - \frac{A_0^2}{2gk^2}} \times h(t) \quad (7.65)$$

where

$$h(t) = \frac{(8 + gt(16 + 9gt))^{1/2}}{(1 + gt)} . \quad (7.66)$$

The variable $h(t)$ is finite at $t = 0$ and changes ‘slowly’ over the CNI region. Figure 7.1 shows the behaviour of $h(t)$ over the range $t \in [0, -0.01]$ $(\text{GeV}/c)^2$, $\sqrt{s} = 19.4 - 62.5$ GeV. Writing $A_0 = k^2\sigma_{\text{tot}}/\pi$ and $\Sigma_{\text{el}} = k^2\sigma_{\text{el}}/\pi$, enables the bound on $|\text{Im } r_5|$ to be expressed as

$$|\text{Im } r_5| \leq m_P \sqrt{\frac{g}{8}} \left(\frac{36\pi g \sigma_{\text{el}}}{\sigma_{\text{tot}}^2} - 1 \right)^{1/2} \times h(t). \quad (7.67)$$

A similar bound can be obtained if the unitarity constraints are excluded [83].

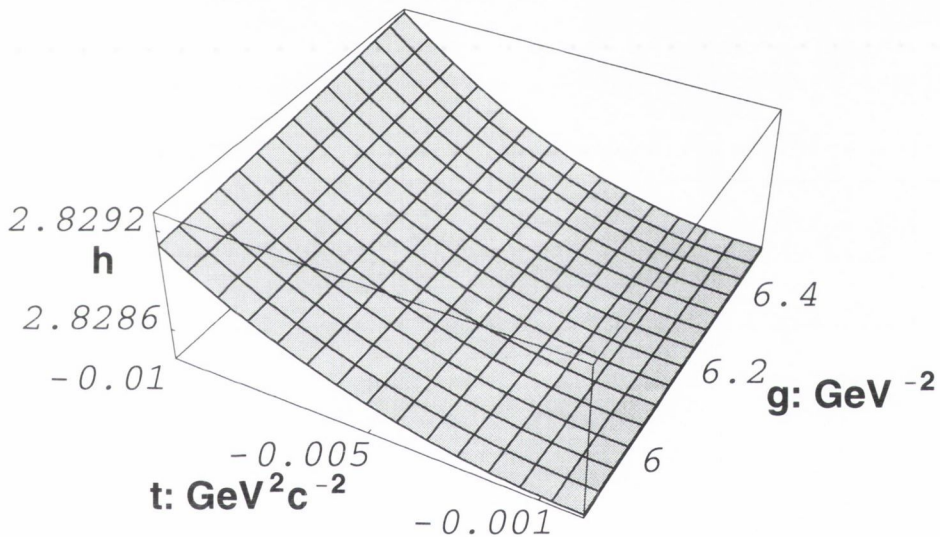


Figure 7.1: Behaviour of $h(t)$ over the CNI region.

The reason why the bound is similar is related to the fact that the inequality multipliers are equal to zero inside the interior unitarity class. Setting the

inequality multipliers equal to zero is like having no unitarity constraints in the system.

3.1 Results

The value of the bound on $|\text{Im } r_5|$ is given in Tables 7.1 and 7.2 plus the values of the equality multipliers. The most noticeable feature of this new bound on $|\text{Im } r_5|$ is its size at low momentum transfers, having a value of 0.89 at $\sqrt{s} = 52.8 \text{ GeV}$, $t = -0.001 \text{ (GeV}/c)^2$. The extra constraint A_0 has a desired effect on the bound, reducing to a value less than unity in the CNI region.

Table 7.1: $|\text{Im } r_5|$ optimized under σ_{el} , $\text{Im } \phi_+$, σ_{tot} and unitarity inside the interior region at $t = -0.001 \text{ (GeV}/c)^2$.

$\sqrt{s} \text{ (GeV)}$	r_1	r_2	β	J_{max}	$ \text{Im } r_5 $
19.4	-12.54	12.77	90	81	0.97
23.5	-12.56	12.79	117	98	0.92
30.7	-12.02	12.24	158	131	0.92
44.7	-11.22	11.44	217	195	1.05
52.8	-11.53	11.76	293	231	0.89
62.5	-11.56	11.79	358	276	0.86

Table 7.2: $|\text{Im } r_5|$ optimized under σ_{el} , $\text{Im } \phi_+$, σ_{tot} and unitarity inside the interior region at $t = -0.01 \text{ (GeV}/c)^2$.

\sqrt{s} (GeV)	r_1	r_2	β	J_{max}	$ \text{Im } r_5 $
19.4	-1.25	1.49	85	81	0.97
23.5	-1.05	1.27	111	98	0.91
30.7	-1.00	1.22	150	131	0.92
44.7	-0.92	1.14	204	195	1.05
52.8	-0.95	1.17	276	231	0.89
62.5	-0.94	1.18	337	276	0.86

The optimized partial waves, at $\sqrt{s} = 52.8 \text{ GeV}$ and $t = -0.001 \text{ (GeV}/c)^2$, are shown in Figures 7.2 and 7.3. Both partial wave series terminate at $J = 231$ which is the upper J limit, M_1 , for the interior unitarity class I . When considering both the interior and boundary unitarity classes, values of $J > M_1$ are permitted.

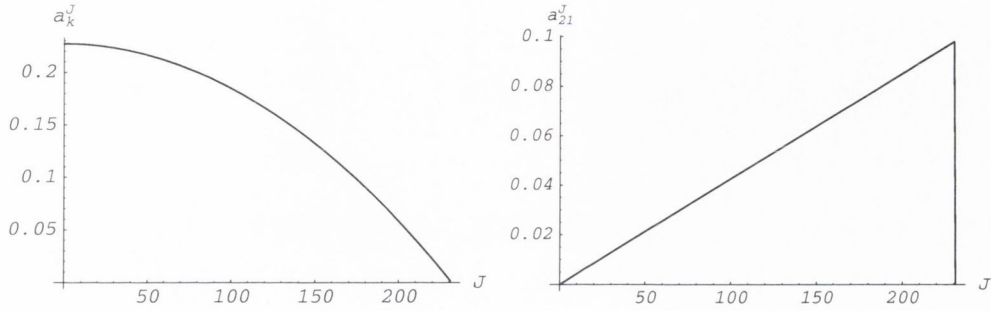


Figure 7.2: a_k^J ($k = 0, 1, 11, 22$) and a_{21}^J optimized under σ_{el} , $\text{Im } \phi_+$, σ_{tot} and unitarity in the interior class; $\sqrt{s} = 52.8 \text{ GeV}$, $t = -0.001 \text{ (GeV}/c)^2$.

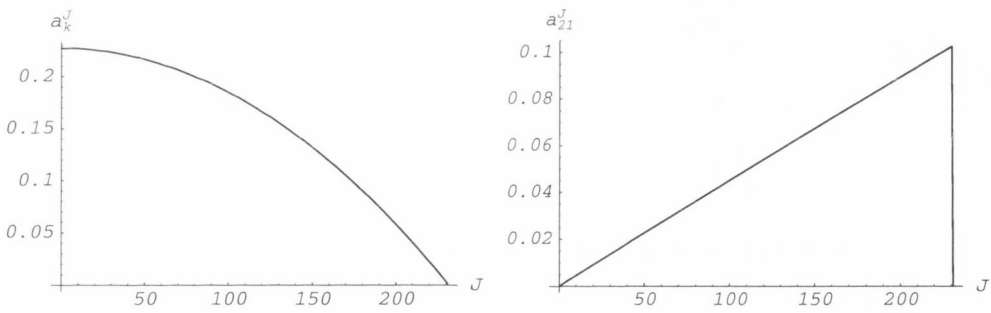


Figure 7.3: a_k^J ($k = 0, 1, 11, 22$) and a_{21}^J optimized under σ_{el} , $\text{Im } \phi_+$, σ_{tot} and unitarity in the interior class; $\sqrt{s} = 52.8 \text{ GeV}$, $t = -0.01 \text{ (GeV}/c)^2$.

The bound on $|\text{Im } r_5|$, under the approximation

$$g \approx \frac{\sigma_{\text{tot}}^2}{32\pi\sigma_{\text{el}}}, \quad (7.68)$$

with momentum transfers in the CNI region can be expressed as

$$|\text{Im } r_5| \leq m_P \sqrt{\frac{g}{64}} \times h(t) \quad (7.69)$$

and in the zero momentum transfer limit, $t \rightarrow 0$, the bound on $|\text{Im } r_5|$ is finite and can be expressed analytically as

$$|\text{Im } r_5| \leq m_p \sqrt{\frac{g}{8}}. \quad (7.70)$$

This approximation generates a ‘stricter’ bound on $|\text{Im } r_5|$ which is shown in Table 7.3 over the CNI region. The bound is considerably lower than the first bound obtained when the system was constrained by the total elastic cross section and by partial wave unitarity; 108.0 compared to 0.84 at $\sqrt{s} = 52.8 \text{ GeV}$, $t = -0.001 \text{ (GeV}/c)^2$.

The bound can be reduced further by considering the behaviour of the polynomial

$$f_2(J) = \tilde{a}_1 + \tilde{a}_2 J^2 + \tilde{a}_3 J^4 + \tilde{a}_4 J^6 \quad (7.71)$$

where $\tilde{a}_1 = (r_1 + r_2)(1 - (r_1 + r_2))$, $\tilde{a}_2 = r_2 \zeta (2(r_1 + r_2) - 1)/4 - 1/(64\beta^2)$, $\tilde{a}_3 = \zeta/(256\beta^2) - r_2^2 \zeta^2/16$ and $\tilde{a}_4 = -\zeta^2/(64\beta)^2$. The interior unitarity class I^X defined in Equation (7.27) can be redefined as

$$I^X \equiv \{J \mid f_2(J) > 0, \tilde{\mu}_J = 0\}. \quad (7.72)$$

Table 7.3: $|\text{Im } r_5|_{\text{max}}$, with an approximation for g , over the CNI region.

\sqrt{s} (GeV)	$t = 0$ (GeV/c) ²	$t = -0.001$ (GeV/c) ²	$t = -0.01$ (GeV/c) ²
19.4	0.803	0.805	0.825
23.5	0.805	0.808	0.827
30.7	0.819	0.821	0.842
44.7	0.839	0.841	0.864
52.8	0.841	0.843	0.866
62.5	0.846	0.848	0.871

The value of J found to satisfy $f_2(J) > 0$ was found to be

$$J^2 < \eta_2^2 \frac{4}{\zeta} \left(1 + \frac{r_1}{r_2} \right) \quad (7.73)$$

with η_2^2 set to unity. The polynomial $f_2(J)$, shown in Figure 7.4, can be plot by substituting the numerical values for r_1 , r_2 and β , at $\sqrt{s} = 52.8$ GeV and $t = -0.001$ (GeV/c)². The maximum J , with $\eta_2^2 = 1$, at $\sqrt{s} = 52.8$ GeV is 231. The maximum J for $f_2(J) > 0$, from Figure 7.4, is 227, implying $\eta_2 = 0.99$. The interior unitarity class I^X , terminating at $J = 227$, is reduced by a small number of partial waves. The effect of this reduction of partial waves on the bound is slight, approximately η_2 times the original bound. This reduction can be applied to the bound all energies over the CNI region

to give a slight improvement on the present $|\text{Im } r_5|$ bound.

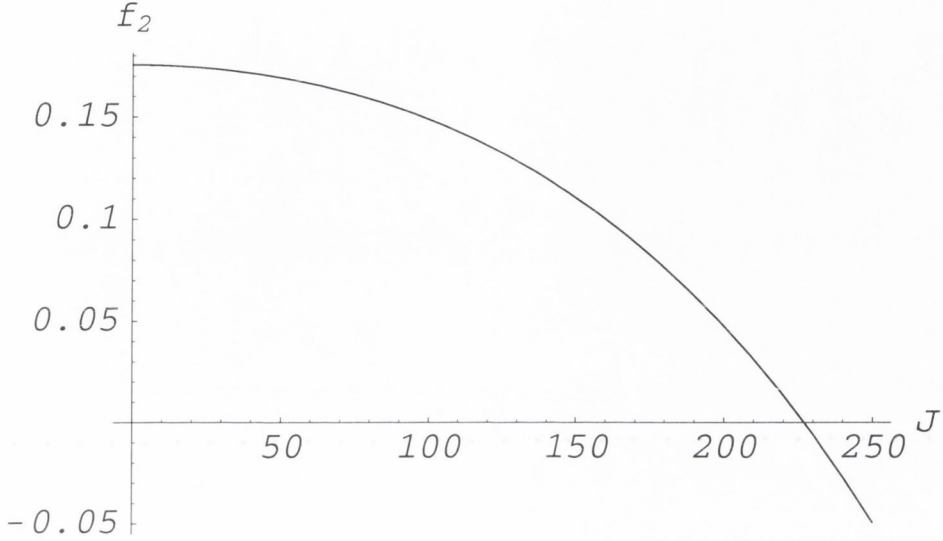


Figure 7.4: The behaviour of the polynomial $f_2(J)$.

4 Solution of Interior and Boundary Classes

Consider the set of classes $I \cup B \equiv I^W \cup I^X \cup B^W \cup B^X$. The boundary unitarity constraints are

$$B^X \equiv \left\{ J | a_{11}^J - a_{11}^{J-2} - a_{21}^{J-2} = 0, M_1 + 1 \leq J \leq M_2 \right\} \quad (7.74)$$

and

$$B^{W_0} \equiv \left\{ J | a_0^J = 0, M_1 + 1 \leq J \leq M_2 \right\} \quad (7.75)$$

where $M_1 = \text{Floor}[\sqrt{4/\zeta(1+r_1/r_2)}]$, $M_2 = \text{Floor}[\sqrt{8/\zeta}]$ and $\zeta = -t/k^2$. The contribution to $|\text{Im } r_5|$ from the boundary unitarity class B can range from 0%–100%. The system with four constraints, when interior and boundary unitarity classes are included, is solved in the same way as described in Chapter 6. With four constraints, three equality and unitarity, the boundary unitarity class is not solvable. The way to solve the system is to convert the three equality constraints into one equality constraint- Σ_{el} . To achieve this the numerical method in Chapter 6 can be employed. The contribution to $|\text{Im } r_5|$ from the boundary unitarity class can be selected without violating any of the constraints and this contribution can be made arbitrarily small.

Consider the case with $\Sigma_{\text{el}}^B = 0.1\Sigma_{\text{el}}$, $\Sigma_{\text{el}}^I = 0.9\Sigma_{\text{el}}$, at $\sqrt{s} = 52.8 \text{ GeV}$ and $t = -0.001 \text{ (GeV}/c)^2$. The maximum contribution to $|\text{Im } r_5|$ is 34.7 where $|\text{Im } r_5^I| \leq 0.5$ and $|\text{Im } r_5^B| \leq 34.2$. The case with $\Sigma_{\text{el}}^B = 0.01\Sigma_{\text{el}}$, $\Sigma_{\text{el}}^I = 0.99\Sigma_{\text{el}}$, leads to $|\text{Im } r_5| \leq 11.6$ where $|\text{Im } r_5^I| \leq 0.8$ and $|\text{Im } r_5^B| \leq 10.6$. Finally, the case with $\Sigma_{\text{el}}^B = 0.001\Sigma_{\text{el}}$, $\Sigma_{\text{el}}^I = 0.999\Sigma_{\text{el}}$, leads to $|\text{Im } r_5| \leq 4.3$ where $|\text{Im } r_5^I| \leq 0.8$ and $|\text{Im } r_5^B| \leq 3.5$. The partial wave amplitudes, a_{11}^J and a_{21}^J , in the boundary interior class, are shown in Figures 7.5, 7.6 and 7.7, where $232 \leq J \leq 2359$. The bound on $|\text{Im } r_5^B|$ falls when the fraction of Σ_{el} in the boundary unitarity class is reduced. The partial wave amplitudes in this region also become smaller in amplitude and contribute less to the

bound on $|\text{Im } r_5^B|$. The fraction of Σ_{el} in the boundary unitarity class can be reduced further and further until the contribution from this class to $|\text{Im } r_5|$ is negligible in comparison with the contribution from the interior unitarity class. In this limit the bound has the expression

$$|\text{Im } r_5| \leq m_P \sqrt{\frac{g}{8}} \left(\frac{36\pi g \sigma_{\text{el}}}{\sigma_{\text{tot}}^2} - 1 \right)^{1/2} \times h(t). \quad (7.76)$$

or, under the approximation $g \approx \sigma_{\text{tot}}^2 / (32\pi\sigma_{\text{el}})$,

$$|\text{Im } r_5| \leq m_P \sqrt{\frac{g}{64}} \times h(t) \quad (7.77)$$

where

$$h(t) = \frac{(8 + gt(16 + 9gt))^{1/2}}{(1 + gt)}. \quad (7.78)$$

The bound is identical to the bound when only the interior unitarity class is considered. Table 7.3 shows the bound on $|\text{Im } r_5|$ over the CNI region under the approximation $g \approx \sigma_{\text{tot}}^2 / (32\pi\sigma_{\text{el}})$. In this system of four constraints, when the interior unitarity class is considered, the solution is an analytic one and the maximum J in this class is much lower than the cases studied in Chapters 5 and 6. The fact that the maximum J is much lower ensures that the sum

$$\text{Im } \tilde{\phi}_5 = \sum_J J^2 a_{21}^J \left(1 - \frac{\zeta}{8} J^2 \right), \quad (7.79)$$

terminating at $J = J_{\text{max}} = 231$, is finite and the upper bound on $|\text{Im } r_5|$ is less than unity.

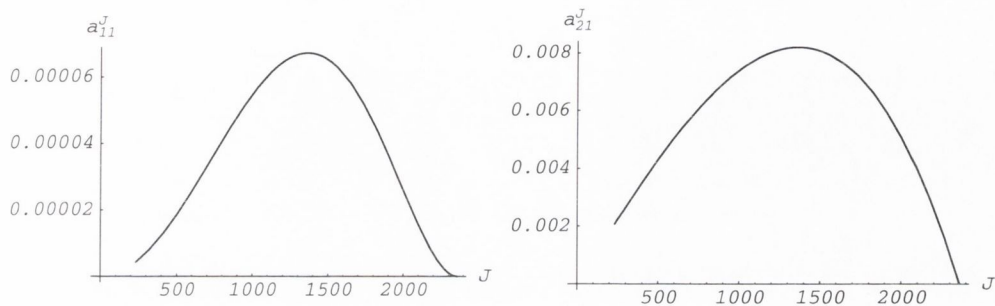


Figure 7.5: a_{11}^J and a_{21}^J optimized under σ_{el} , $\text{Im } \phi_+$, σ_{tot} and unitarity in the boundary unitarity class with $\Sigma_{\text{el}}^B = 0.1\Sigma_{\text{el}}$; $\sqrt{s} = 52.8$ GeV, $t = -0.001$ (GeV/c) 2 .

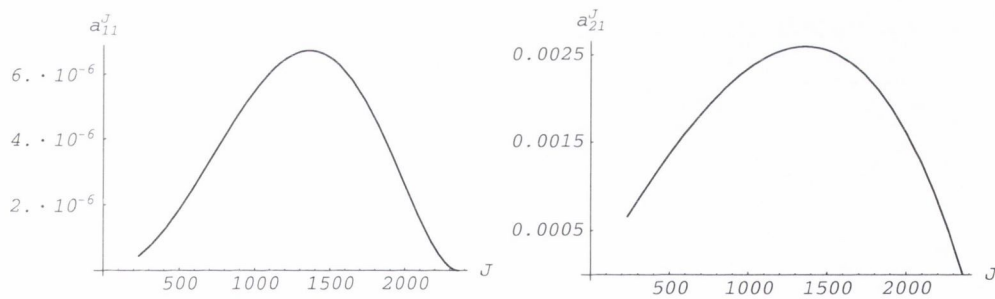


Figure 7.6: a_{11}^J and a_{21}^J optimized under σ_{el} , $\text{Im } \phi_+$, σ_{tot} and unitarity in the boundary unitarity class with $\Sigma_{\text{el}}^B = 0.01\Sigma_{\text{el}}$; $\sqrt{s} = 52.8$ GeV, $t = -0.001$ (GeV/c) 2 .

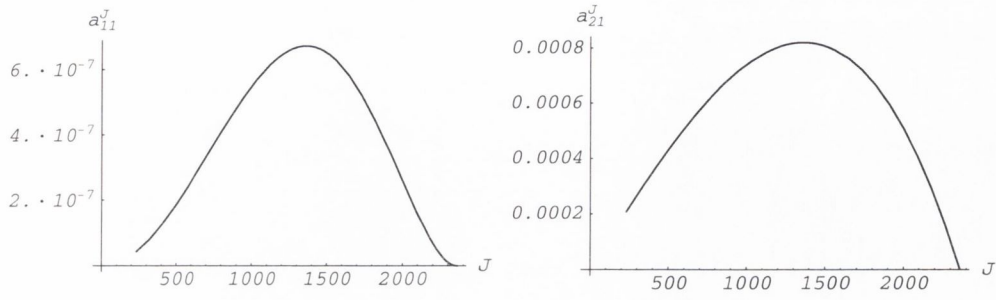


Figure 7.7: a_{11}^J and a_{21}^J optimized under σ_{el} , $\text{Im} \phi_+$, σ_{tot} and unitarity in the boundary unitarity class with $\Sigma_{\text{el}}^B = 0.001 \Sigma_{\text{el}}$; $\sqrt{s} = 52.8 \text{ GeV}$, $t = -0.001 \text{ (GeV}/c)^2$.

In the Thesis the optimization technique of Lagrange multipliers was successfully used to derive bounds on the amplitude $|\text{Im } r_5|$ in the Coulomb Nuclear Interference region. The value of each of the bounds differs and the bound on $|\text{Im } r_5|$ improves as more constraints are added to the system. In Chapter 5 two constraints, the elastic cross section expressed as an equality constraint and unitarity expressed as inequality constraints, are used to bound $|\text{Im } r_5|$. The unitarity constraints split into two classes; an interior unitarity class and a boundary unitarity class. When optimizing $|\text{Im } r_5|$, under the elastic cross section and unitarity, the interior unitarity class is empty and the only non-empty unitarity class is the boundary unitarity class. The system in the boundary unitarity class consists of one equation expressing the normalized dimensionless elastic cross section, $\Sigma_{\text{el}} = k^2 \sigma_{\text{el}} / \pi$, in terms of the equality multiplier β :

$$\Sigma_{\text{el}} \approx \frac{M^2}{2} - 8\beta I_1(M) + 16\beta^2 I_2(M) + I_4(M) - \frac{\zeta}{4} I_6(M) + \frac{\zeta^2}{64} I_8(M) \quad (7.80)$$

where the I_j 's, given in Equation (5.42), are Jacobi-Elliptical integrals. The equation for Σ_{el} , which could not be solved analytically because of the nature of the Jacobi-Elliptical integrals, was solved using `mathematica 3.0`. When there is one unknown in the system of Equations the solution can be easily computed with `mathematica 3.0`. The bound on $|\text{Im } r_5|$, 108.1 at $t = -0.001 (\text{GeV}/c)^2$ and 11.5 at $t = -0.01 (\text{GeV}/c)^2$ with $\sqrt{s} = 52.8 \text{ GeV}$, is not a 'strict' bound and in order to use the pp analyzing power as a polarime-

ter in the Coulomb Nuclear Interference region a bound of 4.48% on $|\text{Im } r_5|$ is required. The value of the bound over the range $\sqrt{s} = 19.4 - 62.5$ GeV, at $t = -0.001 (\text{GeV}/c)^2$ and $t = -0.01 (\text{GeV}/c)^2$, is shown in Table 5.4 and 5.5.

A new constraint, the imaginary spin average non-flip amplitude expressed as an equality constraint, is added to the system with the elastic cross section expressed as an equality constraint and unitarity expressed as inequality constraints. The unitarity constraints again split into different unitarity classes. Three different unitarity classes are considered; the interior class, the boundary class and the union of the interior and boundary classes. The system can be solved analytically when the interior unitarity class is considered and a bound on $|\text{Im } r_5|$ is derived:

$$|\text{Im } r_5| \leq \sqrt{\frac{11}{24}} \frac{m}{k\zeta} \frac{\left(\Sigma_{\text{el}} - \frac{3}{4}\zeta \text{Im } \phi_+^2\right)^{1/2}}{\text{Im } \phi_+} \quad (7.81)$$

where $\zeta = -t/k^2$. The bound on $|\text{Im } r_5|$ has the value 87.9 at $t = -0.001 (\text{GeV}/c)^2$ and 7.7 at $t = -0.01 (\text{GeV}/c)^2$ with $\sqrt{s} = 52.8$ GeV. The values of the bound over the Coulomb Nuclear Interference in the range $\sqrt{s} = 19.4 - 62.5$ GeV are presented in Table 6.2. When only the boundary unitarity class is considered no solutions are possible because inside the boundary class the imaginary spin average amplitude is negative. When both the interior and boundary classes are considered there are two simultaneous equations, one equation for the elastic cross section and the other equation for the imaginary spin

average amplitude. Inside the boundary unitarity class the two equations contain Jacobi-Elliptical integrals. The equations, inside the boundary unitarity class, are not solvable with `mathematica 3.0`; a system of equations with more than one variable is unsolvable in the boundary unitarity class. A numerical technique, designed to solve the system inside the boundary unitarity class by reducing the two simultaneous equations to one equation, is successfully used to solve the system. This leads to a new improved bound on the amplitude $|\text{Im } r_5|$; 59.2 at $t = -0.001 (\text{GeV}/c)^2$ and 5.1 at $t = -0.01 (\text{GeV}/c)^2$ with $\sqrt{s} = 52.8 \text{ GeV}$. The contributions from the unitarity classes to the bound on $|\text{Im } r_5|$ are given in Tables 6.4, 6.5, 6.6 and 6.7.

In the final chapter, four constraints are included in the system; the elastic cross section, the imaginary spin average amplitude and the total cross section, all expressed as equality constraints, and unitarity expressed as inequality constraints. The unitarity classes considered are the interior class and the union of the interior and boundary unitarity classes. The interior unitarity class can be solved analytically and a new, much improved, bound on $|\text{Im } r_5|$ is derived:

$$|\text{Im } r_5| \leq m_P \sqrt{\frac{g}{8}} \left(\frac{36\pi g \sigma_{\text{el}}}{\sigma_{\text{tot}}^2} - 1 \right)^{1/2} \times h(t) \quad (7.82)$$

where

$$h(t) = \frac{(8 + gt(16 + 9gt))^{1/2}}{(1 + gt)}. \quad (7.83)$$

This new bound changes very little over the Coulomb Nuclear Interference region and its value is 0.89 at $\sqrt{s} = 52.8$ GeV. The bound, computed over the range $\sqrt{s} = 19.4 - 62.5$ GeV, is shown in Tables 7.1 and 7.2. The interior and boundary classes, together, lead to an upper bound on $|\text{Im } r_5|$ identical to the bound when just the interior class is considered. This is achieved by reducing the contribution in the boundary unitarity class, without violating the boundary unitarity constraint, until the contribution from the boundary class is negligible in comparison to the contribution from the interior unitarity class. The experimental values for the observables have errors which will have an effect on the $|\text{Im } r_5|$ bound. The approximation $g \approx \sigma_{\text{tot}}^2 / (32\pi\sigma_{\text{el}})$, reduces the final bound on $|\text{Im } r_5|$; 0.89 to 0.84 at $\sqrt{s} = 52.8$ GeV, $t = -0.001$ (GeV/c)². This approximation leads to a reduced number of experimental quantities in the expression for the bound and consequently the error is reduced. A summary of the bounds from each unitarity class in the three studied systems, at $\sqrt{s} = 52.8$ GeV and $t = -0.001$ (GeV/c)², is presented in Table 7.4. The bound of 0.84 is a huge improvement on the first bound of 108.0. Although the value of 0.84 is above the threshold value of 4.48% which is necessary in order to use the pp analyzing power as a polarimeter in the Coulomb Nuclear Interference region with a beam polarization error of, at most 5%, it does

limit the size of the analyzing power. As 0.84 is less than $\kappa_p/2 = 0.896$, the analyzing power in the CNI region is positive.

With more constraints in the system an improved bound would result although to include a new constraint its behaviour must be known experimentally. In the event of future collider experiments measuring pp observables, a greater experimental knowledge of pp observables will be known more accurately at higher energies and over a wider momentum transfer range. With this knowledge new constraints can be added to the Lagrange function and an improved bound less than or equal to 4.48% may be found.

The optimization technique of Lagrange multipliers, applied to elastic proton scattering in the Thesis may also be applied to other physical problems. The method can be used to optimize a function in a system where a number of constraints are given. The constraints can be both equality and inequality constraints. Applications of optimization techniques can be found in public transport models [84] where the Lagrange multiplier method is used to maximize the flow of traffic through a town center with a minimum cost, and in acoustic problems [85] where an optimization technique is used to optimize the acoustical absorption characteristics of an enclosure.

The approved PP2PP RHIC experiment [14] will study, in detail, elastic pp collisions over the Coulomb Nuclear Interference region with center-of-mass energies in the range 50 – 500 GeV. An important issue at RHIC is

polarimetry. It will be interesting to learn what polarimeter will be used in the PHENIX, STAR and PP2PP experiments and what the future will be for other polarimeters which have been investigated theoretically and experimentally including the elastic pC and elastic pp Coulomb Nuclear Interference polarimeters discussed in Chapter 1.

Table 7.4: Summary of the bounds on $|\text{Im } r_5|$; at $\sqrt{s} = 52.8$ GeV and $t = -0.001$ (GeV/c)²

Constraints	Unitarity Classes	$ \text{Im } r_5 _{\text{max}}$
σ_{el} and unitarity	Boundary	108.0
σ_{el} , $\text{Im } \phi_+$ and unitarity	Interior	87.9
	Interior and Boundary	59.2
σ_{el} , $\text{Im } \phi_+$, σ_{tot} and unitarity	Interior	0.84
	Interior and Boundary	0.84

Appendix A

Partial Wave Phase Shifts

In the elastic region the partial wave amplitudes, expressed in terms of the partial wave phase shifts, are given by [86]

$$f_0^J = e^{i\delta_0^J} \sin \delta_0^J, \quad (\text{A.1})$$

$$f_1^J = e^{i\delta_1^J} \sin \delta_1^J, \quad (\text{A.2})$$

$$f_{11}^J = \frac{i}{2} \left[1 - e^{2i\delta_1^J} \left(\cos 2\delta_2^J + i \sin 2\delta_2^J \cos \alpha^J \right) \right], \quad (\text{A.3})$$

$$f_{22}^J = \frac{i}{2} \left[1 - e^{2i\delta_1^J} \left(\cos 2\delta_2^J - i \sin 2\delta_2^J \cos \alpha^J \right) \right], \quad (\text{A.4})$$

and

$$f_{21}^J = \frac{1}{2} e^{2i\delta_1^J} \sin 2\delta_2^J \sin \alpha^J. \quad (\text{A.5})$$

Appendix B

Mathematica Code

```
In[1]:= (* Sample Mathematica file, t=-0.001, W=52.8 *)
```

```
In[2]:= Q=Sqrt[c1 + c2 J^2 + c3 J^4 + c4 J^6]
```

```
Out[2]= (c1 + c2 J^2 + c3 J^4 + c4 J^6)
```

```
In[3]:= f1=J/ Q
```

```
i1=Integrate[f1,J,a, b];
```

```
Out[3]= (J/ (c1 + c2 J^2 + c3 J^4 + c4 J^6) )
```

```
In[5]:= f11=J/(Q^2)
```

```
i2=Integrate[f11,J,a, b];
```

```
Out[5]= (J / (c1 + c2 J^2 + c3 J^4 + c4 J^6) )
```

```
In[7]:= f2=J^3/Q
```

```
i3=Integrate[f2,J,a,b];
```

```
Out[7]= (J^3 / (c1 + c2 J^2 + c3 J^4 + c4 J^6) )
```

```
In[9]:= f22=J^3/( Q^2 )
```

```
i4=Integrate[f22,J,a, b];
```

```
Out[9]= (J^3 / (c1 + c2 J^2 + c3 J^4 + c4 J^6) )
```

```
In[11]:=f3=J^5/Q
i5=Integrate[f3,J,a, b];
Out[11]= (J^5 / (c1 + c2 J^2 + c3 J^4 + c4 J^6 ) )
```

```
In[13]:=f33=J^5/( Q^2 )
i6=Integrate[f33,J,a, b];
Out[13]= (J^5 / (c1 + c2 J^2 + c3 J^4 + c4 J^6 ) )
```

```
In[15]:=f4=J^7/Q
i7=Integrate[f4,J,a, b];
Out[15]= (J^7 / (c1 + c2 J^2 + c3 J^4 + c4 J^6 ) )
```

```
In[17]:= f44=J^7/( Q^2 )
i8=Integrate[f44,J,a, b];
Out[17]= (J^7 / (c1 + c2 J^2 + c3 J^4 + c4 J^6 ) )
```

```
In[19]:=
E0= M ^2 /2 - 8 β i1 + 16 β^2 i2 + i4 -1/4 ζ i6 + 1/64 ζ^2 i8;
```

```
In[20]:= c1=16*β^2 ;
c2=1;
c3=-1/4 ζ ;
c4=1/64 ζ^2 ;
```

```
In[21]:= t=-0.001;
```

```
In[22]:= mp=0.938; W=52.8; k=Sqrt[(W/2)^2 - mp^2]; ζ= (-t/k^2); a=0;
b=Floor[Sqrt[8ζ]]; A=k^2/Pi * (42.906/.3894); E1=k^2/Pi * (7.407/.3894);
g=(12.87/2); phi=k*W/(4*Pi)* (42.906/.3894)*(1 - (-t*g));
```

```
In[23]:= FindRoot[E0==E1,β, 1000,5000, MaxIterations->400]
Out[23]= β → 4372.74929761300423 + 8.36339296256140229*^-9 I
```

```
In[29]:= β1=4372.75
Out[29]= 4372.75
```

```
In[30]:= (* double check solution *)
E1
```

E0 /.β → β1

Out[30]= 4214.59

Out[31]= 4214.59297107105168 - 1.18713820234705313*⁻⁸ I

In[32]:= b1=J/(8β1) (1 - ζ/8 J²);

nu1=1/2(Sqrt[1 + 4 b1²] -1);

a11=nu1/(1 + 2 nu1);

b11=b1/(1 + 2 nu1);

(* Im r5 Bound *)

imr5=mp/k *Sum[J²*b11*(1 - ζ/8 J²),J,a,b]/(phi)

Out[33]= 108.061

Appendix C

Euler-MacLaurin Expansion

The Euler-Maclaurin integration formula allows a sum to be written as an integral:

$$\begin{aligned} \sum_{l=1}^m f(l) &= \int_1^m f(x) dx + \frac{1}{2} [f(m) + f(1)] + \frac{B_2(0)}{2!} [f^1(m) - f^1(1)] \\ &\quad + \frac{B_4(0)}{4!} [f^3(m) - f^3(1)] + \frac{B_6(0)}{6!} [f^5(m) - f^5(1)] + \dots \\ &\quad \dots + \frac{B_{2n}(0)}{2n!} [f^{2n-1}(m) - f^{2n-1}(1)] \end{aligned} \quad (\text{C.1})$$

where, $f^i(m) = \frac{d^i}{dx^i} f(x)|_{x=m}$. and $B_{2n}(0) \equiv B_{2n}$ are Bernoulli numbers with $B_2 = 1/6$, $B_4 = -1/30$, $B_6 = 1/42$, $B_8 = -1/30$, $B_{10} = 5/66$, $B_{12} = -691/2370$, $B_{14} = 7/6$. The following summations can be written as polynomials;

$$\sum_{l=1}^m l = \frac{1}{2} m(m+1) \quad (\text{C.2})$$

$$\sum_{l=1}^m l^2 = \frac{1}{6} m(m+1)(2m+1) \quad (\text{C.3})$$

$$\sum_{l=1}^m l^3 = \frac{1}{4} m^2 (m+1)^2 \quad (\text{C.4})$$

$$\sum_{l=1}^m l^4 = \frac{1}{30} m (m+1) (2m+1) (3m^2 + 3m - 1) \quad (\text{C.5})$$

$$\sum_{l=1}^m l^5 = \frac{1}{12} m^2 (m+1)^2 (2m^2 + 2m - 1) \quad (\text{C.6})$$

and for large m we can approximate the sum as

$$\sum_{l=1}^m J^n \approx \frac{1}{n+1} m^{n+1}. \quad (\text{C.7})$$

Bibliography

- [1] M. Anselmino, A. Efremov and E. Leader, *Phys. Reps.* **261**, 1 (1995).
- [2] E. Leader and E. Predazzi, *An Introduction to Gauge Theories and Modern Particle Theory*, Vol. 1, Cambridge University Press (1996).
- [3] U. Stiegler, *Phys. Reps.* **277**, 1 (1996).
- [4] J. D. Bjorken, *Phys. Rev.* **148**, 1467 (1966), *Phys. Rev.* **D1**, 1367 (1967)
- [5] J. Ellis, R. J. Jaffe, *Phys. Rev.* **D9**, 1444 (1974),
Phys. Rev. **D10**, 1668 (1974).
- [6] J. Ashman *et al.*, *Nucl. Phys.* **B328**, 1 (1989).
- [7] G. Altarelli and G. G. Ross, *Phys. Lett.* **B212**, 391 (1988).
S. J. Brodsky, J. Ellis and M. Karliner, *Phys. Lett.* **B206**, 309 (1988).
G. Veneziano, *Mod. Phys. Lett.* **A4**, 1605 (1989).

R. J. Jaffe, A. Manohar, *Nucl. Phys.* **B337**, 509 (1990).

A. V. Kisselev and V. A. Petrov, *Theor. Math. Phys.* **91**, 234 (1992).

[8] D. Adams *et al.*, *Phys. Lett.* **B357**, 248 (1995),

Phys. Rev. **D 56**, 5330 (1997).

G. Altarelli and G. Ridolfi, *Nucl. Phys. B(Proc. Suppl.)* **39B**, 106 (1995).

I. A. Savin, *The SMC results on polarized muon-nucleon deep inelastic scattering*, Proceedings of the 13th International Symposium on High Energy Spin Physics, Protvino, Russia, 1998, edited by N. Tyurin *et al.* (World Scientific, Singapore, 1999), p. 78.

[9] V. A. Petrov, *Nucleon Spin Puzzle: Ten Years Later...*, in *SPIN98*,

Proceedings of the 13th International Symposium on High Energy Spin Physics, Protvino, Russia, 1998, edited by N. Tyurin *et al.* (World Scientific, Singapore, 1999), p. 107.

H. Y. Cheng, hep-ph/0002157

[10] G. Bunce, *RHIC Spin Physics*, Proceedings of the DESY Workshop, May 1999, edited by A. De Roeck *et al.*, p.283.

[11] T. Roser, *RHIC Spin Program*, Proceedings of the DESY Workshop, May 1999, edited by A. De Roeck *et al.*, p.52.

- [12] S. Vigdor, *Long-Term Overview of STAR Spin Program*, Proceedings of the RIKEN BNL Research Center RHIC Spin Workshop, 1999, eds L. Bland *et al.*, p.17.
- [13] N. Saito, *Progress of PHENIX Spin Program*, Proceedings of the RIKEN BNL Research Center RHIC Spin Workshop, 1999, eds L. Bland *et al.*, p.26.
- [14] W. Guryan *et al.*, *Experiment to Measure Total and Elastic Cross Sections at RHIC*, rev. 1995.
<http://www.rhic.bnl.gov/export1/pp2pp/pp2pp.html>
- [15] C. Prescott *et al.*, Report of RHIC Spin Review Committee, June 1995.
- [16] K. Kuroda in AIP Conf. Proc. No. 95, High Energy Spin Physics, Brookhaven, 1982, ed. G. M. Bunce (AIP, New York, 1983), p. 618.
- [17] D. C. Carey *et al.*, *Phys. Rev. Lett.* **64**, 357 (1990).
- [18] G. Bunce, Proton Polarimetry for RHIC, RIKEN BNL Research Center, Workshop organized by E. Leader (1999).
- [19] M. Froissart, *Phys. Rev.* **123**, 1053 (1961).
- [20] N. H. Buttimore, B. Z. Kopeliovich, E. Leader, J. Soffer and T. L. Trueman, *Phys. Rev.* **D59**, 114010 (1999).

- [21] M. B. Einhorn and R. Blankenbecler, *Ann. Phys.* **67**, 480 (1971).
- [22] M. R. Hestenes, *Calculus of Variations and Optimal Control Theory*, John Wiley and Sons (1966).
- [23] R. J. Eden, *Optimization of Collision Amplitudes under Constraints*, Lecture Notes in Physics, Vol. 17, Springer-Verlag (1973).
- [24] M. M. Denn, *Optimization by Variational Methods*, McGraw-Hill (1969).
- [25] D. P. Bertsekas, *Constrained Optimization and Lagrange Multiplier Methods*, Academic Press (1982).
- [26] M. Jacob and G. C. Wick, *Ann. Phys.* **7**, 404 (1959).
- [27] B. Z. Kopeliovich and L. I. Lapidus, *Sov. J. Nucl. Phys* **19**, 114 (1974).
- [28] N. H. Buttimore, in AIP Conf. Proc. No. 95, High Energy Spin Physics, Brookhaven, 1982, ed. G. M. Bunce (AIP, New York, 1983), p. 634.
- [29] C. Bourrely, E. Leader and J. Soffer, *Phys. Repts.* **59**, 95 (1980).
- [30] M. L. Goldberger, M. T. Grisaru, S. W. MacDowell and D. Y. Wong, *Phys. Rev.* **120**, 2250 (1960).
- [31] R. N. Cahn, *Z. Phys.* **C15**, 253 (1982).
- [32] N. H. Buttimore, E. Gotsman and E. Leader, *Phys. Rev.* **D18**, 694 (1978).

- [33] N. Akchurin, N. H. Buttimore and A. Penzo, *Phys. Rev.* **D51**, 3944 (1995).
- [34] K. Kurita, *A New Polarimeter for RHIC*, Proceedings of the DESY Workshop, May 1999, edited by A. De Roeck *et al.*, p.71.
- [35] N. H. Buttimore, *Fermion boson collisions and swift proton polarimetry*, Proceedings of the RIKEN BNL Research Center RHIC Spin Workshop, 1999, eds L. Bland *et al.*, p.214.
- [36] T. Regge, *Nuovo Cimento* **14**, 951 (1959).
- [37] G. F. Chew, S. C. Frautschi, *Phys. Rev. Lett.* **8**, 41 (1962).
- [38] E. L. Berger, A. C. Irving, C. Sorensen, *Phys. Rev.* **D17**, 2971 (1978).
- [39] A. C. Irving, R. P. Worden, *Phys. Rep.* **34C**, 117 (1977).
- [40] P. D. B. Collins, *An Introduction To Regge Theory and High Energy Physics*, Cambridge University Press (1977).
- [41] P. V. Landshoff and J. C. Polkinghorne, *Nucl. Phys.* **B32**, 541 (1971).
- [42] K. G. Boreskov, A. A. Grigiryan, A. B. Kaidalov and I. I. Levintov, *Sov. J. Nucl. Phys* **27**, 432 (1978).
- [43] C. Bourrely, H. A. Neal, G. A. Ogren, J. Soffer and T. T. Wu, *Phys. Rev.* **D26**, 1781 (1982).

- [44] M. G. Ryskin, *Yad. Fiz.* **46**, 611 (1987), *Sov. J. Nucl. Phys* **46**, 337 (1987).
- [45] B. Z. Kopeliovich and B. G. Zakharov, *Phys. Lett.* **B226**, 156 (1989).
- [46] M. Anselmino and S. Forte, *Phys. Rev. Lett.* **71**, 223 (1993).
- [47] N. Akchurin *et al.*, *Phys. Rev.* **D48**, 3026 (1993).
- [48] G. Mahoux, *Phys. Lett.* **67B**, 75 (1976).
- [49] H. Cornille and A. Martin, *Nucl. Phys.* **B115**, 163 (1976).
- [50] G. Auberson, A. Martin and G. Mennessier, *Phys. Lett.* **67B**, 75 (1977).
- [51] N. H. Buttimore, *Elastic Scattering and The Magnetism of Swift Protons*, Presentation at the Adriatico Research Conference on Trends in Collider Spin Physics, ICTP, Trieste, Italy, December 1995.
- [52] D. P. Hodgkinson, *Phys. Lett.* **39B**, 640 (1972).
- [53] O. W. Greenberg and F. E. Low, *Phys. Rev.* **124**, 2047 (1961).
- [54] K. Yamamoto, *Nuovo Cimento* **27**, 1277 (1963).
- [55] Y. S. Gin and A. Martin, *Phys. Rev.* **135**, B1375 (1964).
- [56] R. J. Eden, *Phys. Lett.* **19**, 695 (1966), *J. Math. Phys.* **8**, 320 (1967).

- [57] A. Martin, *Nuovo Cimento* **59A**, 131 (1969), *Scattering Theory: Unitarity, Analyticity and Crossing*, Lecture Notes in Physics, Vol. 3, Springer-Verlag (1969).
- [58] S. M. Roy and V. Singh, *Phys. Rev.* **D1**, 2638 (1970).
- [59] R. Savit, R. Blankenbecler and M. B. Einhorn, *J. Math. Phys.* **12**, 2092 (1971)
- [60] K. H. Mütter, *Nucl. Phys.* **B31**, 589 (1971).
- [61] B. D. Hahn and D. P. Hodgkinson, *Nucl. Phys.* **B46**, 232 (1972).
- [62] S. M. Roy, *Phys. Repts.* **5**, 125 (1972).
- [63] S. K. Chan and I. A. Sakmar, *Phys. Rev.* **D13**, 603 (1976).
- [64] S. M. Roy, *Phys. Lett.* **70B**, 213 (1977).
- [65] G. Mennessier, S. M. Roy and V. Singh, *Nuovo Cimento* **50A**, 443 (1979).
- [66] K. S. Ramadurai and I. A. Sakmar, *Prog. Theo. Phys.* **63**, 1700 (1980).
- [67] I. A. Sakmar and J. H. Wojtaszek, *Phys. Rev.* **D26**, 2280 (1982), *Nuovo Cimento* **70A**, 132 (1982).
- [68] S. W. MacDowell and A. Martin, *Phys. Rev.* **135**, B960 (1964).

- [69] R. J. Eden, *High Energy Colisions of Elementary Particles*, Cambridge University Press (1967).
- [70] A. D. Martin, T. D. Spearman, *Elementary Particle Theory*, North - Holland Publishing Company, Amsterdam (1970).
- [71] L. Wolfenstein, *Phys. Rev.* **96**, 1654 (1954).
- [72] J. Bystricky, F. Lehar and P. Winternitz, *Journal de Physique* **39**, 1 (1978).
- [73] K. H. Mütter, *Nucl. Phys.* **B27**, 73 (1971).
- [74] M. Andrews and J. Gunson, *J. Math. Phys.* **5**, 1391 (1964).
- [75] W. W. Bell, *Special Functions for Scientists and Engineers*, Van Nostrand (1968).
- [76] Bateman Manuscript, *Higher Transcendental Functions*, McGraw-Hill (1953).
- [77] A. T. Bates and N. H. Buttimore, *Optimisation of the single helicity-flip amplitude in elastic pp collisions*, Talk given at QCD99, Montpellier, France, July 1999, *Nucl. Phys. B (Proc. Suppl.)* **86**, 175 (2000).
- [78] R.P. Boas and C. Stutz, *American Journal of Physics* **39**, 745 (1971).

- [79] G. B. Arfken and H. J. Weber, *Mathematical Methods for Physicists*, Academic Press (1995).
- [80] C. Caso *et al*, *European Physical Journal* **C3**, 1 (1998).
Particle Data Group Web Page, <http://pdg.lbl.gov>
- [81] S. Wolfram, *Mathematica, The Student Book*, Addison-Wesley Publishing Company (1994).
- [82] F. Pereira and E. Ferreira, *Phys. Rev.* **D61**, 07750 (2000).
- [83] A. T. Bates and N. H. Buttimore, *in Spin 98*, Proceedings of 13th International Symposium on High Energy Spin Physics, Protvino, Russia, 1998, edited by N. Tyurin *et al.* (World Scientific, Singapore, 1999), p. 483.
- [84] J. de D. Ortúzar and L. G. Willumsen, *Modelling Transport*, 2nd Ed., John Wiley and Sons, 1994.
- [85] M. Cappelli D'Orazio and D. M. Fontana, *Applied Acoustics* **57**, 139 (1999).
- [86] Talk given by S. MacDowell, Brookhaven National Laboratory, August 1997.